MOISTURE TRANSPORT IN CELLULAR CONCRETE ROOFS

PROEFSCHRIFT

TER VERKRIJGING VAN DE GRAAD VAN DOCTOR IN DE TECHNISCHE WETENSCHAPPEN AAN DE TECHNISCHE HOGESCHOOL TE EINDHOVEN, OP GEZAG VAN DE RECTOR MAGNIFICUS, PROF. DR. IR. A. A. TH. M. VAN TRIER, VOOR EEN COMMISSIE UIT DE SENAAT IN HET OPENBAAR TE VERDEDIGEN OP DINSDAG 18 MEI 1971 DES NAMIDDAGS TE 4 UUR

DOOR

JAN VAN DER KOOI
geboren te Geldrop

UITGEVERIJ WALTMAN – DELFT

DIT PROEFSCHRIFT IS GOEDGEKEURD DOOR DE PROMOTOR
PROF. DR. D. A. DE VRIES

CONTENTS

Chapter 1

INTRODUCTION

In this thesis a method is presented for calculating the moisture transport in roof constructions of cellular concrete. The moisture content of a roof can change for several reasons. In buildings, in which a high inside water vapour pressure is maintained, water vapour penetrates the roof material during the winter season, giving rise to an increase of moisture content in the roof. During summer the roof partly dries out again. Also moisture can be present in roof constructions due to the installation of wet materials or wetting from roofing leaks.

The effect of moisture in roof constructions is, in general, to considerably reduce their insulating value, apart from the tendency to cause physical deterioration of the roof material or other components of the construction, especially under conditions of freezing. Designers of roof constructions, however, usually compute the heat resistance on the basis of values of the thermal conductivities of the dry component materials. Therefore, there is need of a calculation method to predict the moisture content and insulating value of roof constructions for climatic conditions occurring in practice.

Such a method, frequently used in the German speaking countries, is the one of Glaser [1]. With this method the change of moisture content during winter and during summer can be predicted, using well defined boundary conditions with respect to the internal and external temperatures and water vapour pressures [2]. When the increase of moisture content during winter is not harmfull and does not exceed the decrease during summer, the construction is considered to be suitable for the climatic conditions under consideration.

However, in Glaser's method only moisture transport in the vapour phase is considered. Therefore this method can only be used for constructions in which the liquid transport due to capillary forces is negligible in comparison with vapour transport. Such constructions are, for instance, composite structures with air cavities, vapour barriers and insulation materials of mineral wool, polystyrene, etc. For constructions composed of materials with a high capillary liquid transport, such as cellular concrete, the moisture transport calculated in this way is not in agreement with the moisture transport experimentally determined for moisture increase during winter [3, 4], as well as for drying during summer (Section 6.2 in this thesis). A better agreement is found by correlating the moisture content in the roof with the hygroscopic moisture content of the roof material for the relative humidity of the air underneath the roof [5]. In this thesis the moisture content at the lower face of the roof is calculated in a similar way.

The moisture flow inside a porous medium can, according to Philip and De Vries [6], be described by:

$$q_l = -\varrho_l D_\theta \partial\theta/\partial z - \varrho_l D_T \partial T/\partial z,$$

where q_l is the moisture flux density, $\partial\theta/\partial z$ the moisture gradient and $\partial T/\partial z$ the temperature gradient. D_θ and D_T are generalized diffusion coefficients for moisture flow due to those gradients. This theory is applied to roofs made of cellular concrete and compared with experimental results in our work.

In Chapter 2 the theory is discussed in detail. Further a method is developed for the calculation of moisture transport in roof constructions, as is illustrated by an example. For certain conditions the calculation can be carried out in a simplified way. In this chapter Glaser's calculation method is also discussed and applied to the same example, making a comparison between the two methods possible.

Experimental methods have been developed for determining those properties of cellular concrete, that are needed for the calculation of moisture transport. These are the diffusion coefficients D_θ and D_T, the hygroscopic moisture content and the thermal conductivity. These methods and the experiments performed on cellular concrete are described in Chapter 3. Also the structure of the material has been investigated.

In Chapter 4, the diffusion coefficients D_θ and D_T are calculated, using the expressions developed by Philip and De Vries for porous materials with a comparatively simple structure, such as sands. These developments need some extension for the materials with a more complicated structure considered here.

In Chapter 5 experiments are described, performed on specimens of cellular concrete roofs. The specimens have been exposed to several constant internal and external climatic conditions, simulating winter and summer seasons. During these experiments the moisture content in the specimens, as well as the heat insulation value has been measured.

In Chapter 6 the moisture transport and the thermal resistance are calculated for the same climatic conditions as those of the experiments described in Chapter 5. The calculations have been performed with the help of a digital computer, using the physical properties determined in Chapter 3. With the computer a more complete calculation can be carried out than the one described in Chapter 2. For instance, the drying rate of roof constructions exposed to simulated summer conditions can also be calculated. The results of the calculations are compared with experimental results.

It was considered justifiable to calculate the moisture transport in the same way for several kinds of roofs and for several climatic conditions occurring in practice. In Chapter 7 examples of these calculations are given. Some of the theoretical results are compared with the results of measurements carried out on roofs in practice [5].

References

1. H. Glaser, Kältetechnik **11**, 345–349, (1959).
2. W. Caemmerer, Berichte aus der Bauforschung, Heft 51, 55–77, (1968).
3. J. v. d. Kooi, K. T. Knorr, Het vochtgedrag in niet-geventileerde daken van cellenbeton, p. 12, Publikatie Stichting Bouwresearch, no. 33, Samsom, Alphen a/d Rijn (1970).
4. J. v. d. Kooi, K. T. Knorr, Vochthuishouding in niet-geventileerde daken, Werkrapport BII-14, Stichting Bouwresearch (1966).
5. K. Gertis, H. Künzel, K. Gösele, Untersuchungen über die Feuchtigkeitsverhältnisse in Dächern aus Gasbeton, Fachverband Gasbetonindustrie E.V. (1969).
6. D. A. de Vries, De Ingenieur, **74**, 0 45–53, (1962).

Chapter 2

MOISTURE TRANSPORT IN POROUS MEDIA AND ROOF CONSTRUCTIONS

In this chapter several theories will be discussed concerning the moisture transport in porous media. The theories developed by Krischer [1] and Lykow [2] will be discussed briefly; more attention will be paid to a theory by Philip and De Vries [3]. In all these theories vapour transport as well as liquid transport is taken into account.

Next a graphic method will be described to calculate the rate of moisture change in building constructions, due to internal condensation of water vapour as well as to evaporation of water leading to drying. This method, presented by Glaser [4] only allows for water vapour transport. In many constructions, however, liquid transport forms an important contribution to the total moisture transfer. In order to take this contribution also into account and to show its effect we calculated the moisture transport in a cellular flat-roof construction using the theory of Philip and De Vries and compared the results with those obtained from Glaser's method.

2.1 Theories concerning the moisture transport in porous media

2.1.1 *The theory of Philip and De Vries*

Liquid transport

The transport of liquid in a porous medium can macroscopically be described by Darcy's law [5]:

$$q_l = -\varrho_l K \nabla \psi, \tag{2.1}$$

where q_l is the mass flow density, ϱ_l the density of the liquid, K the hydraulic conductivity and ψ the hydraulic potential.

Here the hydraulic potential will be considered as the potential energy of a unit of mass of liquid and can be seen as the algebraic sum of the partial potentials, that result from the different forces working on the mass element under consideration. For each partial-potential ψ_k corresponding with a force $\bar{F}_k$ working on a mass element of water one has:

$$\psi_k = -\int \bar{F}_k \cdot \mathrm{d}\bar{l},$$

where $\mathrm{d}\bar{l}$ is the displacement of the mass element.

The following partial-potentials can be distinguished [6]:

ψ_g = gravity potential;

ψ_m = matrix potential, composed of the adsorbtion potential (due to adhesive forces), the capillary potential (due to curved menisci) and a potential due to the osmotic bond in the double layer;

ψ_p = pressure potential (due to the outside gas pressure).

The hydraulic potential, ψ, can be written as

$$\psi = \psi_g + \psi_m + \psi_p. \tag{2.2}$$

Here only the terms ψ_g and ψ_m will be considered.

ψ_p is neglected because only moisture transport at constant atmospheric pressure is considered. In addition moisture transport due to diffusion under the influence of differences in concentration of solved salts is left out of consideration (see also [29]).

The gravity potential, ψ_g, can be written as

$$\psi_g = gz, \tag{2.3}$$

where g is the acceleration of gravity and z the vertical coordinate, counted positive upwards.

The matrix potential, ψ_m, manifests itself in the suction pressure, which has the effect of a negative pressure namely the moisture tension, P_l. For decreasing moisture content the absolute value of the moisture tension increases. This pressure can be written directly as a potential if the gradient of the pressure is considered as a force (see for instance [6]), so that for the matrix potential holds

$$\psi_m = \frac{P_l}{\varrho_l}. \tag{2.4}$$

In the moisture range where considerable liquid transport occurs P_l, and consequently also the matrix potential ψ_m, is mainly determined by capillarity, so for a cylindrical capillary one has:

$$\psi_m = -\frac{2\sigma \cos \delta}{\varrho_l r}, \tag{2.5}$$

where σ is the surface tension, δ the contact angle and r the radius of the capillary. Like σ, ψ_m is a function of the temperature T. Furthermore ψ_m is a function of the liquid moisture content θ_l, so for Eq. (2.1) can be written:

$$\frac{q_l}{\varrho_l} = -K\left(\frac{\partial \psi_m}{\partial \theta_l}\right)_T \nabla\theta_l - K\left(\frac{\partial \psi_m}{\partial T}\right)_{\theta l} \nabla T - Kgk \tag{2.6}$$

Here k is the unit vector in the positive z-direction so that the term Kgk represents the influence of gravity. The term $(\partial\psi_m/\partial T)_{\theta l}$ can be written as:

$$\left(\frac{\partial\psi_m}{\partial T}\right)_{\theta l} = \frac{\partial\psi_m}{\partial\sigma}\frac{d\sigma}{dT} = \frac{\psi_m}{\sigma}\frac{d\sigma}{dT} = \gamma\psi_m, \tag{2.7}$$

where γ represents the temperature coefficient of the surface tension.

Combining Eqs. (2.6) and (2.7), one finds for the moisture flux:

$$q_l/\varrho_l = -D_{\theta l}\nabla\theta_l - D_{Tl}\nabla T - Kgk, \tag{2.8}$$

with

$$D_{\theta l} = K\left(\frac{\partial\psi_m}{\partial\theta_l}\right)_T, \tag{2.9}$$

$$D_{Tl} = K\gamma\psi_m. \tag{2.10}$$

Vapour transport

The transport of water vapour by molucular diffusion is described macroscopically by Fick's first law, which can be written in various forms according to the variables and the reference system used. A comprehensive treatment is given by De Groot and Mazur [7].

When we consider the air-water vapour system as a binary ideal gas mixture in presence of a temperature gradient the mass flow density of water vapour with respect to air, q_v, is given by ([7] p. 26):

$$q_v = -D\frac{\varrho}{c_2}\nabla c_1 - \varrho c_1 D'\nabla T, \tag{2.11}$$

where D is the binary diffusion coefficient, ϱ the gas density, c_1 the mass fraction of water vapour and c_2 that of air. D' is the thermal diffusion coefficient and T the temperature.

For constant total pressure and an ideal gas mixture Eq. (2.11) can be written as:

$$q_v = -D\frac{P}{P-p_v}\frac{M}{RT}\nabla p_v\left[1 + \frac{D'}{D}\frac{p_v(P-p_v)}{P}\frac{\nabla T}{\nabla p_v}\right], \tag{2.12}$$

where M is the molar mass of water, R the universal gas constant, P the total gas pressure, and p_v the partial pressure of water vapour. For the conditions considered here one can show (see [8]), that the second term between brackets will be small compared to 1, so that the influence of thermal diffusion can be neglected.

Considering the diffusion of gas through a porous material the following two factors have to be taken into account:

- a factor, which represents the total cross-section, available for diffusion. For this we may choose the volumetric air content, a, in the material;
- a tortuosity factor, α, allowing for the extra path length.

So for the mass flow density of water vapour through a porous material one may write:

$$q_v = -\alpha a D \frac{P}{P-p_v} \frac{M}{RT} \nabla p_v. \tag{2.13}$$

For normal atmospheric pressure and room temperature (2.13) can be simplified to:

$$q_v = -\delta \nabla p_v, \tag{2.14}$$

where δ is called the water vapour transmission coefficient.
The vapour pressure p_v can be written as

$$p_v = h p_{vs},$$

where h is the relative humidity and p_{vs} the saturation pressure of water vapour. The relative humidity mainly depends on the moisture content θ_l in the material, while the saturation vapour pressure only depends on the temperature, so that ∇p_v can be written as

$$\nabla p_v = p_{vs}\left(\frac{\partial h}{\partial \theta_l}\right)_T \nabla \theta_l + h \frac{\mathrm{d}p_{vs}}{\mathrm{d}T} \nabla T. \tag{2.15}$$

Combining Eqs. (2.13) and (2.15) for the mass flow density in the vapour phase one finds:

$$q_v/\varrho_l = -D_{\theta v} \nabla \theta_l - D_{Tv} \nabla T, \tag{2.16}$$

with

$$D_{\theta v} = \alpha a D \frac{P}{P-p_v} \frac{M}{RT} \frac{p_{vs}}{\varrho_l} \left(\frac{\partial h}{\partial \theta_l}\right)_T, \tag{2.17}$$

and

$$D_{Tv} = \alpha a D \frac{P}{P-p_v} \frac{M}{RT} \frac{h}{\varrho_l} \frac{\mathrm{d}p_{vs}}{\mathrm{d}T}. \tag{2.18}$$

Combining Eqs. (2.14) and (2.15) we obtain for $D_{\theta v}$ and D_{Tv}

$$D_{\theta v} = \delta \frac{p_{vs}}{\varrho_l} \left(\frac{\partial h}{\partial \theta_l}\right)_T, \tag{2.19}$$

$$D_{Tv} = \delta \frac{h}{\varrho_l} \frac{\mathrm{d}p_{vs}}{\mathrm{d}T}. \tag{2.20}$$

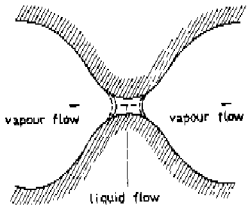

Fig. 2.1
Schematic representation of combined vapour and liquid flow. In the small capillaries liquid flow occurs, in the larger cavities vapour flow.

Here $D_{\theta v}$ represents the diffusivity for vapour transport due to a moisture gradient and D_{Tv} the diffusivity for vapour transport due to a temperature gradient.

A number of workers have done experiments from which data can be derived about the vapour transfer due to a temperature gradient. The measured vapour fluxes are 3 to 10 times higher than those predicted by means of Eqs. (2.18) or (2.20).

Philip and De Vries [9] explained this large value of the vapour transport by considering the following two factors.

a) In fairly moist materials an interaction may be expected between the liquid phase and the vapour phase. As is shown in Fig. 2.1 in such a material the narrow capillaries are filled with liquid, while the larger cavities are filled with air and water vapour. Due to a temperature gradient in the cavities a vapour flux will occur in the direction indicated by the arrows in Fig. 2.1. The resulting condensation at the beginning of the capillary and evaporation at the end, tends to change the curvature of the menisci as given by the dotted lines in Fig. 2.1. This leads to a liquid flow in the capillary in the same direction as the vapour transport. Because the resistance against the liquid flow is negligeable with regard to the resistance against the vapour transport, the diffusion path length will be reduced and the cross section available for vapour diffusion will be enlarged. Now the whole pore volume is available for diffusion except a certain volume of capillaries filled entirely with water, which connect one side of the material with the opposite side.

This influence can be taken into account by replacing αa in Eq. (2.18) by $f(a)$, for which Philip and De Vries propose as a first approximation:

$$\begin{aligned} f(a) &\approx S, && \text{for } \theta_l \leqslant \theta_{lK}\,; \\ f(a) &\approx a + a(S-a)/(S-\theta_{lK}), && \text{for } \theta_l > \theta_{lK}\,. \end{aligned} \tag{2.20a}$$

Here θ_{lK} is a moisture content chosen in such a manner that no liquid continuity exists for $\theta_l < \theta_{lK}$. This is also the moisture content below which the liquid transfer is negligibly small.

b) A second reason for a larger moisture transport is the difference in thermal conductivity between the cavities filled with gas and the rest of the system. Because of the smaller thermal conductivity of cavities filled with gas the temperature gradient

is larger here than in the matrix and the capillaries filled with water. For the same reason the vapour transport in the cavities is also larger than would follow from macroscopic considerations. In the Eqs. (2.18) and (2.20) therefore a factor $(\nabla T)_a/\nabla T$ has to be added, where $(\nabla T)_a$ represents the average temperature gradient in the cavities filled with air and water vapour. The factor $(\nabla T)_a/\nabla T$ for granular materials can be calculated with a method given by De Vries [10].

Taking the two phenomena, mentioned above, into account the diffusion coefficient D_{Tv} can be written as

$$D_{Tv} = \mathrm{f}(a) D \frac{P}{P-p_v} \frac{M}{RT} \frac{h}{\varrho_l} \frac{\mathrm{d}p_{vs}}{\mathrm{d}T} \frac{(\nabla T)_a}{\nabla T}. \tag{2.21}$$

As can be seen from the previous discussion the total moisture transport q can be considered to be composed of a contribution, q_l, in the liquid phase and a contribution, q_v, in the vapour phase. Here we consider as vapour transport, besides the exclusive vapour transport, also the "combined vapour-liquid transport". The total volume flux q/ϱ_l now can be written as

$$q/\varrho_l = q_l/\varrho_l + q_v/\varrho_l = -D_\theta \nabla\theta_l - D_T \nabla T - K g \mathbf{k}, \tag{2.22}$$

where

$$D_\theta = D_{\theta l} + D_{\theta v} \tag{2.23}$$

and

$$D_T = D_{Tl} + D_{Tv}. \tag{2.24}$$

Here D_θ and D_T are the generalized diffusivities for moisture transport due to a moisture gradient or to a temperature gradient respectively.

Throughout this thesis ϱ_l will be considered as a constant. Application of the continuity requirement then leads to:

$$\partial\theta_l/\partial t = -\nabla(q/\varrho_l) = \nabla(D_\theta \nabla\theta_l) + \nabla(D_T \nabla T) + g\partial K/\partial z. \tag{2.25}$$

Here the change of θ_l due to evaporation or condensation inside the pore system has been neglected. More complete equations are given by De Vries [3]. Based on these moisture transport equations De Vries also derived heat transfer equations. For the calculations on roof constructions to be performed later these developments are of minor importance and will be left out of consideration here.

Klute [11] and Philip [12], [13] gave numerical solutions for Eq. (2.25) for isothermal conditions. Philip [14], [15], [16] also developed analytical solutions for horizontal moisture transport, isothermal conditions and certain $D_\theta(\theta_l)$ functions.

2.1.2 *The theory of Krischer*

To describe the moisture transport in porous materials Krischer also considers vapour and liquid transport. The vapour flux, q_v, is written as

$$q_v = -\frac{D}{\mu}\frac{P}{P-p_v}\frac{M}{RT}\nabla p_v. \tag{2.26}$$

The factor μ (>1) in the denominator is called the diffusion resistance factor and describes the decrease of the vapour flow in the considered material in comparison with that in stagnant air. By writing

$$D_1 = D\frac{P}{P-p_v} \qquad \text{and} \qquad \nabla\varrho_v = \frac{M}{RT}\nabla p_v$$

(2.26) changes in

$$q_v = \frac{-D_1}{\mu}\nabla\varrho_v. \tag{2.27}$$

The liquid transport in porous materials is proposed by Krischer to depend only on the moisture gradient, so that the mass flow density in the liquid phase can be written as

$$q_l = -\varkappa\nabla\Gamma_w. \tag{2.28}$$

Here Γ_w represents the moisture content in the material, expressed in kg liquid/m^3 material; $\varkappa$ is called the "Flüssigkeitsleitzahl" and corresponds with the moisture liquid diffusivity $D_{\theta l}$, so that (2.28) can also be written as:

$$q_l = -D_{\theta l}\nabla\Gamma_w = -D_{\theta l}\varrho_l\nabla\theta_l. \tag{2.29}$$

Krischer and Mahler [1], [17] measured this moisture liquid diffusivity for Ytong (a certain manufacture of cellular concrete), where $D_{\theta l}$ proved to be strongly dependent on the moisture content.

Applying the continuity requirement the total moisture transport can be written as:

$$\frac{\partial\theta_l}{\partial t} + S\frac{\partial\varrho_v}{\partial t} = \nabla(D_{\theta l}\nabla\theta_l) + \nabla\left(\frac{D_1}{\mu}\nabla\varrho_v\right). \tag{2.30}$$

Here S is the volume fraction of pores in the material. Krischer also calculated the heat transfer in porous materials, where the heat transfer due to conduction as well as moisture transfer was considered. Assuming a linear relationship between ϱ_v, θ_l and T, and a constant $D_{\theta l}$-value he calculated the moisture transfer for certain drying experiments.

2.1.3 *The theory of Lykow*

While Krischer only allows for vapour tranport due to a vapour gradient and liquid transport due to a moisture gradient, Lykow also considers other moisture transport mechanisms. In connection with the kind of water bond in the material he distinguishes the following kinds of material:

a) capillary porous materials, where the bond is mainly caused by capillary forces;

b) colloidal materials, where the bond is mainly caused by adsorbtion and osmotic forces;

c) capillary porous colloids, where the forces mentioned under a) as well as those mentioned under b) are acting.

Liquid transport occurs as a result of a potential gradient in the material. In colloids, according to Lykow, the adsorbtion and osmotic potentials mainly depend on the moisture content; in capillary porous materials the capillary potential depends on the moisture content as well as on the temperature. So generally the mass flow density q can be presented by the equation:

$$q = -k\varrho_m \nabla u - k\varrho_m \varepsilon \nabla T. \tag{2.31}$$

Here u is the mass fraction of moisture (kg water/kg dry material), ϱ_m the density of the dry material, k is called the "Potential-leitfähigkeit" (corresponding with $D_{\theta l}$) and ε the temperature gradient factor, which is very small for colloids.

The liquid transport in capillary porous materials due to a temperature gradient is, according to Lykow, enlarged by air enclosures in the pores. These enclosures have a smaller volume at lower than at higher temperatures, so that the liquid transport towards the cold side is enlarged (see [2], p. 69).

At constant gas pressure vapour transport in porous materials occurs by diffusion as a result of a vapour pressure gradient. This is the case as long as the mean free path length is small in comparison with the pore diameter (so-called "macro-pores", $r > 10^{-5}$ m). In small pores ($r < 10^{-5}$ m) slip phenomena and Knudsen flow must be taken into consideration (see also Section 4.1.2). In the way discussed in Section 2.1.1 this vapour transport can be split up in two components, one due to the moisture gradient and one due to the temperature gradient. So the vapour flux density can also be described by the general equation (2.31).

Lykow derived equations for the generalized diffusion coefficients k and ε for capillary porous materials ([2], Eqs. 2.41 and 2.43), for colloidal materials ([2], Eqs. 2.50 and 2.59) and for capillary porous colloids ([2], Eqs. 2.61 and 2.62).

Next to the transport mechanisms already discussed Lykow mentions the "thermal slip", by which in capillaries filled with gas or water when an axial temperature gradient is present, a thin layer near the wall moves from the cold to the warm side, thus in a direction opposite to that of the heat flux. This effect is caused by the larger momentum transfer to the capillary wall by molecules coming from the warm side as compared with those coming from the cold side. As a reaction, macroscopically

seen, the particle flux with respect to the wall is in the direction of the temperature gradient. In narrow capillaries filled with gas this effect can be comparable with the vapour diffusion due to a vapour pressure gradient ([2], p. 39). In capillaries filled with liquid this effect is of minor importance and only noticeable in micropores ([2], p. 67).

Another transport mechanism is thermal-diffusion, by which in an air-water-vapour-mixture the heavier air molecules diffuse in the direction of the heat flux and the lighter water vapour molecules in the opposite direction. However, this effect is of minor importance and can be neglected in comparison to the contributions discussed previously.

As was discussed before the total moisture transport can be described by Eq. (2.31). With this equation Lykow calculated the moisture transport introducing a number of dimensionless quantities. In later publications [18] he developed equations based on the principles of irreversible thermodynamics.

2.2 Methods for calculating the moisture transport in roof constructions

2.2.1 *Method of Glaser*

A graphical method to predict the occurrence of condensation in building constructions was – to the author's knowledge – first presented by Rowley, Algren and Lund [19] and later on applied in practice by Johansson and Persson [20], Egner [21], Cammerer and Dürhammer [22]. Schäcke and Schüle [23] attempted to calculate the amount of water condensing in a construction. However, their results were not very satisfactory. Glaser [4] extended their method in a more logical way.

In order to apply Glaser's calculation method the liquid transfer in the construction must be small in comparison with the vapour transfer. Though this condition is not satisfied for most building materials, this method is in fairly widespread use, especially in the German speaking countries cf. [24] to [28]. The method will be explained considering a cellular concrete roof, covered with roofing material, schematically shown in Fig. 2.2.

We suppose the roof to be exposed to stationary winter conditions i.e. a high external relative humidity and a low external temperature, T_e, and a low internal relative humidity combined with a high internal temperature, T_i. The internal vapour

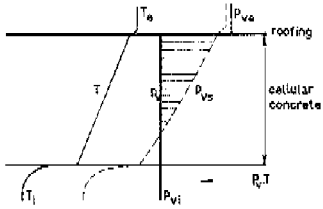

Fig. 2.2
The vapour pressure, p_v; the saturation vapour pressure, p_{vs}; and the temperature, T, in a roof of cellular concrete for winter conditions. In the hatched part condensation might be expected.

pressure is indicated by p_{vi}, the external one by p_{ve}. The vapour pressure distribution in the roof can be derived by dividing the difference in vapour pressure $p_{vi}-p_{ve}$ over the vapour diffusion resistances Z_1 of the layer of cellular concrete and Z_2 of the roofing. Because the roofing has a very great resistance against vapour diffusion, the vapour pressure difference establishes itself almost completely over the roofing and the vapour pressure in the cellular concrete is practically equal to p_{vi}, as is shown in Fig. 2.2. The saturation vapour pressure, p_{vs}, in the roof can be derived from the temperature profile, which is mainly influenced by the heat transfer resistances in the air on both sides of the roof and the heat resistance of the layer of cellular concrete. p_{vs} is shown by the dotted line in Fig. 2.2. In the upper part of the roof the vapour pressure is higher than the saturation vapour pressure, so that in this part of the construction, hatched in Fig. 2.2., condensation can be expected.

To calculate the amount of condensed vapour Glaser [4] plotted the vapour pressure on a transformed thickness scale Z, which has been chosen proportional to the diffusion resistances of the materials, as is done in Fig. 2.3. Because the vapour pressure cannot be higher than the saturation vapour pressure, at first sight a trend of the vapour pressure would be expected as given by the curve A-B-C-D-E.

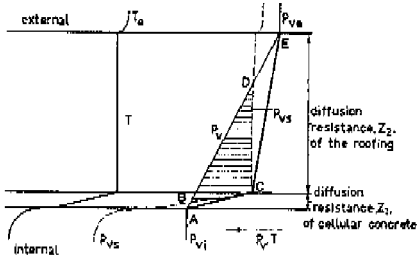

Fig. 2.3
The vapour pressure, p_v; the saturation pressure, p_{vs}; and the temperature, T, in a roof of cellular concrete, plotted as a function of a transformed thickness scale, Z, according to Glaser's method for winter conditions.

For the vapour flux density one has $q_v = \mathrm{d}p_v/\mathrm{d}Z$, where Z is the diffusion resistance. Consequently the slope of the vapour pressure curve in Fig. 2.3 represents the local vapour flux density. This implies that from A to B the vapour flux would be smaller than from B to C. This, however is not possible because a moisture flux can only be constant or decreasing in the direction of transport, at least in the absence of a moisture source. Therefore Glaser concluded that a vapour pressure distribution must be expected as is given by the curve A-C-E. Because the vapour flux density q_{v1} in the zone A-C is larger than the vapour flux density q_{v2} in zone C-E, at C part of the vapour condenses.

The mass of condensed vapour per unit of time and unit of area is given by:

$$q = q_{v1} - q_{v2} = \frac{p_{vA} - p_{vC}}{Z_1} - \frac{p_{vC} - p_{vE}}{Z_2}, \tag{2.32}$$

where p_{vA}, p_{vC} and p_{vE} represent the vapour pressures at A, C and E.

Because $Z_2 \gg Z_1$, Eq. (2.32) can be simplified to:

$$q \approx q_{v1} = \frac{p_{vA} - p_{vC}}{Z_1} = \frac{p_{vi} - p_{vsr}}{Z_1}. \tag{2.33}$$

Here p_{vsr} is the saturated vapour pressure just underneath the roofing.

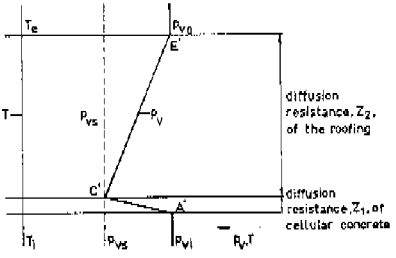

Fig. 2.4
The vapour pressure, p; the saturation pressure, p_{vs}; and the temperature, T, in a roof of cellular concrete, plotted as a function of a transformed thickness scale, Z, according to Glaser's method for summer conditions.

In Fig. 2.4 the vapour pressure curves for the same roof are given for summer conditions, assuming that, just underneath the roofing, there is liquid water in the construction, so that here the vapour pressure is equal to the saturation vapour pressure. The internal and external temperatures and relative humidities are now assumed to be equal. As a consequence of the assumed vapour pressure curve the roof will lose water for the conditions considered here. For the drying rate, q', per unit of area one has:

$$q' = \frac{p_{vC'} - p_{vA'}}{Z_1} + \frac{p_{vC'} - p_{vE'}}{Z_2} \approx \frac{p_{vsr} - p_{vi}}{Z_1}. \tag{2.34}$$

Thus both for winter and summer conditions the rate of moisture change can be calculated from Eq. (2.33).

This result could also have been obtained directly by considering the fact, that the difference in vapour pressure establishes itself mainly over the roofing and the difference in saturation vapour pressure mainly over the layer of cellular concrete, while under the roofing saturation occurs. However, Glaser's method has been discussed at length since, because of its simplicity, it is advantageous to use, especially for complicated constructions.

This for instance can be illustrated by considering the cellular concrete roof for the experimental conditions $T = 23\ ^\circ\text{C}$, $h = 70\%$ internally and $T = 0\ ^\circ\text{C}$ externally. The vapour pressure distribution for these conditions is shown in Fig. 2.5, from which it can be derived that the rate of moisture increase is somewhat larger than would follow from Eq. 2.33, because "tangent condensation" occurs.

Fig. 2.5
The vapour pressure in a roof of cellular concrete (10 cm thick) exposed to the winter conditions: $T_i = 23°C$, $h_i \sim 70\%$, $T_o = 0°C$, according to Glaser's method. Due to "tangent-condensation" the rate of moisture increase is somewhat larger than would follow from Eq. 2.33.

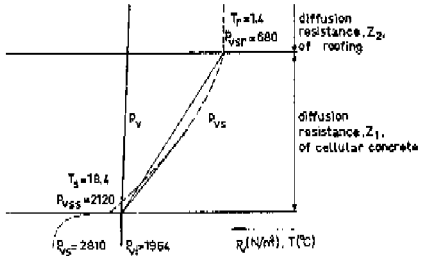

By the method discussed previously the moisture change of a 10 cm thick cellular concrete roof has been calculated for the following winter and summer conditions:

	internal			external
conditions	T(°C)	h(%)	p_i (N/m²)	T(°C)
winter conditions	23	60	1683	0
	23	70	1964	0
summer conditions	23	60	1683	23

The calculations have been based on the following values for the physical parameters (to be discussed in Chapter 3):

vapour diffusion resistance of 10 cm of cellular concrete: $Z_1 = 4.65 \cdot 10^9$ m/s
thermal conductivity of cellular concrete: $\lambda = 0.21$ W/m °C
vapour diffusion resistance of the roofing: $Z_2 = 100 \cdot 10^9$ m/s
heat transfer resistance, internal: 0.129 m² °C/W
heat transfer resistance, external: 0.043 m² °C/W

For the winter conditions considered here the temperature just beneath the roofing $T_r = 1.4°C$, the corresponding saturation pressure $p_{vsr} = 680$ N/m²; for the summer conditions considered here $T_r = 23°C$ and $p_{vsr} = 2806$ N/m². From Eq. (2.33) rates of moisture change are calculated, presented in Table 2.1.

Table 2.1 Rate of moisture change calculated with Glaser's method.

	internal		external	
conditions	T(°C)	h(%)	T(°C)	rate of moisture change
winter conditions	23	60	0	increase: $21 \cdot 10^{-8}$ kg/m²s ≙ 0.54 vol.%/month
winter conditions	23	70	0	increase: $27 \cdot 10^{-8}$ kg/m²s ≙ 0.70 vol.%/month
winter conditions	23	70	0	increase: $31.5 \cdot 10^{-8}$ kg/m²s ≙ 0.81 vol.%/month (from Fig. 2.5 as a result of "tangent condensation")
summer conditions	23	60	23	decrease: $25 \cdot 10^{-8}$ kg/m²s ≙ 0.65 vol.%/month

2.2.2 *Application of Philip and De Vries' theory for the calculation of the moisture transport in roof constructions*

To consider also the influence of liquid transport and combined vapour-liquid transport we tried to calculate the moisture transport in building constructions using Philip and De Vries' theory. For this purpose we consider again the cellular concrete roof discussed previously, with the moisture distribution shown schematically in Fig. 2.6.

The moisture flux density in the cellular concrete is described by:

$$q/\varrho_l = -D_\theta(\partial\theta_l/\partial z) - D_T(\partial T/\partial z). \tag{2.35}$$

This equation can be derived from (2.22) by remembering that in the case considered here we have only to allow for the moisture transport in the vertical z-direction, while for the moisture contents to be expected in the roof construction, the influence of gravity can be neglected.

Initially we suppose the roof to have a uniform moisture content, equal to the hygroscopic moisture content, θ_{l0}, corresponding to the relative humidity of the air underneath the roof. Therefore the moisture gradient $\partial\theta_l/\partial z = 0$ and so Eq. (2.35) reduces to

$$q/\varrho_l = -D_T(\partial T/\partial z). \tag{2.36}$$

During the winter period a temperature gradient exists in the roof, which causes a moisture transport in an upward direction, described by the term $-D_T(\partial T/\partial z)$. Consequently the moisture content under the roofing rises in the course of time as is schematically shown in Fig. 2.6 by the curve marked θ_{l1}. In this case the moisture gradient no longer equals zero and so a second contribution to the moisture transport in a downward direction arises, described by the term $-D_\theta(\partial\theta_l/\partial z)$. As the moisture content under the roofing rises, also this "inverse current" increases, till finally a stationary state will be attained represented by the curve marked θ_{l2}, at which both contributions to the moisture transport will be equal and the moisture increase in the roof will stop. Then one has:

$$-D_\theta(\partial\theta_l/\partial z) - D_T(\partial T/\partial z) = 0. \tag{2.37}$$

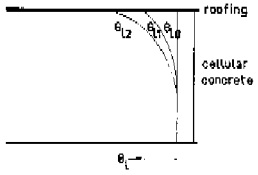

Fig. 2.6
Schematic presentation of the moisture distribution in a roof of cellular concrete.

In practice this stationary state will often not be reached, because of the change from winter to summer conditions. In the summer period the temperature gradient in the roof is smaller than in winter, and so the contribution to the moisture transport downwards, due to the temperature gradient, is also smaller than in the winter period, which results in a decrease of the moisture content in the roof.

It will be clear from the previous discussion that in due course the moisture content in the roof will vary round an average value, being at its highest at the end of winter and at its lowest at the end of the summer period.

To calculate the moisture transport in the roof we must know the following physical properties of the roof material:

- the diffusivities D_ϕ and D_T as functions of the moisture content and the temperature;
- the hygroscopic moisture content as a function of the relative humidity;
- the thermal conductivity as a function of the moisture content.

The determination of these properties will be dealt with in Chapter 3. Using the results given there the following data have been obtained in a simple way:

a) the initial increase of moisture content in a roof under winter conditions starting from a uniform moisture distribution;

b) the moisture distribution in a roof in the stationary state, where the contributions to the moisture transport due to a temperature gradient and due to a moisture gradient do balance under winter conditions.

a) Calculation of the initial rate of moisture increase in the roof under consideration

Assuming that initially everywhere in the roof the moisture content is equal to the hygroscopic moisture content, θ_h, the moisture transport can be calculated from Eq. (2.36). The appropriate D_T-value can be found as follows. First we calculate the temperature T_s at the bottom side of the roof, using the data given in Section 2.2.1.

From the saturated vapour pressure p_{oss} corresponding with this temperature and from the inside vapour pressure p_i, the relative humidity h of the internal air adjacent to the roof follows. The corresponding hygroscopic moisture content θ_h can then be derived from Fig. 3.7, the required D_T-value follows from Fig. 6.1. The results of the calculation are given in Table 2.2.

A comparison with the results presented in Table 2.1 shows that the rates of moisture increase calculated from Philip and De Vries' theory are considerably higher than those calculated with Glaser's method, especially for climatic conditions with a high internal relative humidity. In Section 6.2 this point will be discussed in more detail.

b) Calculation of the moisture distribution in a roof in the stationary state

As we have seen before in the stationary state the moisture transport is described by

Table 2.2 Calculation of the rate of moisture increase for winter conditions, using Philip and De Vries' theory.

	internal	$T = 23$ °C, $h = 60\%$	$T = 23$ °C, $h = 70\%$
conditions	external	$T = 0$ °C	$T = 0$ °C
internal vapour pressure, p_i		1683 N/m²	1964 N/m²
temperature, T_s, at the bottom side of the roof		18.4 °C	18.4 °C
saturation vapour pressure, $p_{v,sat}$, corresponding with T_s		2120 N/m²	2120 N/m²
relative humidity, h		80%	93%
hygroscopic moisture content, θ_h		0.025	0.045
diffusivity, D_T		$1.83 \cdot 10^{-12}$ m²/s °C	$4.17 \cdot 10^{-12}$ m²/s °C
temperature gradient, $\partial T/\partial z$		168 °C/m	168 °C/m
rate of moisture increase		0.8 vol.%/month	1.8 vol.%/month

Eq. (2.37). When we introduce the temperature gradient factor $\varepsilon = D_T/D_\theta$ (see Section 2.1.2), this equation becomes:

$$\partial\theta_l/\partial z = \varepsilon(\partial T/\partial z). \tag{2.38}$$

The quantity ε is known from measurements (see Section 3.7), the temperature gradient in the roof $\partial T/\partial z$ is also known, and so the stationary moisture distribution in the roof can be calculated by a simple stepwize procedure. For this purpose we divide the roof in horizontal layers with a thickness Δz (see Fig. 2.7). The moisture content θ_{l0} at the bottom of the roof ($z = 0$) can be calculated in the same way as presented under a). Using the ε-value for θ_{l0} the difference in moisture content $\Delta\theta_{l1}$ over layer 1 can be calculated from Eq. (2.38), and the moisture content at $z = \Delta z$ becomes $\theta_{l0} + \Delta\theta_{l1}$. In the same way the moisture content at $z = n\Delta z$ ($n = 2, 3, \ldots$) can be calculated. We have to remember that the fore-going calculations were based on an initially uniform moisture distribution and consequently on a uniform temperature gradient in the roof. More exact results can be obtained by applying an itteration procedure, in such a way that for each step the temperature gradient in the roof is based on the moisture distribution that was calculated for the previous step in the procedure.

The calculations have been performed for the winter conditions mentioned in Section 2.2.1 and the results are presented in Table 2.3. The calculations for the inter-

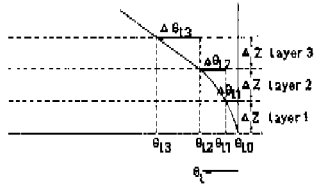

Fig. 2.7
Stepwise calculation of the stationary moisture distribution in a roof exposed to winter conditions, using a simplified calculation procedure.

Table 2.3 Calculation of the moisture distribution at the stationary state for winter conditions.

conditions: internal $T = 23\,°C$, $h = 0.60$; external $T = 0\,°C$

first step					second step				
z (cm)	θ_l (%)	ε ($°C^{-1}$)	$\partial T/\partial z$ (°C/m)	$\Delta\theta_l$ (%)	λ (W/m°C)	$\partial T/\partial z$ (°C/m)	θ_l (%)	ε ($°C^{-1}$)	$\Delta\theta_l$ (%)
0	2.50	$4.6\cdot10^{-3}$	168	0.77	0.22	205	3.1	$6.7\cdot10^{-3}$	1.37
1	3.27	$7.5\cdot10^{-3}$	168	1.26	0.22	205	4.47	$1.2\cdot10^{-2}$	2.46
2	4.53	$1.2\cdot10^{-2}$	168	2.02	0.24	190	6.93	$1.65\cdot10^{-2}$	3.13
3	6.55	$1.6\cdot10^{-2}$	168	2.68	0.26	177	10.06	$1.6\cdot10^{-2}$	2.83
4	9.23	$1.7\cdot10^{-2}$	168	2.85	0.29	158	12.89	$1.3\cdot10^{-2}$	2.05
5	12.08	$1.45\cdot10^{-2}$	168	2.43	0.33	140	14.94	$1.06\cdot10^{-2}$	1.48
6	14.51	$1.1\cdot10^{-2}$	168	1.85	0.35	131	16.42	$8.7\cdot10^{-3}$	1.14
7	16.36	$9\cdot10^{-3}$	168	1.51	0.38	121	17.56	$7.8\cdot10^{-3}$	0.94
8	17.87	$7.5\cdot10^{-3}$	168	1.26	0.39	116	18.50	$6.7\cdot10^{-3}$	0.77
9	19.13	$6\cdot10^{-3}$	168	1.0	0.41	112	19.27	$6\cdot10^{-3}$	0.67
10	20.13				0.42	110	19.94		

conditions: internal $T = 23\,°C$, $h = 0.70$; external $T = 0\,°C$

z (cm)	θ_l (%)	ε ($°C^{-1}$)	$\partial T/\partial z$ (°C/m)	$\Delta\theta_l$ (%)
0	4.50	$1.2\cdot10^{-2}$	168	2.02
1	6.52	$1.6\cdot10^{-2}$	168	2.68
2	9.20	$1.7\cdot10^{-2}$	168	2.85
3	12.05	$1.45\cdot10^{-2}$	168	2.45
4	14.50	$1.1\cdot10^{-2}$	168	1.85
5	16.35	$1\cdot10^{-2}$	168	1.51
6	17.86	$9\cdot10^{-3}$	168	1.26
7	19.12	$7.5\cdot10^{-3}$	168	1.01
8	20.13	$6\cdot10^{-3}$	168	0.89
9	21.02	$5.3\cdot10^{-3}$	168	0.77
10	21.79	$4.6\cdot10^{-3}$		

nal conditions $T = 23\,°C$, $h = 0.60$ have been performed in two steps, the calculations for the internal conditions $T = 23\,°C$, $h = 0.70$ have been stopped after one step, because from the moisture distribution calculated in the first step a surface temperature T_s followed lower than the dewpoint temperature of the inside air, so that condensation against the bottom side of the roof would occur. Consequently no stationary state should be possible for these conditions.

References

1. O. Krischer, Die wissenschaftlichen Grundlagen der Trocknungstechnik, Springer Verlag, Berlin, (1963).
2. A. W. Lykow, Transporterscheinungen in kapillarporösen Körpern, Akademie Verlag, Berlin, (1958).
3. D. A. de Vries, De Ingenieur, 74, 0 45–53, (1962).
4. H. Glaser, Kältetechnik 11, 345–349, (1959).

5. H. P. G. Darcy, Les fontaines publiques de la ville de Dijon, Victor Delmont, Paris, (1856).
6. G. H. Bolt, A. R. P. Janse, F. F. R. Koenigs, Algemene bodemkunde, deel II Bodemnatuurkunde, Landbouwhogeschool Wageningen, (1965).
7. S. R. de Groot, P. Mazur, Non-equilibrium thermodynamics, North-Holland Publ. Cy., Amsterdam, (1962).
8. D. A. de Vries, A. J. Kruger, On the value of the diffusion coefficient of water vapour in air, Colloq. Int. du Cent. Nat. Rech. Sc., (1966).
9. J. R. Philip, D. A. de Vries, Trans. Am. Geoph. Union, **38**, 222–232, (1957).
10. D. A. de Vries, Het warmtegeleidingsvermogen van grond, Meded. Landbouwhogeschool Wageningen, **52**, 1–73, (1952).
11. A. Klute, Soil Sci., **73**, 105–116, (1952).
12. J. R. Philip, Trans. Faraday Soc., **51**, 885–892, (1955).
13. J. R. Philip, Austral. J. Phys., **10**, 29–42, (1957).
14. J. R. Philip, Austral. J. Phys., **13**, 1–12, (1960).
15. J. R. Philip, Soil Sci., **83**, 345–357, 435–448, (1957); **84**, 163–178, 257–264, 329–339, (1957); **85**, 278–286, 333 337, (1958).
16. J. R. Philip, Austral. J. Phys., **14**, 1–13, (1961).
17. O. Krischer, K. Mahler, Ueber die Bestimmung des Diffusionswiderstandes und der kapillaren Flüssigkeitsleitzahl aus stationären und instationären Vorgängen, V.D.I.-Forschungsheft 473, (1959).
18. A. W. Lykow, Y. A. Mikhailow, Theory of heat and mass transfer, S. Monson, Jerusalem, (1965).
19. F. B. Rowley, A. B. Algren, Cl. E. Lund, Methods of moisture control and their application to building construction, University of Minnesota, bull. nr. 17, (1940).
20. C. H. Johansson, G. Persson, Teknisk Tidskrift, **79**, 75, (1949).
21. K. Egner, Feuchtigkeitsdurchgang und Wasserdampfcondensation in Bauten, Fortschritte und Forschungen im Bauwesen, (1950).
22. W. F. Cammerer, W. Dürhammer, Ges. Ing. **71**, 310, (1950).
23. H. Schäcke, Die Durchfeuchtung von Baustoffen und Bauteilen auf Grund des Diffusionsvorganges und ihre rechnerische Abschätzung, Bericht der Forschungsgemeinschaft Bauen und Wohnen, Stuttgart, (1952).
24. J. S. Cammerer, W. Schüle, O. Krischer, Ber. Bauforschung, Heft 23, (1962).
25. W. Caemmerer, Berechnung der Wasserdampfdurchlässigkeit und Bemessung des Feuchtigkeitsschutzes von Bauteilen, Ber. Bauforschung, Heft 51, 55–77, (1968).
26. J. S. Cammerer, Auswertung von Untersuchungen auf dem Gebiet des Wärmeschutzes bei Versuchs- und Vergleichsbauten, Ber. Bauforschung, Heft 40 (1964).
27. K. Moritz, Flachdachhandbuch, Bauverlag G.m.b.H., Wiesbaden-Berlin (1961).
28. J. Fehér, Ges. Ing., **90**, 123, (1969).
29. G. H. Bolt, De Ingenieur, **74**, 0 59, (1962).

Chapter 3

EXPERIMENTAL DETERMINATIONS OF THE STRUCTURE AND THE PROPERTIES OF CELLULAR CONCRETE

3.1 Structure of cellular concrete

Three different types of cellular concrete (trade names Durox (ϱ = 700 kg/m^3), Ytong (ϱ = 680 kg/m^3), Siporex (ϱ = 650 kg/m^3)) have been investigated. They generally are manufactured from the following principal ingredients:

a) a raw material containing quartz i.e. sand, furnace slags, slate;
b) a raw material containing lime i.e. lime and cement.

Mostly lime as well as cement is used. The mutual proportions rather vary depending upon the fabricate. Also a small amount of aluminium powder is added which reacts with the lime and the water. In this reaction hydrogen is formed which is the cause of cell-formation in the material.

As is shown in Fig. 3.1 a very porous material is obtained with rather large cavities of the size of about 1 mm, which are the cause of a comparatively low heat conductivity. Fig. 3.2 shows the structure of cellular concrete enlarged about 100 times. For this purpose a sample of cellular concrete is embedded in an artificial resin and next ground and polished on one side. The cavities initially filled with air now are filled with artificial resin.

Visible are:

- the cavities, recognizable by the grind streaks in the artificial resin;
- the sand grains, recognizable by the shadowed edges caused by the rising above the smooth surface of the harder sand grains;
- the "sponge material", consisting of a cement-lime mass, which provides for the mutual connection in the cellular concrete.

This sponge-material is shown in the Figs. 3.3 and 3.4 enlarged 3500 times respectively 15000 times. The fine pores in this material have been made visible with an electron microscope by preparing, by means of a special technique, slices of about 0.1 μm thick, through which the electron beams of the electron microscope passed.

The cement-lime mass seems, according to these figures, to exist of areas, mainly composed of very fine needle shaped cristals with a thickness of about 0.01 μm, and of areas with cristals of the size of about 1 μm. The space between these cristals forms the pore structure which mainly determines the moisture transport to be discussed in Chapter 4. A more thorough description of the pore structure and the composition of this material is given in [1].

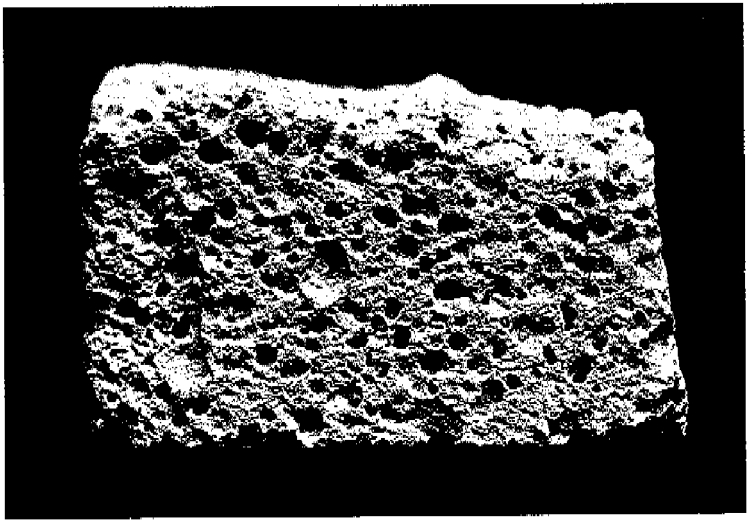

Fig. 3.1 Surface of fracture of cellular concrete (magnification 3×).

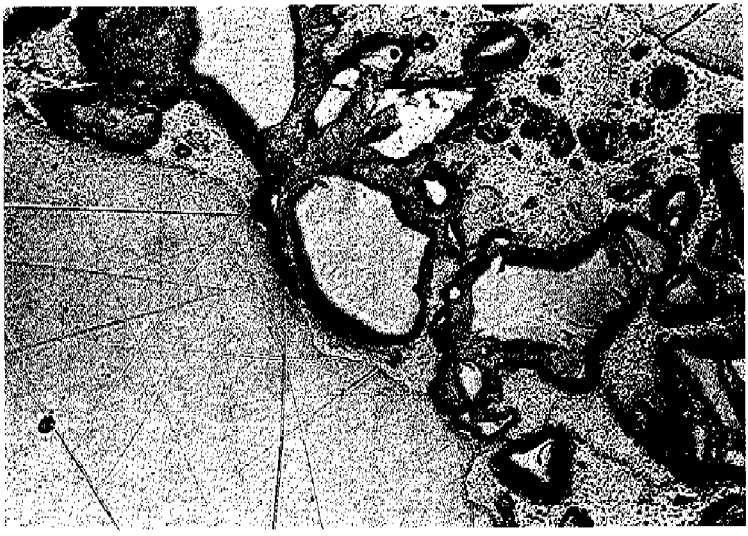

Fig. 3.2 Microscopical photograph of cellular concrete, embedded in artificial resin (striking light, magnification 100×).

Visible are:
- parts of air cavities, now filled with artificial resin and recognizable by grinding streaks,
- sand grains, recognizable by shadowed edges and
- porous cement-lime mass, called "sponge material" here

Fig. 3.3 Electron microscopic exposure of cement-lime mass in cellular concrete (magnification 3500×), obtained by passing the electron beams through a coupe with a thickness of about 100 nm. Visible are crystals with a size of about 1 μm and rather randomly dispersed.

In a planimetric way from these and similar figures the following volume fractions of the composing components and pores have been derived:

40% air-filled cavities,
15% sand grains and
45% sponge material (consisting of 15% solid substance and 30% pore volume).

3.2 Measurements of the suction pressure, ψ_m

To measure the relation between the suction pressure and the moisture content [2], [3], a sample of the material to be examined is brought in contact with water of a known pressure. When the equilibrium state is reached, the moisture pressure in the material is equal to this pressure.

Depending on the amount of the suction pressure the measurements have been carried out as follows:*

* The measurements have been carried out at the Laboratory of Soils and Fertilizers, State Agricultural University, Wageningen.

Fig. 3.4 Electron microscopic exposure of cement-lime mass in cellular concrete (magnification 15000×), obtained by passing the electron beams through a coupe the thickness of about 100 nm. Apart from the crystals, visible in Fig. 3.3 also needle-shaped crystals with a thickness of about 0.01 μm occur, which are arranged more or less parallel.

a) At a suction pressure between 0 and 1 atmosphere by bringing water under suction. For this purpose samples of the materials to be investigated were contacted with a sand bath, in which a suction pressure of 10 cm or 100 cm water column was adjusted. The experiments were started from dry samples to get results for increasing water content; for decreasing water content the experiments were started from samples fully saturated. The moisture content of the sample was determined after 1 week.
b) At a suction pressure higher than 1 atmosphere by bringing the water under pressure. For this purpose the samples were put into special membrane presses, after which at a pressure difference of 1 atmosphere, respectively 16 atmosphere across the membrane water was removed from the samples. The remaining moisture content in the samples was determined after about 1 week.
c) At very high suction pressures by bringing the samples in equilibrium with an environment of known relative humidity. In the experiments discussed here the samples were placed in a desiccator partly filled with a saturated NaCl solution. The equivalent suction pressure in this case amounted to about 500 atmosphere.

Fig. 3.5
Suction pressure, w_m, of cellular concrete as a function of the moisture content, θ_l (measurements have been performed at the Laboratory of Soils and Fertilizers, State Agricultural University, Wageningen).

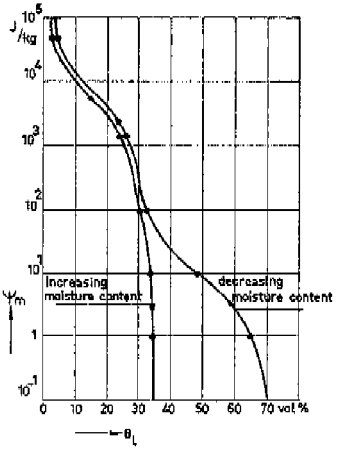

The relation between the suction pressure and the moisture content, determined in this way is given in Fig. 3.5 for Durox for increasing as well as for decreasing moisture content. At moisture contents higher than about 30 vol.% a large hysteresis is found which is mainly caused by air enclosures. This can be illustrated by the following experiment.

We put several samples of cellular concrete with a volume of about 1 cm^3 under water and regularly determined the moisture increase by weighing. Directly after immersion the volumetric moisture content increased rapidly, i.e. in several minutes, up to 25 or 30%. The further increase of the moisture content occurred very slowly; only after six months the final volumetric moisture content of about 75% was reached. This slow moisture increase is caused by the fact that after immersion the fine capillaries in the sponge-material fill themselves with water first, while the bigger cavities still remain filled with air. After some time the sponge-material is completely filled with water (corresponding with a volumetric moisture content of about 30%), so that the air from the bigger cavities cannot escape any more. As is shown by the experiment the moisture content in the material gradually increases further. This is made possible because the air dissolves into the water, so that the larger cavities can also be filled. The hysteresis considered in this region of moisture contents therefore turns out to be dependent upon time and to disappear in the long run.

Some experiments discussed before were started with samples of cellular concrete fully saturated with water. These samples were obtained by placing them under water level in a desiccator, after which the space above the water surface was evacuated and brought up to normal atmospheric pressure again several times. In this way the larger cavities could fill themselves with water.

3.3 Measurements of the transmission coefficient for water vapour, δ

As is seen in Section 2.1.3 the equation of vapour diffusion in a porous material may be written as

$$q_v = -\delta \nabla p_v . \tag{2.14}$$

To determine the vapour transmission coefficient, δ, a layer of cellular concrete was sealed on a dish, partly filled with a desiccant (see Fig. 3.6). The assembly was placed in an atmosphere of high relative humidity (95%) and a temperature of 23 °C. The vapour flux q_v in Eq. (2.14) next was determined from the weight gain of the assembly; the gradient of the vapour pressure ∇p_v was known from the conditions in- and outside the dish and so the vapour transmission coefficient could be calculated. A more detailed description of this measuring method is given in [4]. In this way for all types of cellular concrete investigated we found $\delta \approx 2.1 \cdot 10^{-11}$ s.

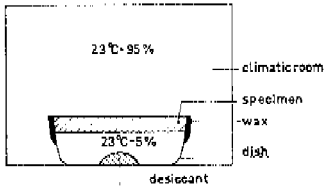

Fig. 3.6
Measurement of the water vapour transmission coefficient, δ.

δ is dependent on the temperature because it is proportional to the term DM/RT (see Eq. (2.13)). Here D is the diffusion coefficient of water vapour in air, for which De Vries and Kruger [5] proposed:

$$D = 2.17 \cdot 10^{-5} \left(\frac{p_0}{p} \right) \left(\frac{T}{T_0} \right)^{1.88} \text{m}^2/\text{s} . \tag{3.1}$$

δ depends also on the moisture content in the material. Wissmann [6] determined for several building materials the μ-value which is inversely proportional to δ (see Section 2.1.2). He carried out these measurements for different values of the vapour pressure difference over the material and consequently also for different values of the hygroscopic moisture content. For Siporex ($\varrho = 760$ kg/m^3) and Ytong ($\varrho = 630$ kg/m^3) he found μ-values varying from $\mu = 11$ (for a low moisture content) to $\mu = 5$ (for a high moisture content), corresponding with δ-values of respectively $\delta = 1.6 \cdot 10^{-11}$ s and $\delta = 3.6 \cdot 10^{-11}$ s.

3.4 Measurements of the hygroscopic moisture content, θ_h

For porous materials a connection exists between the moisture content in the material

and the relative humidity, h, of the surrounding air. At low relative humidities the hygroscopic moisture content is mainly caused by physical adsorption of water molecules by the wall of the capillaries in the material, at higher relative humidities the dominant water binding process is capillarity which is connected with a decrease of the vapour pressure above a curved water surface. The relation between the decrease of the vapour tension and the radius of a circular capillary may be expressed by Thomson's law ([7] p. 15):

$$\frac{p_v}{p_{vs}} = \exp\left[-\frac{2M\sigma}{\varrho_l RTr}\right], \tag{3.2}$$

where r is the radius of the capillary.

The hygroscopic moisture content as a function of the relative humidity can be found by placing a sample of the material into an atmosphere with a constant relative humidity, the moisture content in the material being determined by weighing. In the investigations considered here samples of cellular concrete of about 1 cm^3 in volume were placed into several desiccators in each of which a constant relative humidity was obtained by means of a saturated salt solution.

The following salt solutions were used [8, 9]:

solid phase	h (%)
$Pb(NO_3)_2$	98
$NH_4H_2PO_4$	93
$(NH_4)_2SO_4$	81
NH_4NO_3	67
$NaBr \cdot 2H_2O$	58
$MgCl_2 \cdot 6H_2O$	33

The initial moisture content varied from 0 to 30 vol.%. In all cases the equilibrium state was reached within three weeks. For Durox the course of the hygroscopic mois-

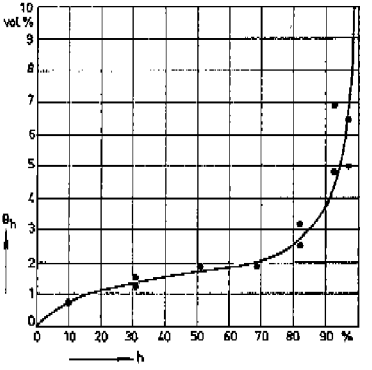

Fig. 3.7
Hygroscopic moisture content, θ_h, of cellular concrete as a function of the relative humidity, h.

ture content is given in Fig. 3.7. The differences for experiments with increasing respectively decreasing moisture contents are only small.

3.5 Measurements of the thermal conductivity, λ

The relation between the thermal conductivity λ and the moisture content θ_l has been determined for several types of cellular concrete by means of the cylindrical probe method. This method was first suggested by Schleiermacher [10] and independently by Stålhane and Pyk [11].

The method was used for measuring the thermal conductivity of liquids [12–17], soils [18–28], insulating materials [29–32] and gases [33–35]. A survey of the probes used by various investigators is given by De Vries and Peck [36].

These measurements for the greater part have been carried out by using cylindrical needle-shaped probes, which contain as a heat source a thin metal wire, heated electrically. The temperature near the centre is measured by means of a thermocouple, or by a resistance method. In its simplest form only a single heating wire is used. The measurements are carried out by switching on the electrical current and measuring the temperature rise, which is related to the thermal properties of the surrounding material.

With certain simplifications the following equation can be derived for the thermal conductivity of the material:

$$\lambda = \frac{q'}{4\pi} \frac{\ln (\tau_2/\tau_1)}{t_2 - t_1} \tag{3.3}$$

where λ is the heat conductivity, q' the energy produced in the heating wire per unit of length and t_1, t_2 the temperatures measured at times τ_1, τ_2 respectively.

The measurements on cellular concrete described here have been performed with a needle-shaped probe of own construction, which is shown in Fig. 3.8. In a sample of the material a hole was bored, that fitted the probe tight enough to assure a good thermal contact between the probe and the material. The results for Durox are given in Fig. 3.9 for several moisture contents. Other measurements on cellular concrete have been carried out by Jespersen [37], using a guarded hot plate apparatus in which the moist materials were exposed to a stationary temperature difference.

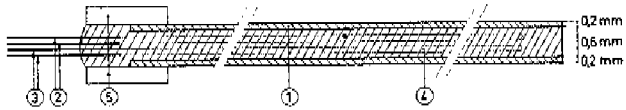

Fig. 3.8 Cross section of probe, used for the measurements of the thermal conductivity. 1. capillary of stainless steel; 2. Fe-Co thermocouple (⌀ 60 μm); 3. heating wire of constantan (⌀ 40 μm); 4. araldite; 5. perspex.

Fig. 3.9
Thermal conductivity, λ, of cellular concrete as a function of the moisture content, θ_l.

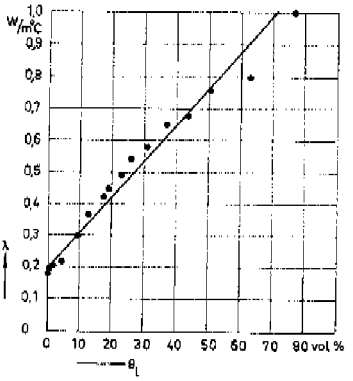

3.6 Measurements of the moisture diffusivity, D_θ

The diffusivity D_θ (diffusivity for moisture transfer due to a moisture gradient) as a function of the moisture content θ_l has been determined by two different methods, viz.

a) by means of drying experiments,
b) by means of a stationary moisture flux.

3.6.1 *Measurements of D_θ by means of drying experiments*

In this method the course of the diffusivity D_θ was determined during drying from the moisture distributions in samples of cellular concrete with sizes of 10 cm × 5 cm × 5 cm. First these samples were fully filled with water and next provided with a vapour-tight layer all along the outside surface, except for one side with an area of 5 cm × 5 cm which was left open in order to make drying possible.

The moisture distributions during drying were determined by measuring the electrical resistances at different places in the samples as is shown schematically in Fig. 3.10. For this purpose in two lateral faces, facing each other, pairs of electrodes were introduced at a distance of 1 cm. Between each pair of electrodes the electrical resistance was measured with a measuring bridge. By means of a calibration performed

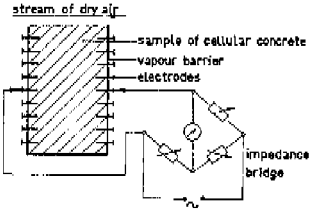

Fig. 3.10
Measurement of D_θ by means of drying experiments.

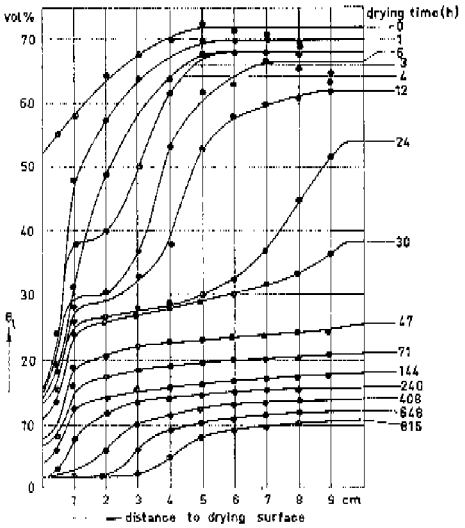

Fig. 3.11
Moisture distributions in a sample of cellular concrete during drying experiments.

previously the moisture distributions in the samples could be derived. To increase the rate of drying a stream of dry air (conditions 20 °C and 20% relative humidity) was led along the open surfaces of the samples.

These measurements have been performed for three types of cellular concrete namely Durox, Ytong and Siporex. By way of illustration the moisture distributions measured after several drying times in a sample of Durox are given in Fig. 3.11. From these and similar results the values of the diffusivity D_θ were calculated from the equation

$$q/\varrho_l = -D_\theta(\partial\theta_l/\partial x), \tag{3.4}$$

which holds for the isothermal case, when the x-axis is supposed to be perpendicular to the drying surface.

The moisture flux density q/ϱ_l can be derived from the curves in Fig. 3.11 by determination of the amount of moisture, passing through a given cross-section in the period between two successive measurements. This amount of moisture is proportional to the area between the two curves on the right-hand side of the considered cross-section. The moisture gradient $\partial\theta_l/\partial x$ can be derived by determining the average slope of the two moisture distribution curves at the considered cross-section.

The average moisture content at the cross-section can also be derived from Fig. 3.11 and so with Eq. (3.4) a D_θ-value can be calculated. By repeating this calculation for other cross-sections and combinations of moisture distributions a D_θ-curve has been determined as shown in Fig. 3.12.

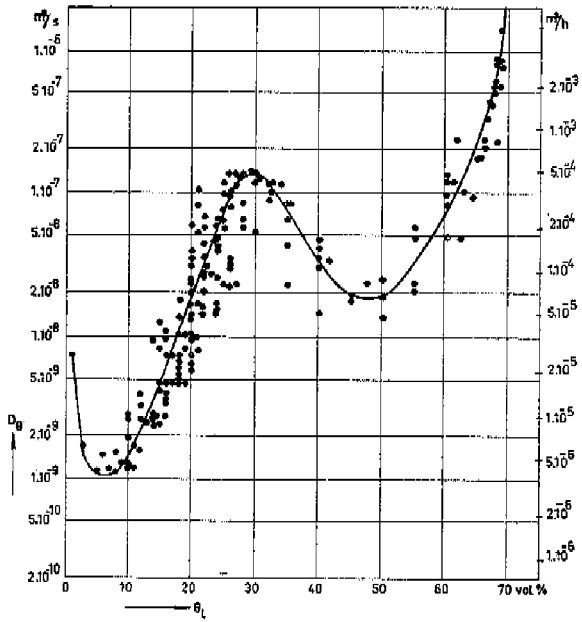

Fig. 3.12 Diffusion coefficient, D_θ, for cellular concrete, determined by means of drying experiments (20 °C).

In the same way measurements have been performed on Ytong and Siporex. These results are presented in [38]; they show no essential differences with those obtained for Durox.

3.6.2 *Measurements of D_θ by means of a stationary moisture flux*

The diffusivity D_θ has also been determined from the moisture distribution in a sample in which a constant moisture flux was realised. For these measurements samples of

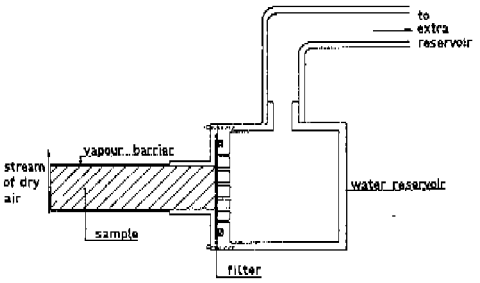

Fig. 3.13
Measurement of D_θ by means of a stationary moisture flux.

cellular concrete were used with sizes of 12 cm × 3 cm × 3 cm. These samples were provided with a vapour barrier along the surfaces in the longitudinal direction and placed into a "filterholder" as is shown schematically in Fig. 3.13. This filterholder consisted of a reservoir, filled with distilled water, and a filter, situated in such a way that the water had to pass the filter before reaching the sample. The moisture flux in the sample could be controlled by using a filter with a higher or lower flow resistance.

In this way on one end of the sample a constant moisture flux was supplied while at the opposite end water was withdrawn by a stream of dry air (conditions 20 °C, 20% relative humidity) along the surface, so that after some time in the sample a constant moisture distribution was attained. The values of the diffusivity D_θ could be calculated from the moisture distribution in the samples, by means of Eq. (3.4).

The moisture flux q/ϱ_l was derived by weighing the assembly (filter-holder with sample) regularly. The moisture gradient $\partial\theta_l/\partial x$ was derived from the moisture distribution in the samples which was determined by splitting up the samples in slices of 1 cm thickness, from each of which the moisture content was measured by weighing and drying. In Figs. 3.14 and 3.15 the moisture distributions determined in this way are shown for different values of the moisture flux.

The measurements have been performed in two ways namely starting with dry samples and starting with samples completely filled with water. Starting with wet samples D_θ-values were determined for "moisture decrease", while the measurements

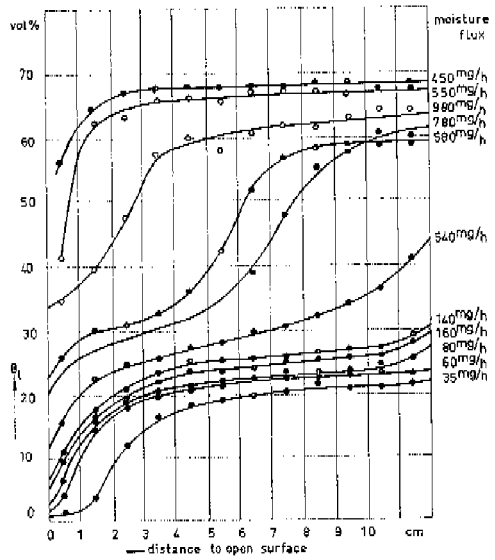

Fig. 3.14
Moisture distributions in samples of cellular concrete for several stationary moisture fluxes (decreasing moisture content, 20 °C)

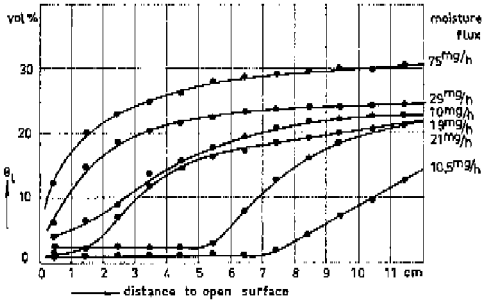

Fig. 3.15
Moisture distributions in samples of cellular concrete for several stationary moisture fluxes (increasing moisture content, 20 °C).

with originally dry samples yielded D_0-values for "moisture increase". For Durox the D_θ-curves for moisture decrease and moisture increase respectively have been given in Figs. 3.16 and 3.17.

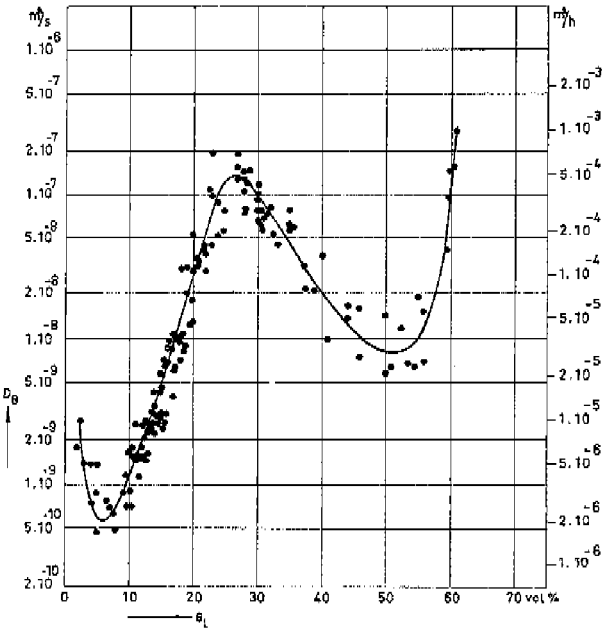

Fig. 3.16 Diffusion coefficient D_0 for cellular concrete, determined by means of a stationary moisture flux (decreasing moisture content, 20 °C).

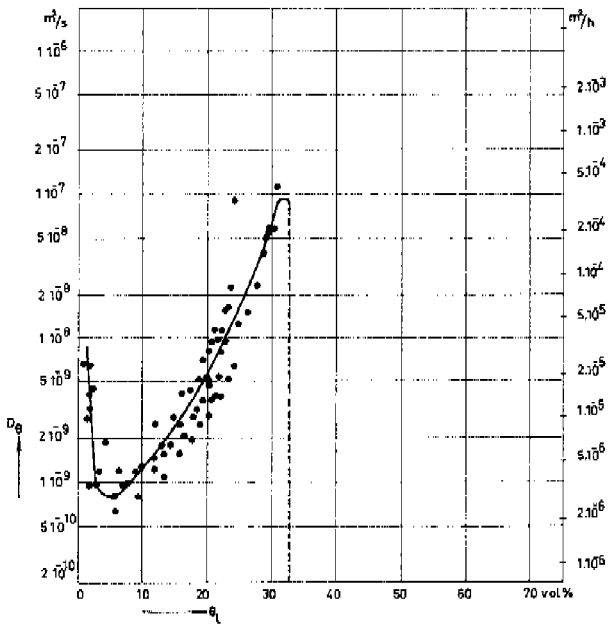

Fig. 3.17 Diffusion coefficient D_0 for cellular concrete, determined by means of a stationary moisture flux (increasing moisture content, 20 °C).

3.6.3 *Discussion of the results*

From the theory given in Section 4.1.2 it follows that the D_θ-curves must have a maximum at a moisture content of about 2% or less. As from the measurements only D_θ-values for moisture contents higher than 2% could be derived, only the right-hand part of the curve leading to this maximum could be determined. By calculation it can be shown that for $\theta_l \approx 2\%$ a maximum does occur, as a consequence of vapour transport.

For higher moisture contents (6% and higher) the moisture transport mainly takes place in the liquid phase. The D_θ-curve for moisture increase (Fig. 3.17) rises with increasing moisture content untill at $\theta_l \approx 32\%$ a sharp fall occurs, due to the presence of entrapped air which impedes a further increase in moisture content (see Section 3.2).

Both D_θ-curves for moisture decrease (Figs. 3.12 and 3.16) also show for $\theta_l > 7\%$ initially a rise with increasing moisture content, followed by a fall at $\theta_l = 25$ to 30% and a rise at $\theta_l = 50$ to 60%, while for fully saturated materials (θ_l = about 75%) D_θ approaches infinity. This can be understood by considering a material, fully filled with water, where on one side water is supplied, while on the opposite side water is

discharged. In this material moisture transport occurs in absence of a moisture gradient, consequently from Eq. (3.4) follows $D_\theta = \infty$.

The presence of the second maximum at $\theta_l = 25$ to 30% is connected with the pore size distribution and the arrangement of the pores in the material. In Chapter 4 this subject will be discussed in more detail.

Krischer et al. ([39] p. 239, [40]) did experiments on Ytong in approximately the same way as has been described previously, be it only for decreasing θ_l. In the method with drying experiments they determined the moisture distributions in the samples by measuring the electrical capacity; in the experiments discussed here this was done by measuring the resistance. The results of Krischer et al. have been given in Fig. 3.18, together with our results. For low and high moisture contents the results correspond quite well; in the intermediate area (θ_l between 30 and 60%) the results differ considerably, because Krischer et al. did not find the second maximum, although this

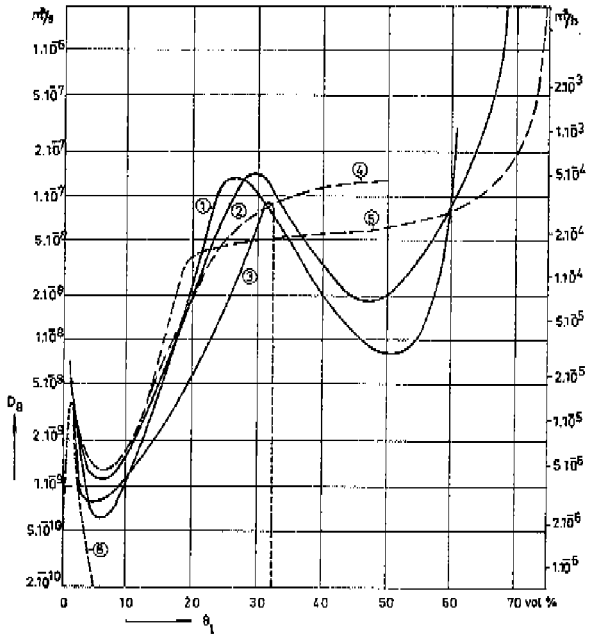

Fig. 3.18 Diffusion coefficient D_θ for cellular concrete determined by:
1. drying experiments (decreasing moisture content)
2. a stationary moisture flux (decreasing moisture content) } own experiments
3. a stationary moisture flux (increasing moisture content)
4. drying experiments (decreasing moisture content)
5. a stationary moisture flux (decreasing moisture content) } experiments of Krischer et al.
6. theoretical curve for contribution of vapour transport ($D_{\theta v}$)

maximum can be derived directly from their measurements. They, however, ascribed these D_θ-values to incorrect moisture distributions at the ends of the samples.

3.7 Measurements of the thermal diffusivity for moisture transport, D_T

The diffusivity D_T (diffusivity for moisture transfer due to a temperature gradient) as a function of the moisture content θ_l has been determined from the moisture distribution in the stationary state. This method was among others suggested by Lykow ([41] p. 154).

For these measurements samples of cellular concrete have been used with sizes of 10 cm × 3 cm × 3 cm, which were provided with a vapour barrier all along the outside surface. These samples were filled with water to a certain moisture content and placed in an apparatus, which is shown schematically in Fig. 3.19. The apparatus consisted of two reservoirs of which one was filled with melting ice and the other with water, at a constant temperature of 40 °C, controlled by means of electrical heating. Between

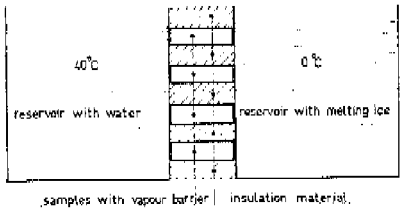

Fig. 3.19
Apparatus for the determination of the diffusion coefficient, D_T.

these reservoirs the samples were placed, in order to obtain a temperature gradient in the longitudinal direction. To obtain a one-dimensional distribution of temperature the samples were supplied with an insulation material all around the surface.

The moisture transfer in the samples can be written as

$$q/\varrho_l = -D_\theta(\partial\theta_l/\partial x) - D_T(\partial T/\partial x), \tag{3.5}$$

when the x-axis is in the longitudinal direction of the samples. Because no moisture transfer out of the samples is possible, in the stationary state an equilibrium is reached for which holds:

$$q/\varrho_l = 0 = -D_\theta(\partial\theta_l/\partial x) - D_T(\partial T/\partial x). \tag{3.6}$$

After one, respectively two months the samples were taken out of the apparatus and the moisture distribution was measured in a gravimetric way.

Next with Eq. (3.6) values of D_T could be calculated since the moisture gradient $\partial\theta_l/\partial x$ at different locations in the sample could be derived from the moisture distri-

bution, the value of D_θ for the corresponding moisture content was known (see Section 3.6), and the temperature gradient $\partial T/\partial x$ in the sample was known from the temperature difference adjusted in the apparatus; the influence of θ_l on λ was neglected in calculating $\partial T/\partial x$, which seemed to be permissible in comparison with other inaccuracies.

For a better interpretation of the results first the temperature gradient factor $\varepsilon = D_T/D_\theta$ (see Section 2.1.3) has been derived with the equation

$$\varepsilon = D_T/D_\theta = -\frac{\partial\theta_l/\partial x}{\partial T/\partial x}, \tag{3.7}$$

while afterwards, by multiplying with the measured D_θ-values, the D_T-curve was obtained. These measurements have been carried out on Durox, Ytong and Siporex. Only the results of the measurements on Durox will be given here, because the mutual differences are only small. The other ones are presented in [38]. The measurements are grouped in the following four series, depending on the place where initially the moisture was added to the samples and dependent on the time the samples stayed in the apparatus:

series	moisture originally applied to	moisture distributions measured after
1	cold side	1 month
2	cold side	2 months
3	warm side	1 month
4	warm side	2 months

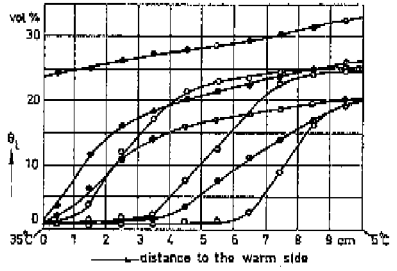

Fig. 3.20a
Stationary moisture distributions in samples exposed to a temperature difference (moisture originally applied to the cold side).

○ series 1: moisture distribution determined after 1 month
● series 2: moisture distribution determined after 2 months

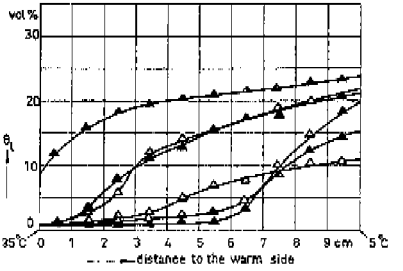

Fig. 3.20b
Stationary moisture distributions in samples exposed to a temperature difference (moisture originally applied to the warm side)

△ series 3: moisture distribution determined after 1 month
▲ series 4: moisture distribution determined after 2 months

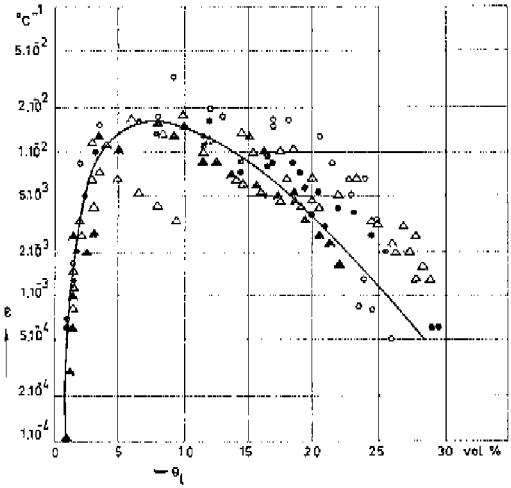

Fig. 3.21
Temperature gradient factor, $\varepsilon\,(=D_T/D_\theta)$, for cellular concrete determined from moisture distributions in the stationary state. ○, △ – from distributions found after one month, ●, ▲ – from distributions found after two months.

The moisture distributions measured for these series are given in Fig. 3.20, while the ε-values derived from these curves are represented in Fig. 3.21. In these figures the results for each series of measurements are indicated by the same mark, which therefore shows the correspondance between results and the series of measurements.

The results show a rather wide spread, which may be due to the following reasons:

a) When the samples stayed too short in the apparatus, the moisture distributions were determined before the stationary state was reached. For the measurements of series 1 and 2, in which water was added to the cold side of the samples, this would result in too high values of $\partial\theta/\partial x$ and consequently in too high ε-values. For measurements of series 3 and 4 this would result in too low ε-values. Since series 1 and 3 stayed one month in the apparatus and series 2 and 4 two months, the last series are the most reliable ones.

b) Possibly the ε-values are dependent upon the fact whether the moisture content is increasing or decreasing. From the measurements of series 1 and 2 on the cold side (and for relatively high moisture content) ε-values were derived with decreasing moisture content, and on the warm side (and for low moisture content) with increasing moisture content. From the measurements 3 and 4 on the cold side ε-values were derived with increasing moisture content and on the warm side with decreasing moisture content. In connection with the calculations about moisture transport in roof constructions to be performed later, we are interested in ε-values for increasing moisture content, so that by preference we have to take the results from series 2 for low moisture contents and the results from series 4 for higher moisture contents.

c) Possibly the ε-values are dependent upon the temperature. The ε-values at low moisture content have been derived from moisture distributions in the warm part of the samples, while the ε-values at high moisture content have been derived from moisture distributions in the cold part of the samples.

As can be seen from Fig. 3.21 the spread in the results probably is mainly caused by the fact that the stationary state is not yet reached, while the difference between moisture increase and decrease seems to be less important. The influence of the temperature cannot be derived from the results, because all experiments for high moisture content give ε-values for low temperature and all experiments for low moisture content give ε-values for high temperature.

Allowing for the previous discussion the average ε-curve has been determined, from which the average D_T-curve for increasing moisture content has been derived by multiplying with the D_θ-curve for moisture increase.

The D_T-curve obtained in this way is shown in Fig. 3.22. With a dotted line the D_{Tv}-curve is presented, calculated with Eq. (2.20) where only vapour transport is considered. Apparently the really existing moisture transport is till 10 times higher as a consequence of combined liquid-vapour transport. In Section 4.2 this subject will be discussed more thoroughly.

For moisture contents higher than 32% the D_T-values are very small, a fact that has been derived from supplementary experiments, carried out on samples with a moisture content between 40 and 75%. From these samples the moisture distributions were determined after a stay of 2 or 4 months in the apparatus. The moisture distributions are given in Fig. 3.23. They turn out to be very irregular and not at all in

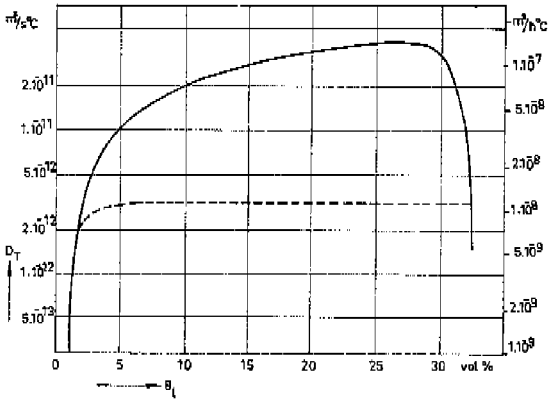

Fig. 3.22 Diffusion coefficient D_T for cellular concrete as a function of the moisture content θ_l (for increasing moisture content)

——— measured values.
– – – – – calculated from Eq. (2.20).

Fig. 3.23
Stationary moisture distributions in samples exposed to a temperature difference (high moisture contents).

- ● moisture distributions determined after 2 months
- ○ moisture distributions determined after 4 months

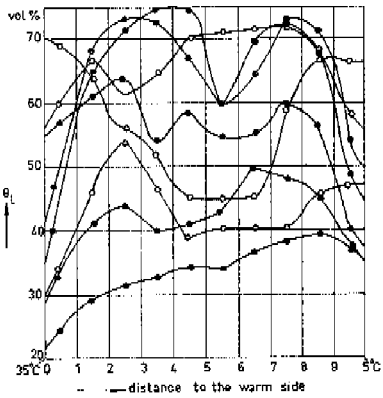

agreement with the expectations. Apparently the moisture distributions have hardly been changed during the exposure period, so that the stationary state is not reached and consequently the D_T-values cannot be calculated in the way discussed previously. From the fact that even after 4 months a uniform moisture distribution was not reached one can derive that the D_T-values for these high moisture contents cannot be higher than $1.4 \cdot 10^{-12}$ m^2/s°C.

These low D_T-values are probably caused by the influence of air-enclosures. For high moisture contents the larger cavities filled with air are surrounded by water. Due to the temperature gradient water and water vapour try to penetrate into these cavities, which tendency is opposed because of the presence of entrapped air. Only because the air dissolves into the water the moisture content in the cold side of the samples can rize. This proces is a very slow one, so that very low D_T-values will be found for increasing moisture content.

In addition to the experiments mentioned before also measurements have been carried out with an exposure period of 8 months. These measurements indeed produced higher D_T-values, which in fact must be equal to the values for decreasing moisture content. Exact measurements however are not possible in this way because the time necessary for reaching the stationary state might be very long. Perhaps D_T-values could be determined more succesfully by drying experiments under the influence of a temperature gradient. These experiments, however, need a non-destructive measuring method for determining the moisture distributions in the samples. The determination of the moisture distributions by measuring the electrical resistance, as described in Section 3.6.1, is too inaccurate because of the dependence of the electrical resistance on temperature. For this reason no D_T-values have been measured for decreasing moisture content.

References

1. B. J. Spit and S. C. van der Knaap, Klei en Keramiek, **20**, (1970), 331–337.
2. M. G. M. Bruggenwert, A. R. P. Janse, F. F. R. Koenigs, Algemene Bodemkunde, handl. kand. pract., Landb. hogeschool, Wageningen (1966).
3. L. A. Richards, Soil science, **68** (1949), 95.
4. A.S.T.M. Designation: E96–53T. Tentative methods of test for measuring water vapor transmission of materials in sheet form (1953).
5. D. A. de Vries and A. J. Kruger, On the value of the diffusion coefficient of water vapour in air, Phénomènes de transport avec changement de phase dans les milieux poreux au colloïdaux, Paris, (1966).
6. W. Wissmann, Ueber das Verhalten von Baustoffen gegen Feuchtigkeitseinwirkungen aus der umgebenden luft, diss. Darmstadt (1954).
7. A. W. Lykow, Transporterscheinungen in Kapilarporösen Körpern, Akademie-Verlag, Berlin (1958).
8. F. E. M. O'Brien, J. of Scientific Instr., **25**, (1948) 73–77.
9. J. S. Carr and B. L. Harris, Ind. and Eng. Chem. (1949), 2014–2015.
10. A. L. E. F. Schleiermacher, Wied. Ann. Phys. **34** (1888), 623.
11. B. Stålhahne and S. Pyk, Tekn. Tidskr. **61**, (1931), 389–393.
12. J. Weishaupt, Forsch. Arb. Ing. Wes. **11** (1940), 20–35.
13. E. F. M. van der Held and F. G. van Drunen, Physica, **15**, (1949) 865–881.
14. E. F. M. van der Held, J. Hardebol and J. Kalshoven, Physica, **19**, (1953), 208–215.
15. D. G. Gillam and O. Lamm, Acta Chem. Scand., **9**, (1955), 657–660.
16. D. G. Gillam, L. Rombén, H. E., Nissen and O. Lamm, Acta Chem. Scand. **9** (1955), 641–656.
17. R. A. W. Will, Proc. Roy. Soc. A 239 (1957), 476–486.
18. F. C. Hooper, Highway Research Board, Special Rep. no. 2 (1952), 57–59.
19. G. Skeib, Z. Met. **4** (1950), 32–29.
20. V. V. Mason, and M. Kurtz, Trans. Amer. Inst. Electr. Engrs. A 103 (1956) 453–470.
21. D. A. de Vries, Soil Sci, **73**, (1952), 83–89.
22. D. A. de Vries, Meded. Landb. Hogesch. Wageningen, **52**, (1952), 1–72.
23. D. A. de Vries, Neth. J. Agric. Sci. **1** (1953) 115–121.
24. R. H. A. van Duin and D. A. de Vries, Neth. J. Agric. Sci. 2 (1954).
25. D. A. de Vries and C. T. de Wit, Met. Rdsch., 7, (1954), 41–45.
26. K. Buettner, Trans Amer. Geophys. Un., **36**, (1955), 827–830.
27. M. W. Makowski and K. Mochlinski, Proc. Instn. Electr. Engrs. A 103 (1956), 453–470.
28. E. C. Bullard, A. E. Maxwell and R. Revelle, Advanc. Geophys. **3**, (1956), 153–181.
29. F. C. Hooper and F. R. Lepper, Heat. Pip. Air Condit. **1950** (1950) 129–135.
30. D. d'Eustachio and R. E. Schreiner, Heat. Pip. Air Condit. **1952** (1952), 113–117.
31. G. Mann and F. G. Forsyth, Mod. Refrig. **59** (1956), 188–191.
32. B. H. Vos, De Ingenieur **73** (1961), 0 7–21.
33. J. W. Haarman, Een nauwkeurige methode voor het bepalen van de warmtegeleidingscoëfficiënt van gassen, diss. Delft (1969).
34. D. G. Briggs, R. J. Goldstein and W. E. Ibele, Proc. of the fourth Symposium on Thermophysical Properties, (1968), 452.
35. J. J. C. Picot, Can. J. Chem. Eng., **47** (1969) 17.
36. D. A. de Vries and A. J. Peck, Austr. J. Phys., **11** (1958), 255–271.
37. H. B. Jespersen, J. Inst. Heat. Vent. Eng., 21 (1953), 157–174.
38. J. van der Kooi, Het vochttransport in dakconstructies, rapport no. 803.011, Techn. Phys. Dienst T.N.O.-T.H. (1968).
39. O. Krischer, Die Wissenschaftlichen Grundlagen der Trocknungs-Technik, Springer Verlag, Berlin (1963).
40. O. Krischer and K. Mahler, Ueber die Bestimmung des Diffusionswiderstandes und der Kapillaren Flüssigkeitsleitzahl aus stationären und instationären Vorgängen, VDI-Forschungsheft 473 (1959).
41. A. W. Lykow, Transporterscheinungen in Kapillarporösen Körpern, Akademie-Verlag, Berlin (1958).

Chapter 4

CALCULATION OF THE DIFFUSION COEFFICIENTS D_θ AND D_T

Philip and De Vries derived equations for the diffusion coefficients D_θ and D_T which can be found from Eq. (2.23) together with (2.9) and (2.17) and Eq. (2.24) together with (2.10) and (2.21). In this chapter we shall compare the results calculated in this way with the results determined experimentally.

4.1 Calculation of D_θ

4.1.1 *Liquid transport*

To calculate the contribution $D_{\theta l}$ the hydraulic conductivity K as well as the matrix potential ψ_m have to be known in dependence of θ_l for the material under consideration. Measurements of ψ_m have been discussed in Section 3.2. K has not been measured, at least not in the usual way by measuring in a porous medium the gradient of the potential as well as the liquid transport due to this gradient. Actually there is hardly any difference between this method and the method described in Section 3.6.2 in which D_θ is derived from the moisture gradient and the corresponding moisture transport. For by reducing this moisture gradient to a ψ_m-gradient with the known (ψ_m versus θ_l) relation, K instead of D_θ can be derived from these measurements.

An independent way of determining K is given by Childs and Collis-George [1], who calculate K from the relation $\psi_m = \psi_m(\theta_l)$. Then with Eq. (2.9) $D_{\theta l}$ can be obtained. By comparing the $D_{\theta l}$-values derived in this way with the D_θ-values determined experimentally it will be seen how far Childs and Collis-George's method, evolved originally for a medium with a simple structure such as sand, can be applied for a material with a more complicated structure such as cellular concrete. First this method will be discussed briefly.

Let us consider the pores to be cylindrical with radius r and let $f(r)$ be the distribution function of the pore volume, which means that the term $f(r)dr$ gives the fraction of the total apparent volume which is occupied by capillaries with a radius ranging from r to $r+dr$.

For a column of sand with unit cross-sectional area a section at any chosen plane normal to the axis of the column will exhibit two similar faces showing similar pore-size distributions; the column may be regarded as the random juxtaposition of these two faces. If a_ϱ is the fractional area occupied by pores of radius ϱ to $\varrho+dr$ and a_σ the fractional area occupied by pores in the range σ to $\sigma+dr$, then

$$a_\varrho = f(\varrho)dr \quad \text{and} \quad a_\sigma = f(\sigma)dr\,. \tag{4.1}$$

The area of cross-section connected with the pore sequence $\varrho \to \sigma$ is given by:

$$a_{\varrho-\sigma} = \mathrm{f}(\varrho)\mathrm{d}r\ \mathrm{f}(\sigma)\mathrm{d}r. \tag{4.2}$$

Childs and Collis-George now make two assumptions, which introduce errors of opposite sign. First all the effective resistance to flow in the sequence is supposed to be due entirely to the smaller one of the two pores, owing to the operation of the factor r^4 in Poiseuille's equation. This assumption results in an over-estimation of the contribution of this sequence to the total permeability but frees us from the necessity of considering the probability of more than one of the smaller pores leading into the same larger pore. Second only direct sequences of the kind described are considered, i.e. we ignore by-passing sequences of, may be, several pores. This results in an under-estimation to compensate for the previous over-estimation.

The distribution of pore sequences given by Eq. (4.2) is repeated wherever the cross-section is taken and is characteristic of the material. The number of pores of size σ accommodated in the area $a_{\varrho\to\sigma}$ is proportional to σ^{-2}, the rate of flow according to Poiseuille's equation is proportional to σ^4, so that the contribution $\mathrm{d}K$ of this group of sequences to the total permeability K is given by:

$$\mathrm{d}K = \sigma^2 M\ \mathrm{f}(\varrho)\mathrm{d}r\ \mathrm{f}(\sigma)\mathrm{d}r, \tag{4.3}$$

and the total permeability due to all possible sequences by:

$$K = M \sum_{\varrho=0}^{\varrho=R} \sum_{\sigma=0}^{\sigma=R} \sigma^2 \mathrm{f}(\varrho)\mathrm{d}r\ \mathrm{f}(\sigma)\mathrm{d}r. \tag{4.4}$$

Here M is a constant which cannot be calculated except for very simple pore geometries. In the case considered here it will be adapted in such a way that the best correspondance is found between the calculated and experimentally determined K-values. In Eq. (4.4) σ^2 has to be replaced by ϱ^2 in any term of the summation in which $\varrho < \sigma$. For any given moisture content the summation is stopped at that pore-size, R, corresponding with the largest pore filled with water.

Childs and Collis-Georges have presented a form of tabulation to perform this calculation in a systematic way. For that purpose they plotted the moisture content against the reciprocal value of the suction pressure, ψ_m, for the considered material. According to Eq. (2.5) $1/\psi_m$ is proportional to the equivalent radius R of the largest capillary filled with water at the considered moisture content. So from the relation $\theta_l = \mathrm{f}(1/\psi_m)$ for the different pore groups the terms $\mathrm{f}(r)\mathrm{d}r$ can be derived, after which with Eq. (4.4) the course of K/M can be calculated in dependence of θ_l.

In the same way as proposed by Childs- and Collis George, we carried out the calculation for cellular concrete. Starting from the suction pressure curve (see Section 3.2) in Table 4.1 for the different pore groups the terms $\mathrm{f}(r)\mathrm{d}r$ have been derived, after

Table 4.1 The moisture characteristic of cellular concrete and the derivation of the pore-size distribution.

experimental results			data interpolated from the graph of moisture content against reciprocal of tension			
moisture content (vol.%)	tension (J/kg)	reciprocal of tension (kg/J)	reciprocal of tension (kg/J)	moisture content (vol.%)	vol. contribution to pore group, $f(r)dr$ (vol.%)	mean radius of pore groep, r (m)
2.5	$1.0 \cdot 10^{6}$	$1.0 \cdot 10^{-6}$	$1 \cdot 10^{-6}$	2.5	0.0	0
5	$3.6 \cdot 10^{4}$	$2.78 \cdot 10^{-5}$	$3 \cdot 10^{-6}$	5.25	2.75	$3.0 \cdot 10^{-9}$
7.5	$2.1 \cdot 10^{4}$	$4.77 \cdot 10^{-5}$	$6 \cdot 10^{-6}$	9.0	3.75	$6.75 \cdot 10^{-9}$
10	$1.5 \cdot 10^{4}$	$6.65 \cdot 10^{-5}$	$1 \cdot 10^{-4}$	13.5	4.5	$1.2 \cdot 10^{-8}$
12.5	$1.05 \cdot 10^{4}$	$9.5 \cdot 10^{-5}$	$3 \cdot 10^{-4}$	22.5	9.0	$3.0 \cdot 10^{-8}$
15	$8.5 \cdot 10^{3}$	$1.18 \cdot 10^{-4}$	$6 \cdot 10^{-4}$	25.6	3.1	$6.75 \cdot 10^{-8}$
17.5	$6.75 \cdot 10^{3}$	$1.48 \cdot 10^{-4}$	$1 \cdot 10^{-3}$	27.0	1.4	$1.2 \cdot 10^{-7}$
20	$5.0 \cdot 10^{3}$	$2.0 \cdot 10^{-4}$	$3 \cdot 10^{-3}$	28.2	1.2	$3.0 \cdot 10^{-7}$
22.5	$3.5 \cdot 10^{3}$	$2.85 \cdot 10^{-4}$	$6 \cdot 10^{-3}$	30.2	2.0	$6.75 \cdot 10^{-7}$
25	$2.0 \cdot 10^{3}$	$5.0 \cdot 10^{-4}$	$1 \cdot 10^{-2}$	32.0	1.8	$1.2 \cdot 10^{-6}$
27.5	$8.5 \cdot 10^{2}$	$1.18 \cdot 10^{-3}$	$3 \cdot 10^{-2}$	38.0	6.0	$3.0 \cdot 10^{-6}$
30	$1.8 \cdot 10^{2}$	$5.55 \cdot 10^{-3}$	$6 \cdot 10^{-2}$	43.5	5.5	$6.75 \cdot 10^{-6}$
32.5	$9.0 \cdot 10$	$1.11 \cdot 10^{-2}$	$1 \cdot 10^{-1}$	49.0	5.5	$1.2 \cdot 10^{-5}$
35	$5.5 \cdot 10$	$1.82 \cdot 10^{-2}$	$3 \cdot 10^{-1}$	58.2	9.2	$3.0 \cdot 10^{-5}$
37.5	$3.7 \cdot 10$	$2.7 \cdot 10^{-2}$	$6 \cdot 10^{-1}$	62.5	4.3	$6.75 \cdot 10^{-5}$
40	$2.5 \cdot 10$	$4.0 \cdot 10^{-2}$	1	64.2	1.7	$1.2 \cdot 10^{-4}$
42.5	$1.9 \cdot 10$	$5.25 \cdot 10^{-2}$	3	66.2	2.0	$3.0 \cdot 10^{-4}$
45	$1.5 \cdot 10$	$6.7 \cdot 10^{-2}$	6	67.0	0.8	$6.75 \cdot 10^{-4}$
47.5	$1.2 \cdot 10$	$8.32 \cdot 10^{-2}$	10	67.5	0.5	$1.2 \cdot 10^{-3}$
50	9.5	$1.05 \cdot 10^{-1}$				
52.5	7.2	$1.39 \cdot 10^{-1}$				
55	5.4	$1.85 \cdot 10^{-1}$				
57.5	3.8	$2.63 \cdot 10^{-1}$				
60	2.6	$3.85 \cdot 10^{-1}$				
62.5	1.6	$6.25 \cdot 10^{-1}$				
65	0.7	1.43				
67.5	0.1	10				

which in Table 4.2 in tabular form the terms have been calculated, which lead to K/M. Next with Eq. (2.9) the course of $D_{\theta l}/M$ is calculated. In Fig. 4.1 the $D_{\theta l}$-curve calculated in this way is plotted together with the D_θ-curve determined experimentally, where at moisture contents between 10 and 30% the best agreement is found with $M = 37 \cdot 10^3$ s/m^2. For a pore system consisting of parallel cylindrical capillaries with their axis in the flow direction the value of M would be $M' = 1/8\nu_l S$, [15], where ν_l is the kinematic viscosity of water. In our case, with $\nu_l = 1.0 \cdot 10^{-6}$ m^2/s (at 20°C) and $S = 0.75$, we find $M' = 167 \cdot 10^3$ s/m^2. The ratio $M/M' = 0.22$ can be ascribed to the influence of the pore space geometry. It is somewhat surprising that the method of Childs and Collis-George, developed for rather coarse granular materials, also applies to cellular concrete with a distinctly different pore geometry and much smaller pore sizes.

Table 4.2 Calculation of K and D_{θ_l} (according to Childs and Collis-George's method) for decreasing θ_l.

0	1	2	3	4	5	6	7	8	9	10	11
θ_l	r	$f(r)dr$	$r^2f(r)dr$	$\Sigma r^2f(r)dr$	$f(r)dr$ $\Sigma r^2f(r)dr$	$2\Sigma\{f(r)dr$ $\Sigma r^2f(r)dr\}$	$r^2(f(r)dr)^2$	$\Sigma r^2(f(r)dr)^2$	(=6–8) K/M	$\partial\psi_m/\partial\theta_l$	D_{θ_l}(m²/s) (M=37·10³ s/m²)
(%)	(m)	(–)	(m²)	(m²)	(m²)	(m²)	(m²)	(m²)	(m²)	(J/kg)	
2.5	0	0	0	0	0	0	0	0	0	–	–
5.2	$3.0\cdot10^{-9}$	$2.75\cdot10^{-2}$	$2.47\cdot10^{-19}$	$2.47\cdot10^{-19}$	$6.83\cdot10^{-21}$	$1.36\cdot10^{-20}$	$6.80\cdot10^{-21}$	$6.80\cdot10^{-21}$	$6.80\cdot10^{-21}$	$1.7\cdot10^{6}$	$4.30\cdot10^{-10}$
9.0	$6.75\cdot10^{-9}$	$3.75\cdot10^{-2}$	$1.71\cdot10^{-18}$	$1.96\cdot10^{-18}$	$7.32\cdot10^{-20}$	$1.60\cdot10^{-19}$	$6.40\cdot10^{-20}$	$7.10\cdot10^{-20}$	$8.92\cdot10^{-20}$	$4.4\cdot10^{5}$	$1.45\cdot10^{-9}$
13.5	$1.2\cdot10^{-8}$	$4.5\cdot10^{-2}$	$6.47\cdot10^{-18}$	$8.42\cdot10^{-18}$	$3.80\cdot10^{-19}$	$9.20\cdot10^{-19}$	$2.90\cdot10^{-19}$	$3.60\cdot10^{-19}$	$5.39\cdot10^{-19}$	$1.3\cdot10^{5}$	$2.60\cdot10^{-9}$
22.5	$3.0\cdot10^{-8}$	$9.0\cdot10^{-2}$	$8.10\cdot10^{-17}$	$8.92\cdot10^{-17}$	$8.03\cdot10^{-18}$	$1.70\cdot10^{-17}$	$7.30\cdot10^{-18}$	$7.65\cdot10^{-18}$	$9.30\cdot10^{-18}$	$6.0\cdot10^{4}$	$2.07\cdot10^{-8}$
25.6	$6.75\cdot10^{-8}$	$3.1\cdot10^{-2}$	$1.41\cdot10^{-16}$	$2.30\cdot10^{-16}$	$7.10\cdot10^{-18}$	$3.12\cdot10^{-17}$	$4.40\cdot10^{-18}$	$1.20\cdot10^{-17}$	$1.91\cdot10^{-17}$	$6.0\cdot10^{4}$	$4.25\cdot10^{-8}$
27.0	$1.2\cdot10^{-7}$	$1.4\cdot10^{-2}$	$2.02\cdot10^{-15}$	$4.32\cdot10^{-16}$	$6.07\cdot10^{-18}$	$4.32\cdot10^{-17}$	$2.82\cdot10^{-18}$	$1.48\cdot10^{-17}$	$2.83\cdot10^{-17}$	$6.0\cdot10^{4}$	$6.30\cdot10^{-8}$
28.2	$3.0\cdot10^{-7}$	$1.2\cdot10^{-2}$	$1.08\cdot10^{-15}$	$1.51\cdot10^{-15}$	$1.81\cdot10^{-17}$	$7.95\cdot10^{-17}$	$1.29\cdot10^{-17}$	$2.77\cdot10^{-17}$	$5.18\cdot10^{-17}$	$5.5\cdot10^{4}$	$1.06\cdot10^{-7}$
30.2	$6.75\cdot10^{-7}$	$2.0\cdot10^{-2}$	$9.10\cdot10^{-15}$	$1.06\cdot10^{-14}$	$2.12\cdot10^{-16}$	$5.01\cdot10^{-16}$	$1.82\cdot10^{-16}$	$2.10\cdot10^{-16}$	$2.92\cdot10^{-16}$	$2.6\cdot10^{4}$	$2.80\cdot10^{-7}$
32.0	$1.2\cdot10^{-6}$	$1.8\cdot10^{-2}$	$2.60\cdot10^{-14}$	$3.65\cdot10^{-14}$	$6.53\cdot10^{-16}$	$1.82\cdot10^{-15}$	$4.65\cdot10^{-16}$	$6.75\cdot10^{-16}$	$1.14\cdot10^{-15}$	$9.6\cdot10^{3}$	$4.02\cdot10^{-7}$
38.0	$3.0\cdot10^{-6}$	$6.0\cdot10^{-2}$	$5.40\cdot10^{-13}$	$5.77\cdot10^{-13}$	$3.46\cdot10^{-14}$	$7.10\cdot10^{-14}$	$3.24\cdot10^{-14}$	$3.31\cdot10^{-14}$	$3.80\cdot10^{-14}$	$7.5\cdot10^{2}$	$1.06\cdot10^{-6}$
43.5	$6.75\cdot10^{-6}$	$5.5\cdot10^{-2}$	$2.52\cdot10^{-12}$	$3.08\cdot10^{-12}$	$1.70\cdot10^{-13}$	$4.10\cdot10^{-13}$	$1.38\cdot10^{-13}$	$1.72\cdot10^{-13}$	$2.38\cdot10^{-13}$	$1.9\cdot10^{2}$	$1.68\cdot10^{-6}$
49.0	$1.2\cdot10^{-5}$	$5.5\cdot10^{-2}$	$7.93\cdot10^{-12}$	$1.10\cdot10^{-11}$	$6.06\cdot10^{-13}$	$1.62\cdot10^{-12}$	$4.35\cdot10^{-13}$	$6.05\cdot10^{-13}$	$1.01\cdot10^{-12}$	$8.0\cdot10^{1}$	$3.00\cdot10^{-6}$
58.2	$3.0\cdot10^{-5}$	$9.2\cdot10^{-2}$	$8.25\cdot10^{-11}$	$9.35\cdot10^{-11}$	$8.57\cdot10^{-12}$	$1.88\cdot10^{-11}$	$7.60\cdot10^{-12}$	$8.20\cdot10^{-12}$	$1.06\cdot10^{-11}$	$4.0\cdot10^{1}$	$1.58\cdot10^{-5}$
62.5	$6.75\cdot10^{-5}$	$4.3\cdot10^{-2}$	$1.96\cdot10^{-10}$	$2.89\cdot10^{-10}$	$1.24\cdot10^{-11}$	$4.36\cdot10^{-11}$	$8.40\cdot10^{-12}$	$1.66\cdot10^{-11}$	$2.70\cdot10^{-11}$	$3.8\cdot10^{1}$	$3.80\cdot10^{-5}$
64.2	$1.2\cdot10^{-4}$	$1.7\cdot10^{-2}$	$2.45\cdot10^{-10}$	$5.34\cdot10^{-10}$	$9.10\cdot10^{-12}$	$6.18\cdot10^{-11}$	$4.17\cdot10^{-12}$	$2.08\cdot10^{-11}$	$4.10\cdot10^{-11}$	$3.5\cdot10^{1}$	$5.30\cdot10^{-5}$
66.2	$3.0\cdot10^{-4}$	$2.0\cdot10^{-2}$	$1.80\cdot10^{-9}$	$2.33\cdot10^{-9}$	$4.66\cdot10^{-11}$	$1.55\cdot10^{-10}$	$3.60\cdot10^{-11}$	$5.68\cdot10^{-11}$	$9.82\cdot10^{-11}$	$5.0\cdot10^{1}$	$1.82\cdot10^{-4}$
67.0	$6.75\cdot10^{-4}$	$8.0\cdot10^{-3}$	$3.65\cdot10^{-9}$	$5.98\cdot10^{-9}$	$4.77\cdot10^{-11}$	$2.50\cdot10^{-10}$	$2.92\cdot10^{-11}$	$8.60\cdot10^{-11}$	$1.64\cdot10^{-10}$	$1.0\cdot10^{2}$	$6.10\cdot10^{-4}$
67.5	$1.2\cdot10^{-3}$	$5.0\cdot10^{-3}$	$7.20\cdot10^{-9}$	$1.32\cdot10^{-8}$	$6.60\cdot10^{-11}$	$3.82\cdot10^{-10}$	$3.60\cdot10^{-11}$	$1.22\cdot10^{-10}$	$2.60\cdot10^{-10}$	∞	∞

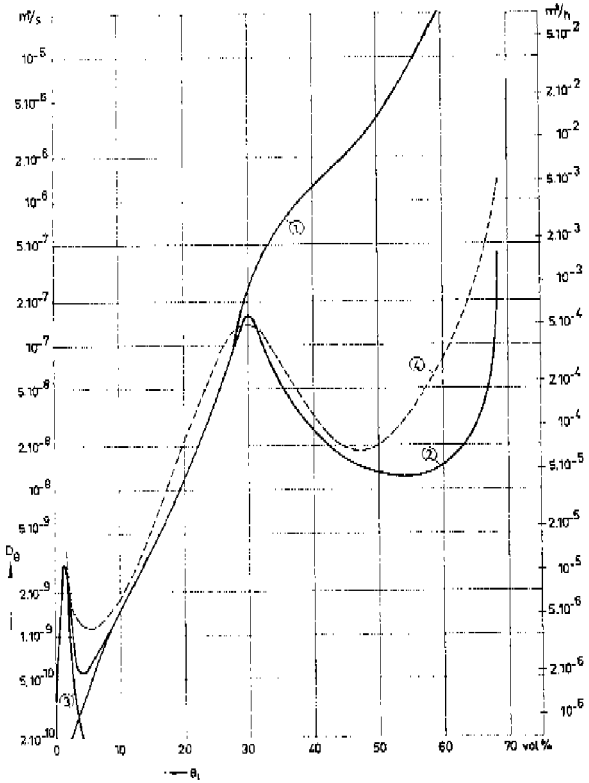

Fig. 4.1 Diffusioncoefficients D_θ for cellular concrete as a function of the moisture content θ_l.

1. D_{θ_l} calculated with the method of Childs and Collis-George
2. Same, but with constant r-value for $\theta_l > 28\%$
3. D_{θ_v} according to Eq. (2.19)
4. D_θ experimentally determined by means of a stationary moisture flux

For moisture contents higher than 30% however the curves differ considerably, since the experimental D_θ-values first decrease with increasing θ_l, while the calculated D_θ-curve continues to increase.

At first sight one would conclude that Childs and Collis-George's method could not be applied for the case considered here. However one should keep in mind that the method was developed for homogeneous granular materials in which no conglomerates of pores or cavities exist. These however do exist in the material considered here. As is seen in Section 3.1 the material consists of a skeleton of sponge material in which rather big cavities occur, mutually connected by small pores. Therefore it is

Table 4.3 Calculation of K and D_{θ_l} (according to a modification of the method of Childs-Collis George, r constant from $3 \cdot 10^{-9}$ m onwards) for decreasing θ_l.

0	1	2	3	4	5	6	7	8	9	10	11
θ_l	r	$f(r)dr$	$r^2f(r)dr$	$\Sigma r^2f(r)dr$	$\frac{f(r)dr}{\Sigma r^2f(r)dr}$	$\frac{2\Sigma\{f(r)dr}{\Sigma r^2f(r)dr\}}$	$r^2\{f(r)dr\}^2$	$\Sigma r^2\{f(r)dr\}^2$	$(=6\text{–}8)$ K/M	$\partial\psi_m/\partial\theta_l$	$D_{\theta_l}(m^2/s)$ $(M=37\cdot10^3$ $s/m^2)$
(%)	(m)	(–)	(m^2)	(m^2)	(m^2)	(m^2)	(m^2)	(m^2)	(m^2)	(J/kg)	
2.5	0	0	0	0	0	0	0	0	0	–	–
5.2	$3.0\cdot10^{-9}$	$2.75\cdot10^{-2}$	$2.47\cdot10^{-19}$	$2.47\cdot10^{-19}$	$6.83\cdot10^{-21}$	$1.36\cdot10^{-20}$	$6.80\cdot10^{-21}$	$6.80\cdot10^{-21}$	$6.80\cdot10^{-21}$	$1.7\cdot10^{6}$	$4.30\cdot10^{-10}$
9.0	$6.75\cdot10^{-9}$	$3.75\cdot10^{-2}$	$1.71\cdot10^{-18}$	$1.96\cdot10^{-18}$	$7.32\cdot10^{-20}$	$1.60\cdot10^{-19}$	$6.40\cdot10^{-20}$	$7.10\cdot10^{-20}$	$8.92\cdot10^{-20}$	$4.4\cdot10^{5}$	$1.45\cdot10^{-9}$
13.5	$1.2\cdot10^{-8}$	$4.5\cdot10^{-2}$	$6.47\cdot10^{-18}$	$8.42\cdot10^{-18}$	$3.80\cdot10^{-19}$	$9.20\cdot10^{-19}$	$2.90\cdot10^{-19}$	$3.60\cdot10^{-19}$	$5.39\cdot10^{-19}$	$1.3\cdot10^{5}$	$2.60\cdot10^{-9}$
22.5	$3.0\cdot10^{-8}$	$9.0\cdot10^{-2}$	$8.1\cdot10^{-17}$	$8.92\cdot10^{-17}$	$8.03\cdot10^{-18}$	$1.70\cdot10^{-17}$	$7.30\cdot10^{-18}$	$7.65\cdot10^{-18}$	$9.30\cdot10^{-18}$	$6.0\cdot10^{4}$	$2.07\cdot10^{-8}$
25.6	$6.75\cdot10^{-8}$	$3.1\cdot10^{-2}$	$1.41\cdot10^{-16}$	$2.30\cdot10^{-16}$	$7.10\cdot10^{-18}$	$3.12\cdot10^{-17}$	$4.40\cdot10^{-18}$	$1.20\cdot10^{-17}$	$1.91\cdot10^{-17}$	$6.0\cdot10^{4}$	$4.25\cdot10^{-8}$
27.0	$1.2\cdot10^{-7}$	$1.4\cdot10^{-2}$	$2.02\cdot10^{-16}$	$4.32\cdot10^{-16}$	$6.07\cdot10^{-18}$	$4.32\cdot10^{-17}$	$2.82\cdot10^{-18}$	$1.48\cdot10^{-17}$	$2.83\cdot10^{-17}$	$6.0\cdot10^{4}$	$6.30\cdot10^{-8}$
28.2	$3.0\cdot10^{-7}$	$1.2\cdot10^{-2}$	$1.08\cdot10^{-15}$	$1.51\cdot10^{-15}$	$1.81\cdot10^{-17}$	$7.95\cdot10^{-17}$	$1.29\cdot10^{-17}$	$2.77\cdot10^{-17}$	$5.18\cdot10^{-17}$	$5.5\cdot10^{4}$	$1.06\cdot10^{-7}$
30.2	$3.0\cdot10^{-7}$	$2.0\cdot10^{-2}$	$1.8\cdot10^{-15}$	$3.30\cdot10^{-15}$	$6.60\cdot10^{-17}$	$2.12\cdot10^{-16}$	$3.60\cdot10^{-17}$	$4.12\cdot10^{-17}$	$1.71\cdot10^{-16}$	$2.6\cdot10^{4}$	$1.64\cdot10^{-7}$
32.0	$3.0\cdot10^{-7}$	$1.8\cdot10^{-2}$	$1.62\cdot10^{-15}$	$4.93\cdot10^{-15}$	$8.90\cdot10^{-17}$	$3.90\cdot10^{-16}$	$2.92\cdot10^{-17}$	$7.00\cdot10^{-17}$	$3.20\cdot10^{-16}$	$9.6\cdot10^{3}$	$1.11\cdot10^{-6}$
38.0	$3.0\cdot10^{-7}$	$6.0\cdot10^{-2}$	$5.4\cdot10^{-15}$	$1.03\cdot10^{-14}$	$6.20\cdot10^{-16}$	$1.63\cdot10^{-15}$	$3.25\cdot10^{-16}$	$3.93\cdot10^{-16}$	$1.24\cdot10^{-15}$	$7.5\cdot10^{2}$	$3.43\cdot10^{-6}$
43.5	$3.0\cdot10^{-7}$	$5.5\cdot10^{-2}$	$4.95\cdot10^{-15}$	$1.53\cdot10^{-14}$	$8.40\cdot10^{-16}$	$3.31\cdot10^{-15}$	$2.72\cdot10^{-16}$	$6.65\cdot10^{-16}$	$2.63\cdot10^{-15}$	$1.9\cdot10^{2}$	$1.85\cdot10^{-6}$
49.0	$3.0\cdot10^{-7}$	$5.5\cdot10^{-2}$	$4.95\cdot10^{-15}$	$2.03\cdot10^{-14}$	$1.11\cdot10^{-15}$	$5.52\cdot10^{-15}$	$2.72\cdot10^{-16}$	$9.40\cdot10^{-16}$	$4.60\cdot10^{-15}$	$8.0\cdot10^{1}$	$1.36\cdot10^{-6}$
58.2	$3.0\cdot10^{-7}$	$9.2\cdot10^{-2}$	$8.3\cdot10^{-15}$	$2.86\cdot10^{-14}$	$2.63\cdot10^{-15}$	$1.08\cdot10^{-14}$	$7.6\cdot10^{-16}$	$1.70\cdot10^{-15}$	$9.10\cdot10^{-15}$	$4.0\cdot10^{1}$	$1.34\cdot10^{-6}$
62.5	$3.0\cdot10^{-7}$	$4.3\cdot10^{-2}$	$3.87\cdot10^{-15}$	$3.25\cdot10^{-14}$	$1.40\cdot10^{-15}$	$1.36\cdot10^{-14}$	$1.67\cdot10^{-15}$	$1.87\cdot10^{-15}$	$1.17\cdot10^{-14}$	$3.8\cdot10^{1}$	$1.65\cdot10^{-6}$
64.2	$3.0\cdot10^{-7}$	$1.7\cdot10^{-2}$	$1.53\cdot10^{-15}$	$3.40\cdot10^{-14}$	$5.80\cdot10^{-16}$	$1.48\cdot10^{-14}$	$2.60\cdot10^{-15}$	$1.89\cdot10^{-15}$	$1.29\cdot10^{-14}$	$3.5\cdot10^{1}$	$1.52\cdot10^{-6}$
66.2	$3.0\cdot10^{-7}$	$2.0\cdot10^{-2}$	$1.80\cdot10^{-15}$	$3.58\cdot10^{-14}$	$7.16\cdot10^{-16}$	$1.62\cdot10^{-14}$	$3.60\cdot10^{-15}$	$1.93\cdot10^{-15}$	$1.43\cdot10^{-14}$	$5.0\cdot10^{1}$	$2.65\cdot10^{-6}$
67.0	$3.0\cdot10^{-7}$	$8.0\cdot10^{-2}$	$7.20\cdot10^{-15}$	$3.65\cdot10^{-14}$	$2.92\cdot10^{-15}$	$1.68\cdot10^{-14}$	$5.80\cdot10^{-15}$	$1.93\cdot10^{-15}$	$1.49\cdot10^{-14}$	$1.0\cdot10^{2}$	$5.50\cdot10^{-6}$
67.5	$3.0\cdot10^{-7}$	$5.0\cdot10^{-2}$	$4.50\cdot10^{-15}$	$3.69\cdot10^{-14}$	$1.84\cdot10^{-15}$	$1.71\cdot10^{-14}$	$2.25\cdot10^{-15}$	$1.94\cdot10^{-15}$	$1.52\cdot10^{-14}$	∞	∞

not surprising that the $D_{\theta l}$-curve calculated in this way is far different from the D_θ-curve determined experimentally. A much better agreement is obtained when the calculation is performed in the following way.

For moisture contents lower than 30% only the small pores in the sponge material are filled with water. As all these pores are more or less connected with each other the sponge material can be considered as a rather homogeneous material and the calculation for these moisture contents can be carried out in the way indicated before. When the moisture content is higher also the larger cavities inside the skeleton are filled with water. These cavities are not directly connected with each other and so the mutual liquid transport between the cavities can only take place via the small pores in the sponge material. For these higher moisture contents it is therefore not correct to connect the term σ^2 in Eq. (4.4) with the smallest of the cavities which have just been filled at this moisture content. A better approach is obtained if the term σ^2 is connected with the largests of the pores, existing in the sponge material, which mainly are responsible for the flow resistance between the cavities.

The calculation has been performed in this way in Table 4.3, where for moisture contents higher than $\theta_l = 28\%$ r is held at a constant value of $3 \cdot 10^{-7}$ m. The D_θ-curve calculated in this way is also plotted in Fig. 4.1 and corresponds reasonably well with the curve determined experimentally. The D_θ-curve calculated in this way holds for water decrease.

For increasing θ_l the D_θ-curve can be calculated in the same way, starting from the relation $\psi_m = f(\theta_l)$ for increasing θ_l.

4.1.2 *Vapour transport*

As discussed in Section 2.1.1 the vapour flux due to a vapour pressure gradient can be represented by the Eqs. (2.13) and (2.14). Combining these equations gives

$$\delta = \alpha a D \frac{P}{P - p_v} \frac{M}{RT}. \tag{4.5}$$

From experiments in Section 3.3 we found $\delta = 2.1 \cdot 10^{-11}$ s, so with $a = 0.7$ (see Section 3.1), $T = 293$ K, $D = 27.4 \cdot 10^{-6}$ m^2/s, $M = 18$ kg/kmol, and $R = 8.31$ kJ/kmol K follows $\alpha a = 0.11$ and $\alpha = 0.15$.

This rather low α-value in comparison to other materials (for sand for instance $\alpha \approx 0.7$) is partly caused by the inhomogeneous structure of the material as will appear from the considerations given below. First we will give a short description of the theories to be used.

De Vries [2] calculated the gas diffusion in a granular material by considering this material as a continuous medium (in this case air with diffusivity D_a) in which ellipsoidal particles with diffusivity $D = 0$ are embedded. The mathematical treatment is the same as that for calculating the dielectric constant of granular materials, for which originally theories were developed by:

a. Maxwell [3] – Burger [4] – Eucken [5],
b. Ollendorf [6],
c. Böttcher [7] – Polder and Van Santen [8],
d. Bruggeman [9].

A survey of these theories is given by De Vries [10]. Here it will suffice to give a short description of the theory of Maxwell–Burger, because the diffusion coefficients, calculated by this theory proved to be in rather good agreement with experimental values of Penman [11] for the diffusion of CS_2, aceton and CO_2 through soils and of De Vries [10] for the diffusion of water vapour through sand.

In this connection it can be remarked that the same type of theory has been used to calculate the magnetic permeability μ, the electrical conductivity σ and the heat conductivity λ. De Vries [10] calculated in this way the heat conductivity of soils, while Krischer and Mahler [12] in a similar way carried out calculations on the dielectric constant of "Dachziegel" (a material of which roof tiles consist).

Apart from this Krischer ([13] p. 275) tried to make the experiments of the thermal conductivity of moist building materials accessible to calculation by considering the heat transfer in the material as series transport as well as parallel transport through the composing components. By adjusting the mutual proportion of both contributions a good agreement was obtained between experimental and calculated results. As will appear in Section 4.2 this method turns out to be useful too for the calculation of the vapour transport due to a temperature gradient.

With the theory of Maxwell-Burger we shall calculate the gas diffusion in dry cellular concrete. For this purpose we consider the material as consisting of a continuous medium of sponge-material in which air-cavities and quartz grains are randomly dispersed. Maxwell originally developed this theory for the electric conductivity of an isotropic medium with spherical enclosures. Burger extended the theory for ellipsoidal enclosures, while Eucken first applied it to calculate the heat conductivity. In these theories the mutual influence of the particles is neglected. De Vries has shown that they provide a useful first approximation in case the ratio of the conductivities of the enclosures and the continuous medium is less than about 10.

The diffusivity of the material can be written as:

$$D = \frac{\sum_{i=0}^{i=N} D_i v_i k_i}{\sum_{i=0}^{i=N} v_i k_i}, \tag{4.6}$$

where D_i is the diffusivity of the particles of kind i, v_i their volume fraction and k_i a factor depending on the form of the particles. If these particles are embedded in a medium with diffusivity D_0 one has:

$$k_i = \frac{3D_0}{2D_0 + D_i} \qquad (4.7)$$ for spherical particles,

$$k_i = \frac{5D_0 + D_i}{3(D_0 + D_i)} \qquad (4.8)$$ for elongated cylindrical particles with circular cross section,

$$k_i = \frac{D_0 + 2D_i}{3D_i} \qquad (4.9)$$ for disc-shaped particles.

For the material considered here (4.6) changes into:

$$D_c = \frac{D_s v_s + D v_a k_a + D_q v_q k_q}{v_s + v_a k_a + v_q k_q} \qquad (4.10)$$

where D_c, D_s, D and D_q are respectively the diffusivities in cellular concrete, sponge-material, stagnant air and quartz and v_s, v_a and v_q the volume fractions of the last three components.

To calculate the diffusivity D_c of cellular concrete, first the diffusivity D_s of the sponge material has to be considered. When α_s is the labyrinth factor and a_s the volume fraction of air in sponge material, one has :

$$D_s = \alpha_s a_s \beta_s D. \qquad (4.11)$$

Here the factor β_s provides for the reduction of the diffusivity, caused by the small dimensions of the pores in the sponge-material, which causes Knudsen flow to occur. At atmospheric pressure this is the case for $r < 10^{-7}$ m.

While the diffusion in the larger pores can be written as

$$q = -D f \frac{P}{P - p_v} \frac{M}{RT} \nabla p_v, \qquad (4.12)$$

for Knudsen-flow applies ([13] p. 170, [14] p. 77):

$$q = -\frac{8}{3} f r \sqrt{\frac{M}{2\pi RT}} \nabla p_v, \qquad (4.12a)$$

where f is the cross-section available for diffusion.

So the reduction of the diffusion due to Knudsen-flow is given by:

$$\beta_s = \frac{8}{3} \frac{r}{D} \sqrt{\frac{RT}{2\pi M}}. \qquad (4.13)$$

For the temperature and pressure range considered here one has:

$$\beta_s \approx 14 \cdot 10^6 r, \tag{4.13a}$$

where r is expressed in m.

The factor $\bar{\beta}_s$ for sponge-material can be calculated from the suction pressure curve for cellular concrete, by remembering that the part of this curve between 0 and 30% is mainly connected with the pores in the sponge material.
So from this part of the suction pressure curve for each pore group in the sponge-material the average pore radius and volume fraction can be derived, where after the β_s-value for each pore group and also the average value $\bar{\beta}_s$ for sponge-material can be calculated with Eq. (4.13a). This calculation is carried out in Table 4.5, where is found $\bar{\beta}_s = 0.37$.
Starting from a labyrinth factor $\alpha_s = 0.75$, which can be derived for a simplified model of isotropically distributed cylindrical capillaries, and a volume fraction of air $a_s = 0.66$ (see Section 3.1), we find with Eq. (4.11):

$$D_s = 0.75 \cdot 0.66 \cdot 0.37 D = 0.18 D$$

Table 4.5 Calculation of the coefficient $\bar{\beta}_s$

$\Delta\theta_l$ (vol.%)	ψ_m (J/kg)	r (m)	β_s	$(\beta_s \Delta\theta_l)/30$
0–2.5	$3 \cdot 10^5$	$0.5 \cdot 10^{-5}$	$7 \cdot 10^{-3}$	$0.58 \cdot 10^{-3}$
2.5–5	$6 \cdot 10^4$	$2.5 \cdot 10^{-5}$	$35 \cdot 10^{-3}$	$2.9 \cdot 10^{-3}$
5–7.5	$2.6 \cdot 10^4$	$6 \cdot 10^{-5}$	$84 \cdot 10^{-3}$	$7.0 \cdot 10^{-3}$
7.5–10	$1.7 \cdot 10^4$	$9 \cdot 10^{-5}$	$126 \cdot 10^{-3}$	$10.5 \cdot 10^{-3}$
10–15	$1.1 \cdot 10^4$	$1.4 \cdot 10^{-5}$	$195 \cdot 10^{-3}$	$32.5 \cdot 10^{-3}$
15–20	$5.3 \cdot 10^3$	$2.8 \cdot 10^{-5}$	$390 \cdot 10^{-3}$	$65 \cdot 10^{-3}$
20–25	$4.0 \cdot 10^3$	$3.7 \cdot 10^{-5}$	$520 \cdot 10^{-3}$	$87 \cdot 10^{-3}$
25–30	$1 \cdot 10^3$	$1.5 \cdot 10^{-7}$	1	$166 \cdot 10^{-3}$
				$\bar{\beta}_s = 0.37$

Assuming spheroidal air-cavities and quartz-grains, the diffusivity D_c of cellular concrete can be calculated from Eqs. (4.7) and (4.10). Therefore we find from $D_q = 0$ and $v_s = 0.45$, $v_a = 0.40$, $v_q = 0.15$ (see Section 3.1): $D_c = 0.29D$. From the experiments we derived $\alpha a = 0.11$, so that $D_c = 0.11D$. This low value of the diffusivity found experimentally therefore cannot be explained fully by the inhomogeneous structure of the material and the reducing influence of Knudsen-flow, but must be caused also by the fact that a large amount of the pores in the sponge material is blocked.

The vapour diffusivity $D_{\theta v}$ can be calculated from Eq. (2.17) using the following data: $\alpha a = 0.11$, $D = 27.4 \cdot 10^{-6}$ m^2/s, $M = 18$ kg/kmol, $R = 8.31$ kJ/kmol K, $T = 293K$, $p_{vs} = 2.34 \cdot 10^3$ N/m^2 (for 20°C), and $(\partial h/\partial\theta_l)_T$ derived from the $\theta_l = \theta_l(h)$

Table 4.6 Calculation of D_{θ_v}

θ_l (vol. %)	$(\partial h/\partial\theta_l)_T$	D_{θ_v} (m²/s)
0	5	$2.6\cdot10^{-10}$
0.5	13.6	$7.1\cdot10^{-10}$
1	31	$16.1\cdot10^{-10}$
1.5	60	$31\cdot10^{-10}$
2	44	$23\cdot10^{-10}$
2.5	13	$16\cdot10^{-10}$
3	9	$4.7\cdot10^{-10}$
4	5	$2.6\cdot10^{-10}$
5	3	$1.6\cdot10^{-10}$
6	1	$0.5\cdot10^{-10}$
7	1	$0.5\cdot10^{-10}$

relation (see Section 3.3). The results are given in Table 4.6. In Fig. 4.1 the calculated D_θ-curve, found by summation of the calculated $D_{\theta v}$- and $D_{\theta l}$-values, have been presented together with the D_θ-curve determined experimentally. The curves turn out to correspond reasonably well.

4.2 Calculation of D_T

4.2.1 *Vapour transport*

Philip and De Vries derived for the vapour transport due to a temperature gradient Eq. (2.21), where f(a) depends on the volume fraction air in the material. For granular materials with a simple structure, such as sand, they proposed as a first approach Eq. (2.20a). Due to the rather complicated structure of the cellular concrete material considered here, the considerations which have lead to Eq. (2.20a) need some extension.

For this purpose we consider the moisture transport in the material as to be represented by *parallel transport* (i.e. in a part of the pores only vapour transport occurs and in the other ones only liquid transport) or by *series transport* (i.e. in all pores liquid islands occur, so that only combined vapour liquid transport takes place). By combining the contributions calculated in this way in a certain proportion, we shall try to bring the calculated results in agreement with the experiments.

The contribution $(D_{Tv})_p$ by parallel transport can be represented by Eq. (2.18) in unchanged form, so that

$$(D_{Tv})_p = \alpha a D \frac{P}{P-p_v} \frac{M}{RT} \frac{h}{\varrho_l} \frac{\mathrm{d}p_{os}}{\mathrm{d}T}. \tag{4.14}$$

Here a decreases with increasing moisture content, according to

$$a = S-\theta_l. \tag{4.15}$$

For series transport the factor αa has to be replaced by S, because now the total volume, occupied by water and air, is available for diffusion. Next to this the enlargement of the temperature gradient $(\nabla T)_a$ in the air-filled cavities, with regard to the average temperature gradient ∇T in the material has to be taken into account, because the heat conductivity of moist air is smaller than that of liquid water. The enlargement of the temperature gradient can be calculated according to the theory of Maxwell-Burger, so that

$$[(\nabla T)_a/(\nabla T)_l] = k_a, \tag{4.16}$$

and

$$a(\nabla T)_a + (S-a)(\nabla T)_l = S\nabla T, \tag{4.17}$$

where $(\nabla T)_l$ is the temperature gradient in the liquid.
Combination of (4.16) and (4.17) gives:

$$[(\nabla T)_a/\nabla T] = \frac{k_a S}{S-a+k_a a}. \tag{4.18}$$

For low a-values spheroidal air-cavities are assumed, for higher a-values cylindrical ones which results in the use of Eqs. (4.7) respectively (4.8), which are adapted for the problem considered here by replacing D_0 by λ_l (heat conductivity of liquid water) and D_l by λ_a (heat conductivity of moist air).
So for series transport we have:

$$(D_{Tv})_s = \frac{k_a S^2}{S-a+k_a a} D \frac{P}{P-p_v} \frac{M}{RT} \frac{h}{\varrho_l} \frac{\mathrm{d}p_{ns}}{\mathrm{d}T}. \tag{4.19}$$

The contributions of series- and parallel transport can be combined as follows:

$$D_{Tv} = \beta(D_{Tv})_s + (1-\beta)(D_{Tv})_p, \tag{4.20}$$

where we propose:

$$\beta = 0 \quad \text{for} \quad a = 0 \text{ and } a = S,$$

$$\beta = 1 \quad \text{for} \quad a = S/2. \tag{4.21}$$

In this way in Table 4.7 the diffusivity D_{Tv} is calculated, using the following data: $\alpha = 0.15$; $S = 0.70$; $D = 0.27 \cdot 10^{-4}$ m^2/s; $\lambda_a = 0.28$ W/m°C (temperature 20°C) and $\lambda_l = 0.55$ W/m°C. The calculated values are plotted in Fig. 4.2.

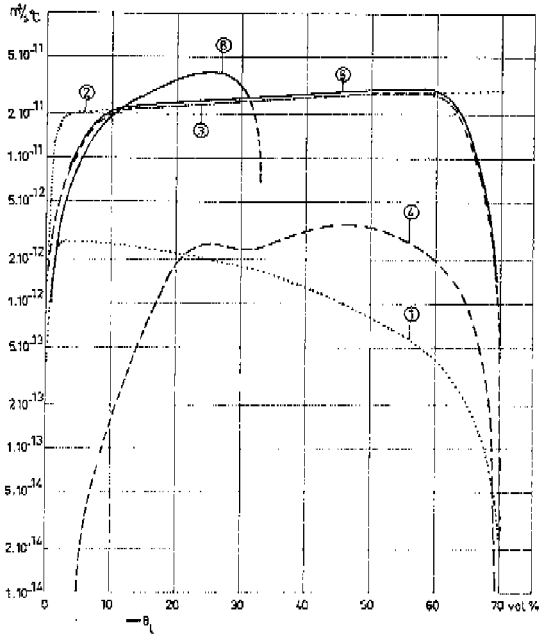

Fig. 4.2 Diffusivity, D_T, in relation to moisture content, θ_l, for cellular concrete.

1. diffusivity $(D_{Tv})_p$ calculated for parallel transport in vapour phase
2. diffusivity $(D_{Tv})_s$ calculated for series transport in vapour phase
3. diffusivity D_{Tv} calculated for vapour transport from Eq. 4.20
4. diffusivity D_{Tl} calculated for liquid transport
5. general diffusivity D_T calculated by summation of D_{Tv} and D_{Tl}
6. general diffusivity D_T determined experimentally

Table 4.7 Calculation of the diffusivity D_{Tv}

θ_l (vol.%)	$(D_{Tv})_p$ (m²/s °C)	$(D_{Tv})_s$ (m²/s °C)	β (–)	D_{Tv} (m²/s °C)
0	0	0	0	0
2.5	$0.275 \cdot 10^{-11}$	$1.90 \cdot 10^{-11}$	0.2	$0.60 \cdot 10^{-11}$
5	$0.273 \cdot 10^{-11}$	$2.02 \cdot 10^{-11}$	0.45	$1.06 \cdot 10^{-11}$
10	$0.255 \cdot 10^{-11}$	$2.10 \cdot 10^{-11}$	0.99	$2.09 \cdot 10^{-11}$
20	$0.215 \cdot 10^{-11}$	$2.20 \cdot 10^{-11}$	1	$2.20 \cdot 10^{-11}$
40	$0.129 \cdot 10^{-11}$	$2.50 \cdot 10^{-11}$	1	$2.50 \cdot 10^{-11}$
60	$0.043 \cdot 10^{-11}$	$2.86 \cdot 10^{-11}$	0.99	$2.83 \cdot 10^{-11}$
65	$0.021 \cdot 10^{-11}$	$2.86 \cdot 10^{-11}$	0.45	$1.29 \cdot 10^{-11}$
67.5	$0.011 \cdot 10^{-11}$	$2.86 \cdot 10^{-11}$	0.2	$0.58 \cdot 10^{-11}$
70	0	$2.86 \cdot 10^{-11}$	0	0

4.2.2 *Liquid transport*

For the diffusioncoefficient D_{Tl} for liquid transport due to a temperature gradient Eq. (2.10) was derived. The calculation is carried out in Table 4.8. starting from the following data:

- the hydraulic conductivity K, calculated in Table 4.3,
- the temperature coefficient of surface tension $\gamma = 2.1 \cdot 10^{-3}\ °C^{-1}$, and
- the matrixpotential ψ_m, determined experimentally in Section 3.2.

Summation of D_{Tl} and D_{Tv} yields the generalized diffusivity D_T. The D_T-values calculated in this way are, together with the experimental ones, shown in Fig. 4.2. For moisture contents below 30% both types of results agree fairly well, for higher moisture contents the calculated D_T-values are much higher than the experimental ones. As discussed in Section 3.7 the low experimental results are ascribed to the influence of air-enclosures.

Table 4.8 Calculation of the diffusion coefficients D_{Tl} and D_T

θ_l (vol.%)	K (kgm^4/Js)	ψ_m (J/kg)	D_{Tl} (m^2/s °C)	D_{Tv} (m^2/s °C)	D_T (m^2/s °C)
2.5	–	$1 \cdot 10^5$		$6.0 \cdot 10^{-12}$	$6.0 \cdot 10^{-12}$
5.2	$2.53 \cdot 10^{-16}$	$3.2 \cdot 10^4$	$1.7 \cdot 10^{-14}$	$1.1 \cdot 10^{-11}$	$1.1 \cdot 10^{-11}$
9.0	$3.30 \cdot 10^{-16}$	$1.7 \cdot 10^4$	$1.2 \cdot 10^{-13}$	$1.9 \cdot 10^{-11}$	$1.9 \cdot 10^{-11}$
13.5	$2.0 \cdot 10^{-14}$	$9.5 \cdot 10^3$	$4.0 \cdot 10^{-13}$	$2.1 \cdot 10^{-11}$	$2.1 \cdot 10^{-11}$
22.5	$3.45 \cdot 10^{-13}$	$3.5 \cdot 10^3$	$2.5 \cdot 10^{-12}$	$2.2 \cdot 10^{-11}$	$2.4 \cdot 10^{-11}$
27.0	$1.05 \cdot 10^{-12}$	$1.1 \cdot 10^3$	$2.4 \cdot 10^{-12}$	$2.2 \cdot 10^{-11}$	$2.4 \cdot 10^{-11}$
32.0	$1.18 \cdot 10^{-11}$	$9.5 \cdot 10$	$2.3 \cdot 10^{-12}$	$2.3 \cdot 10^{-11}$	$2.6 \cdot 10^{-11}$
38.0	$4.60 \cdot 10^{-11}$	$3.2 \cdot 10$	$3.1 \cdot 10^{-12}$	$2.4 \cdot 10^{-11}$	$2.7 \cdot 10^{-11}$
43.5	$9.70 \cdot 10^{-11}$	$1.7 \cdot 10$	$3.6 \cdot 10^{-12}$	$2.6 \cdot 10^{-11}$	$2.9 \cdot 10^{-11}$
49.0	$1.69 \cdot 10^{-10}$	$1 \cdot 10$	$3.5 \cdot 10^{-12}$	$2.8 \cdot 10^{-11}$	$3.1 \cdot 10^{-11}$
58.2	$3.37 \cdot 10^{-10}$	3.6	$2.3 \cdot 10^{-12}$	$2.8 \cdot 10^{-11}$	$3.0 \cdot 10^{-11}$
62.5	$4.35 \cdot 10^{-10}$	1.6	$1.5 \cdot 10^{-12}$	$2.5 \cdot 10^{-11}$	$2.6 \cdot 10^{-11}$
65.0	$5.03 \cdot 10^{-10}$	0.7	$7.4 \cdot 10^{-13}$	$1.3 \cdot 10^{-11}$	$1.4 \cdot 10^{-11}$
67.5	$5.60 \cdot 10^{-10}$	0.1	$1.2 \cdot 10^{-13}$	$5.8 \cdot 10^{-12}$	$5.9 \cdot 10^{-12}$

References

1. E. C. Childs, N. Collis George, Proc. Roy. Soc., London, A 201, 392–405, (1950).
2. D. A. de Vries, Trans. 4th Int. Congr. of Soil Sc. II, 41–43, (1950).
3. C. Maxwell, Treatise on electricity and magnetism I, Oxford (1873).
4. H. C. Burger, Phys. Zs. **20**, 73–76, (1915).
5. A. Eucken, VDI-Forschungsheft 353, (1932).
6. F. Ollendorf, Arch. für Elektrotechn. **25**, 436–447, (1931).
7. C. J. F. Böttcher, Rec. Trav. Chim. **64**, 47–51, (1945).
8. D. Polder, J. H. van Santen, Physica **12**, 257–271 (1946).
9. D. A. G. Bruggeman, Arm. der Phys. V, **24**, 636–679, (1935).
10. D. A. de Vries, Med. Landb. Hogeschool Wageningen, **52**, 1–73, (1952).
11. H. L. Penman, J. of Agric. Sc. **30**, 437–462, 570–581, (1940).

12. O. Krischer and K. Mahler, Ueber die Bestimmung des Diffusionswiderstandes und der Kapillären Flüssigkeitsleitzahl aus stationären und instationären Vorgängen, VDI-Forschungsheft 473, (1959).
13. O. Krischer, Die Wissenschaftlichen Grundlagen der Trocknungstechnik, Springer Verlag, Berlin, (1963).
14. A. W. Lykow, Transporterscheinungen in Kapillärporösen Körpern, Akademie-Verlag, Berlin, (1958).
15. D. A. de Vries, De Ingenieur, **74**, 0 45–53, (1962).

Chapter 5

EXPERIMENTS ON THE MOISTURE TRANSPORT IN ROOF CONSTRUCTIONS FOR CONTROLLED EXPOSURE CONDITIONS

5.1 Experimental procedure

In order to obtain data about the behaviour of roofs of cellular concrete specimens were exposed to several climatic conditions in one of the climate rooms, shown in Fig. 5.1, in a similar way as discussed in [1]. The climate rooms were constructed as two sections of a box; the insulated top half could be raised by cables for obtaining access to the interior. The specimens were mounted horizontally dividing the box in an upper and a lower chamber, in each of which the air was maintained at selected conditions. In the lower chamber internal conditions were simulated and in the upper chamber external ones. The climate in the lower chamber was for some measurements adjusted at an internal temperature $T_i = 23\,^{\circ}\mathrm{C}$ and a relative humudity $h_i = 60\%$, for other measurements the exposure conditions were $T_i = 23\,^{\circ}\mathrm{C}$, $h_i = 70\%$. These conditions were realised by means of electrical heating and an air humidifier. In the upper chamber summer as well as winter conditions were simulated. For winter

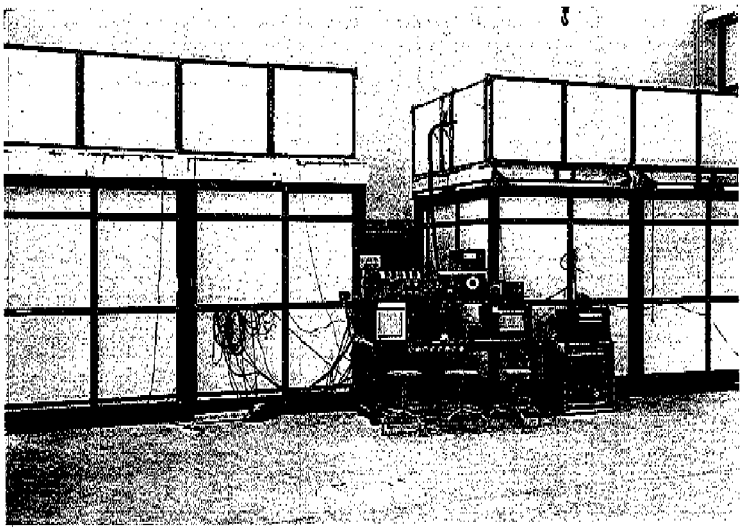

Fig. 5.1 Climate rooms for the investigation of the moisture behaviour of specimens.

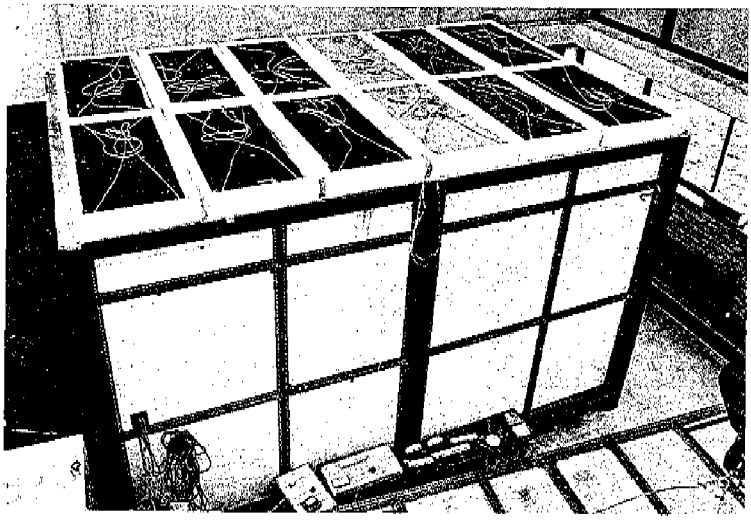

Fig. 5.2 Specimens provided with roofing and insulation, mounted on the lower chamber; the upper chamber is in a raised position.

conditions a temperature $T_e = 0°C$ was maintained, by means of a refrigerator. For summer conditions the refrigerator was switched off and consequently the temperature in the upper chamber increased untill about $T_e = 23°C$.

The floor surface of the climate room, and consequently also the surface available for the specimens amounted to 4×2.5 m^2. This area was divided in twelve parts, making it possible to investigate twelve specimens at the same time (see Fig. 5.2). The specimens consisted of parts of cellular concrete slabs, with a size of about 50×110 cm^2, which on the upper face and along the sides were provided with roofing and also were insulated along the sides, to reduce the transverse flow of heat and the influence of edge effects in each specimen. During the exposure periods the moisture content in the specimens was determined at regular intervals by weighing.

Also the heat resistance of the specimens was measured by means of heat-flow meters (manufactured by the Institute of Applied Physics, TNO-TH), [2], in contact with the upper side of the specimens.

The measurements have been performed on the three manufactures of cellular concrete mentioned in Chapter 3. From each manufacture two identical specimens were investigated, the data of which are given in Table 5.1. The measurements have been carried out for simulated summer conditions as well as for simulated winter conditions. During the summer conditions the moisture content in the specimens decreased, while during winter conditions the moisture content increased. Therefore

Table 5.1 Data concerning the specimens investigated

construction	specific mass without reinforcing (kg/m^3)	horizontal dimensions (cm × cm)
10 cm Durox with roofing	700	50 × 110
10 cm Siporex with roofing	730	50 × 110
10 cm Ytong with roofing	680	60 × 110

the winter periods were started with "dry" specimens (2 vol.% moisture), while for the summer periods the initial moisture content amounted to 25 vol.%.

5.2 Results

In the Figs. 5.3 and 5.4 the course of the moisture content in the specimens, averaged over the thickness, is given during the summer and winter exposure conditions. The three types of cellular concrete turned out to behave in about the same manner; therefore only the average course of the moisture content is given.

The rate of increase of the average moisture content during winter conditions turned out to be quite constant – at least during the exposure period of six months – and relatively low. The drying rate during summer conditions turned out to be much higher and strongly dependent on the moisture content in the specimens. During the first months when the moisture content was high the drying rate was much higher than in a later stage, at a lower moisture content. Therefore in Table 5.2, where the most important results are presented, the drying rate is given for several values of the average moisture content in the specimens.

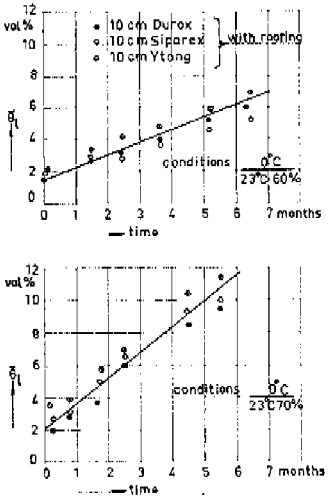

Fig. 5.3
Increase of the average moisture content, $\bar{\theta}_l$, in specimens of cellular concrete exposed to winter conditions.

Fig. 5.4
Decrease of the average moisture content, $\bar{\theta}_t$, in specimens of cellular concrete exposed to summer conditions.

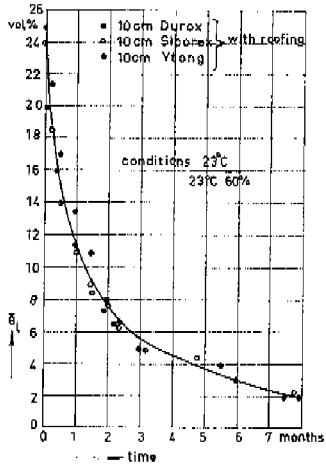

Table 5.2 Rate of change of the average moisture content in cellular concrete specimens, 10 cm thick, exposed to controlled winter and summer conditions.

conditions				average moisture content	rate of change of the average moisture content	
winter/summer	T_i(°C)	h_i(%)	T_e(°C)	(vol.%)	increase/decrease	vol.%/month
winter	23	60	0	–	increase	0.8
	23	70	0	–	increase	1.6
summer	23	60	23	20	decrease	25
	23	60	23	15	decrease	10
	23	60	23	10	decrease	4
	23	60	23	5	decrease	1

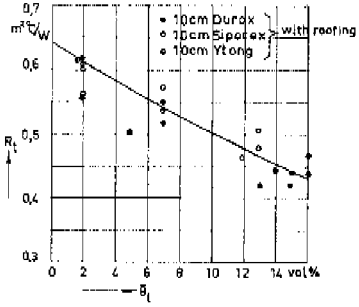

Fig. 5.5
Thermal resistance, R_t, (inclusive heat transfer resistances) of specimens of cellular concrete as a function of the average moisture content $\bar{\theta}_t$.

In Fig. 5.5 the measured heat resistances of the specimens are given as a function of the average moisture content. Strictly speaking the heat resistance does not depend on the average moisture content only, but also on the moisture distribution. So for instance the heat resistance for a uniform moisture distribution is lower than in the case where the moisture is mainly present underneath the roofing. However for increasing as well as for decreasing moisture content the moisture is for the greater part assembled under the roofing, so that similar moisture distributions can be expected, and the heat resistance can be represented as a function of the average moisture content without the occurrence of great deviations.

References

1. F. J. Powel and H. E. Robinson, Measurement of effect of moisture on heat transfer through insulated flat-roof constructions, Special technical report No. 312, Symposium on methods on testing building constructions, American Society for Testing and Materials, (1960).
2. J. de Jong and L. Marquenie, Instr. Pract. **16**, 45 (1962).

Chapter 6

CALCULATIONS OF THE MOISTURE TRANSPORT IN ROOF CONSTRUCTIONS FOR CONTROLLED EXPOSURE CONDITIONS

As discussed in Section 2.2.2 for certain simplified circumstances – such as constant climatic conditions and a uniform initial moisture content in the roof – the moisture change in roof constructions can be calculated with a simplified calculation procedure. The complete calculation of the moisture transport however is much more complicated and in fact can only be done by means of a digital computer. In Section 6.1 this calculation is performed for the climatic conditions for which the experiments discussed in Chapter 5 were carried out. In Section 6.2 the results calculated in this way are compared with the experimental ones.

6.1 Calculation method

The moisture transport in a roof construction can be described by Eq. (2.35). Application of the continuity requirement yields

$$\partial \theta_l/\partial t = \partial/\partial z[D_\theta(\partial \theta_l/\partial z) + D_T(\partial T/\partial z)], \tag{6.1}$$

which gives the change of moisture content as a result of the moisture and temperature gradients in the vertical direction.

If the roof extends from $z = 0$ to $z = d$ the boundary conditions are:

$$q/\varrho_l = 0, \quad t > 0, \quad z = d, \tag{6.2}$$

and

$$q/\varrho_l = \beta(p_i - p_s), \quad t > 0, \quad z = 0. \tag{6.3}$$

Condition (6.2) is connected with the presence of the watertight roofing; condition (6.3) represents the moisture flux at the lower face of the roof. Here β is the mass transfer coefficient, p_i the vapour pressure in the air underneath the roof and p_s the vapour pressure in the roof material on the lower face. Also the initial condition:

$$\theta = \theta_0(z), \quad t = 0, \quad 0 \leqslant z \leqslant d \tag{6.4}$$

has to be satisfied where $\theta_0(z)$ is the initial distribution of the moisture content in the roof.

The temperature gradient $\partial T/\partial z$ at the different places in the roof can be calculated from the temperature difference over the roof, the heat-transfer coefficients on the

upper and lower face of the roof and the thermal conductivity of the material. Here the dependance of λ on θ_l has to be taken into account. The (apparent) thermal conductivity of a moist material however, is not a unique function of the moisture content, since it is connected with the amount of moisture transport. Strictly speaking the boundary conditions for moisture transport have to be fixed and horizontal or vertical transport and stationary or instationary circumstances have to be distinguished. A theoretical analysis of the influence of moisture transport on thermal conductivity has been given by De Vries and Peck [1], for the case of instationary measurements with the cylindrical probe method. A similar analysis for our case shows that the influence mentioned above only gives rise to small corrections for the temperatures to be expected in roof constructions (usually below 40°C). Therefore the calculation of the temperature gradients in the roof has been based on the relation $\lambda = \lambda(\theta_l)$, determined in Section 3.5.

To solve non-linear differential equations with concentration dependent diffusion coefficients of the type of Eq. (6.1) Klute and Philip (see Section 2.1.1) have given analytical as well as numerical solution methods, be it only for isothermal circumstances. These methods however, are not applicable to the case considered here, because the diffusion coefficients D_θ and D_T vary greatly with θ_l, and because the circumstances are not isothermal, so that the moisture transport due to a temperature gradient has to be considered too.

We also tried to solve the problem under consideration by means of an electrical analogue. Casanova [2] investigated the drying processes of moist materials for isothermal conditions with an electrical R-C network similar to the well-known Beukenmodel [3]. For this purpose he used the transport equations given by Krischer (see Section 2.1.2).

By choosing convenient scale factors the analogue could be operated stepwise on a slow time-scale, making it possible to adjust the resistance values as a function of the electrical potential in correspondance with the variation of the analogous moisture diffusivity as a function of the moisture content.

In this way moisture transport equations of the type of Eq. (6.1) can also be solved be it only for isothermal circumstances. In order to allow for moisture transport under non-isothermal circumstances as well, we extended the electrical analogue in such a way that it was possible to determine alternatively the contribution of the moisture transport due to the moisture gradient and the contribution due to the temperature gradient.

A description of this analogue is given in [4]. In this way we examined the moisture transport in roof constructions under winter as well as summer conditions. The method turned out to be only partly suitable for the problems considered here, mainly as a consequence of the strong variability of the diffusivities D_θ and D_T, especially for low moisture contents (2–5 vol.%). For this reason the time increments had to be reduced strongly to get accurate results.

In a more suitable way the calculations could be performed with a digital computer.

In order to be able to compare the values calculated in this way with the experimental ones obtained in the climate rooms, the calculations were carried out for the same conditions as for which the experiments were performed. In the numerical method applied here the coordinate z, and consequently the thickness of the roof, is divided into increments Δz and the time t in increments Δt. The time increments are indicated by m, the place increments by k, so layer k in the roof extends between the boundaries $(k-\frac{1}{2})\Delta z$ and $(k+\frac{1}{2})\Delta z$. The moisture content of layer k in time $m\Delta t$ is given by θ_k^m, where the subscripts denote the position increment and the superscripts the time increment.

The left-hand side of Eq. (6.1) now can be approximated by:

$$\frac{\partial \theta}{\partial t} \rightarrow \begin{cases} \dfrac{\theta_k^{m+1} - \theta_k^m}{\Delta t} & (6.5) \\ \text{or} & \\ \dfrac{\theta_k^m - \theta_k^{m-1}}{\Delta t} & (6.6) \end{cases}$$

The right-hand side is approximated by:

$$\frac{\partial}{\partial z}\left(D_\theta \frac{\partial \theta}{\partial z} + D_T \frac{\partial T}{\partial z}\right) \rightarrow \left[D_{\theta_{k-\frac{1}{2}}} \frac{(\theta_{k+1}^m - \theta_k^m)}{(\Delta z)^2} + D_{T_{k+\frac{1}{2}}} \frac{\Delta T}{(\Delta z)^2}\right] - \left[D_{\theta_{k-\frac{1}{2}}} \frac{(\theta_k^m - \theta_{k-1}^m)}{(\Delta z)^2} + D_{T_{k-\frac{1}{2}}} \frac{\Delta T}{(\Delta z)^2}\right]. \quad (6.7)$$

Here the difference equation (6.5) is associated with point k, $m+\frac{1}{2}$ and the difference equation (6.6) with the point k, $m-\frac{1}{2}$, while the difference equation (6.7) is associated with the point k, m. The diffusivities D_θ and D_T are connected, for the time being, with the moisture contents at the boundaries $(k-\frac{1}{2})\Delta z$ and $(k+\frac{1}{2})\Delta z$.

The difference equations now can be combined in several manners. According to the Schmidt method [5] Eqs. (6.5) and (6.7) are combined, leading to:

$$\frac{\theta_k^{m+1} - \theta_k^m}{\Delta t} = \left[D_{\theta_{k+\frac{1}{2}}} \frac{(\theta_{k+1}^m - \theta_k^m)}{(\Delta z)^2} + D_{T_{k+\frac{1}{2}}} \frac{\Delta T}{(\Delta z)^2}\right] - \left[D_{\theta_{k-\frac{1}{2}}} \frac{(\theta_k^m - \theta_{k-1}^m)}{(\Delta z)^2} + D_{T_{k-\frac{1}{2}}} \frac{\Delta T}{(\Delta z)^2}\right]. \quad (6.8)$$

In this method the calculation procedure is fairly simple because in this equation three known θ_l-values occur (on time m) and one unknown (on time $m+1$), which can be calculated easily. A disadvantage however is the instability of the method. It can be proved that the method has a good stability only when the condition

$$D_0 \frac{\Delta t}{(\Delta z)^2} \leqslant \tfrac{1}{2} \tag{6.9}$$

is satisfied.

A better stability is obtained with the methods of Crank and Nicholson [6] or Liebmann [7]. Crank and Nicholson combined Eq. (6.5) with the average value of the second order differential coefficient associated with the points (k, m) and $(k, m+1)$. In this way an expression was obtained for which the left-hand side as well as the right-hand side pertained to the point $(k, m+\frac{1}{2})$. According to this method Hanks et al. [8] solved the moisture flow equation for infiltration into layered soils, using a IBM 650 computer. Liebmann combined Eqs. (6.6) and (6.7). In both methods each of the resulting equations comprises 3 unknowns i.e. the moisture contents at the points $k-1$, k and $k+1$ at the time $m+1$ or at the time m respectively. Combination of all equations however leads to k equations with k unknowns making it possible to solve the system of equations.

Here the calculation is performed according to the Schmidt-method. The change of moisture content $(\theta_k^{m+1} - \theta_k^m)$ in Eq. (6.8) is considered as to be consisting of a component DTO, as a result of the moisture transport at the boundary $(k-\frac{1}{2})\Delta z$ and a component DTK, as a result of the moisture transport at the boundary $(k+\frac{1}{2})\Delta z$. Thus

$$(\theta_k^{m+1} - \theta_k^m) = \text{DTO} - \text{DTK} \tag{6.10}$$

where

$$\text{DTO} = \left[D_{\theta_{k-\frac{1}{2}}} \frac{(\theta_{k-1}^m - \theta_k^m)}{\Delta z} - D_{T_{k-\frac{1}{2}}} \frac{\Delta T}{\Delta z} \right] \frac{\Delta t}{\Delta z}, \tag{6.11}$$

and

$$\text{DTK} = \left[D_{\theta_{k+\frac{1}{2}}} \frac{(\theta_k^m - \theta_{k+1}^m)}{\Delta z} - D_{T_{k+\frac{1}{2}}} \frac{\Delta T}{\Delta z} \right] \frac{\Delta t}{\Delta z}. \tag{6.12}$$

Since the component DTK devoted to layer k is equal to the component DTO devoted to layer $k+1$, only the component DTK for the several layers have to be calculated. For the top layer (layer DIKTE) DTK $= 0$ as a consequence of the watertight roofing (condition (6.2)).

The component DTO for the first layer is related to the moisture flux density between the adjacent air layer and the first layer of the roof, given by Eq. (6.3). Here p_s can be written as

$$p_s = h p_{vss}, \tag{6.14}$$

where h is the relative humidity, corresponding with the moisture content in the material by the relation $h = h(\theta_l)$ and p_{vss} is the saturation vapour pressure, corresponding with the temperature T_s on the bottom side of the roof.

The component DTO of layer I now can be written as:

$$\mathrm{DTO} = \frac{\beta(p_i - h p_{oss})\Delta t}{\Delta z} = \frac{\beta p_i \Delta t}{\Delta z} - \frac{\beta h p_{oss}\Delta t}{\Delta z}. \tag{6.15}$$

The component DTK of layer I can than be calculated from Eq. (6.12).

The moisture content θ_i of layer I calculated in this way turns out to be hardly different from the hygroscopic moisture content θ_h. In spite of this the calculation is performed with this comprehensive method for making it possible to calculate also the moisture transport when temporarily condensation occurs against the bottom side of the roof as a consequence of a high internal vapour pressure.

The calculations have been performed on a TR 4 computer, by means of the program given on pages 76 to 79. The following symbols have been used:

DC11.10^{-6} = diffusivity D_θ due to a moisture gradient.
TETA[K] = moisture content θ_k of layer k.
DX = thickness Δz of a layer.
XD = $1/\Delta z$.
STAP = time increment Δt, over which the change of moisture content is calculated.
TX[K] = temperature difference ΔT over layer k.
DC22. 10^{-8} = diffusivity D_T due to a temperature gradient.
DTO = moisture change of layer k, due to moisture flow at the boundary $(k-\frac{1}{2})\Delta z$.
DTK = moisture change of layer k, due to moisture flow at the boundary $(k+\frac{1}{2})\Delta z$.
HEATRES = thermal resistance R_i of the roof.
LABDATET = thermal conductivity λ.
BETA = mass transfer coefficient β.
RVO = relative humidity h.
CMAX = saturation vapour pressure p_{vs}.
DIKTE = thickness of the roof.
START = first month for which moisture transport is calculated.
EINDE = last month for which moisture transport is calculated.
PIEK = time interval during which a high inside-vapour pressure exists.
MTE = average monthly outside temperature.
MTI = average monthly inside temperature.
MCI = average monthly inside vapour pressure.
MCIP = high inside vapour pressure during time interval PIEK.

The program is illustrated by means of a simplified flow diagram, given on page 80. For that purpose the main calculations are denoted with the labels A to F, corresponding with the lables in the program.

Label A

At A the following data, given on page 79, are read:

a. D_θ-values (10^{-6} m^2/h) as a function of θ_l,
b. D_T-values (10^{-8} m^2/h °C) as a function of θ_l,
c. h-values (−) as a function of θ_l,
d. p_{vs}-values (N/m^2) as a function of T,
e. λ-values (W/m °C) as a function of θ_l.

Each of these quantities have been given for 71 points namely from 0 to 10 vol.% (or °C) in steps of 0.25 and from 11 to 40 vol.% (or °C) in steps of 1 unit. In the range 0 to 10 vol.% the data have been given with a smaller step in connection with the strong variation of the D_θ-, D_T- and h-values. These quantities are interpolated in steps of 0.05 vol.% (or °C) by the procedure LEES(ARR) and stored in a memory, so that during the calculation the data for the moisture contents (or temperatures) under consideration are available.

Label B

At B the data given on page 79 are read, relating to the calculation of the moisture increase of a 10 cm thick cellular concrete roof, exposed to the conditions 23 °C 60% internal and 0 °C external. For the conditions considered here these successively are:

DIKTE: thickness of the roof = 10.
START: first month, for which moisture transport is calculated = 1.
EINDE: last month, for which moisture transport is calculated = 6.
BETA: mass-transfer coefficient $\beta = 1.08 \times 10^{-7}$.
STAP: time interval over which the change of moisture content is calculated = 1.
PIEK: time interval, during which a high inside-vapour pressure exists = 1.
MTE: average monthly outside-temperatures = 0 (12 ×).
MTI: average monthly inside-temperatures = 23 (12 ×).
MCI: average monthly inside-vapour pressures = 1686 (12 ×).
MCIP: average monthly high inside-vapour pressures = 1686 (12 ×).
TETA: initial moisture distribution = 1.5 (10 ×).

The data PIEK and MCIP are connected with the calculation of the moisture flow during periods of high vapour production, which especially occur in bathrooms and kitchens. During these periods, PIEK, the calculation is performed with the inside vapour pressure MCIP instead of MCI. When the value of MCIP is higher than the saturation vapour pressure corresponding with the surface temperature of the roof, „surface condensation" occurs. During the remaining part of the day the roof partly dries out again. The numerical values of MCIP and MCI are the same in the example given above, because they refer to a case where no peak values are taken into account.

Label D

At D the temperature gradients in the roof, the thermal resistance, R_t, of the roof, the surface temperature, T_s, at the lower side of the roof, and the saturation vapour pressure, p_{vss}, at this temperature are calculated. These calculations are given below, together with the equations, expressed in the usual symbols, which are placed between brackets.

D1: HEATRES = 0.043+0.129; (R_i+R_o)
D2: J = 2000×TETA[K]; TX[K] = DX/LABDATET[J]; ($R_k=\Delta z/\lambda_k$)
D3: HEATRES = HEATRES+TX[K]; ($R_t = R_i+R_e+\Sigma R_k$)
D4: GRAD = T/HEATRES; ($\Delta T/R_t$)
D5: TX[K] = GRAD×TX[K]; ($\Delta T_k = (R_k/R_t)(T_i-T_e)$)
D6: TX[0] = 0.129×GRAD; TOPP = TIN−TX[0]; ($T_s=T_i-(R_i/R_t)(T_i-T_e)$)
D7: B = 20× TOPP; J = ENTIER(B); (calculation p_{vss} at T_s)
D8: C4 = CMAX[J]+(B−J)×(CMAX[J+1]−CMAX[J]);
(linear interpolation)

Label E

At E the moisture flow penetrating into the roof is calculated, according to Eq. (6.15). This calculation has been included in the program at E1 to E7.

E1: C3 = BETA×XD×STAP; $\left(C3=\frac{\beta\Delta t}{\Delta z}\right)$
E2: RV[H] = C3×RVO[H]; $\left(RV=\frac{\beta h\Delta t}{\Delta z}\right)$
E3: A = TETA[1]; AA = 2000×A; L = AA; (calculation h for θ_1)
E4: C5 = RV[L]; C5 = C5+(AA−L)×(RV[L+1]−C5); (linear interpolation)
E5: C1 = C3×MCI[N]; $\left(C1=\frac{\beta p_i\Delta t}{\Delta z}\right)$
E6: C4 = CMAX[J]+(B−J)×(CMAX[J+1]−CMAX[J]); (calculation p_{vss} for T_s)
E7: DTO = C1−C4×C5; $\left(DTO=\frac{\beta p_i\Delta t}{\Delta z}-\frac{\beta h p_{vss}\Delta t}{\Delta z}\right)$

Label F

At F the change of moisture content of layer k is calculated due to the moisture flow from layer k to layer $k+1$. This calculation has been carried out with Eq. (6.12) and has been included in the program at F1 to F7.

F1: C1 = 10^{-6}×XD×XD×STAP; $\left(C1=\frac{10^{-6}\Delta t}{\Delta z\,\Delta z}\right)$
C2 = 10^{-2}×C1; $\left(C2=\frac{10^{-8}\Delta t}{\Delta z\,\Delta z}\right)$

F2: DC1[H] = C1 × DC11[H]; $\left(DC1 = \frac{D_\theta 10^{-6}\Delta t}{\Delta z\,\Delta z}\right)$

DC2[H] = C2 × DC22[H]; $\left(DC2 = \frac{D_T 10^{-8}\Delta t}{\Delta z\,\Delta z}\right)$

F3: A = TETA[1]; $(A = \theta_k)$

AA = 2000 × A; L = AA;

F4: B = TETA[k+1]; $(B = \theta_{k+1})$

AA = 1000 × (A+B); J = AA; DC = DC1[J]; (calculation of D_θ for $\theta_l = \frac{\theta_k+\theta_{k+1}}{2}$ with linear interpolation)

F5: DC = DC+(AA−J) × (DC1[J+1]−DC)

F6: DTK = (A−B) × DC+TX[K] × DC2[L];

$\left(DTK = \frac{D_\theta(\theta_k-\theta_{k+1})10^{-6}\Delta t}{\Delta z\,\Delta z} - \frac{D_T 10^{-8}\Delta T\Delta t}{\Delta z\,\Delta z}\right)$

F7: TETA[K] = A+DTO−DTK; $(\theta_k^{m+1} = \theta_k^m + DTO - DTK)$

```
BEREKENING VOCHTGEHALTE IN EEN DAKCONSTRUCTIE.
*****************************************************************
'BEGIN'   'REAL' A,AA,B,C,BETA,CS,CI,T,DX,START,STAP,EINDE,HH,DTO,DTK
          TDAUW,DC,CIP,TIN,TOPP,GRAD,C1,C2,C3,C4,C5,HEATRES,XD,
          RECDIK,PIEK;
          'INTEGER' D,I,J,H,K,L,M,N,TIJD,DIKTE,DIKMIN,BTIJD,LTIJD;
          'REAL' 'ARRAY' HULP[0:40],MTE,MTI,MCI,MCIP[1:12],
          DC11,DC22,RVO,LABDATET,DC1,DC2,RV,CMAX[0:800];
          'BOOLEAN' ALFA;
          'PROCEDURE' LEES(ARR); 'REAL' 'ARRAY' ARR;
          'COMMENT' DE WAARDEN ZIJN VAN 0-10 PROCENT GEGEVEN IN
          STAPPEN VAN 0,25 PROCENT, VAN 10-40 PROCENT IN STAPPEN
          VAN 1 PROCENT. DEZE PROCEDURE INTERPOLEERT LINEAIR
          EN PRODUCEERT EEN REEKS WAARDEN MET STAPPEN VAN
          0,05 PROCENT;
  'BEGIN'   READ(HULP);
            'FOR' H:=0 'STEP' 1 'UNTIL' 39 'DO'
    'BEGIN'   A:=HULP[H]; B:=0,2*(HULP[H+1]-A); K:=5*H;
              'FOR' L:=0 'STEP' 1 'UNTIL' 4 'DO'
              ARR[K+L]:=A+L*B;
    'END';
              HULP[0]:=HULP[40];
              'FOR' H:=1 'STEP' 1 'UNTIL' 30 'DO' READ(HULP[H]);
              'FOR' H:=0 'STEP' 1 'UNTIL' 29 'DO'
    'BEGIN'   A:=HULP[H]; B:=0,05*(HULP[H+1]-A); K:=20*H+200;
              'FOR' L:=0 'STEP' 1 'UNTIL' 19 'DO' ARR[K+L]:=A+L*B;
    'END';
              ARR[800]:=HULP[30];
  'END';

        'PROCEDURE' TYD;
   'BEGIN' TIJD:=KLOK;
        PRINT(''
              REKENTIJD IS'',TIJD-LTIJD,''TOTAAL'',TIJD-BTIJD);
        LTIJD:=TIJD;
   'END';


  PRINT(''HB 4953/7-1-69/VISSER, VOCHTGEHALTE DAKCONSTRUCTIES'');
        BTIJD:=LTIJD:=KLOK;
        LEES(DC11);LEES(DC22);LEES(RVO);LEES(CMAX);LEES(LABDATET);
NOGEEN: READ(HULP); NLCR(3); PRINT(HULP); NLCR(3);
        READ(DIKTE,START,EINDE,BETA,STAP,PIEK,MTE,MTI,MCI,MCIP);
        PRINT(''DIKTE   BEGINMAAND   EINDMAAND''); NLCR(1);
        SPACE(2);TYPE(DIKTE);SPACE(8);TYPE(START);
        SPACE(11); TYPE(EINDE); WRITE(''
                                        STAP '');VASKO(1,2,STAP);
        WRITE('' UUR      '');WRITE(''PIEKTIJD'');VASKO(1,2,PIEK);
        WRITE(''UUR'');
        WRITE(''

              MAANDELIJKSE GEGEVENS:'');
        WRITE(''

              BUITENTEMPERATUREN'');VASKO(2,2,MTE,12);
        WRITE(''
              BINNENTEMPERATUREN'');VASKO(2,2,MTI,12);
        WRITE(''

              BINNENDAMPDRUKKEN     ''); VASKO(4,0,MCI,12);
        WRITE(''
              PIEK-BINNENDAMPDRUKKEN''); VASKO(4,0,MCIP,12);
```

```
'BEGIN''ARRAY' TETA[1:DIKTE],TX,DT[0:DIKTE];

        'PROCEDURE' TEMPDIST(TIK); 'BOOLEAN' TIK;
    'BEGIN'HEATRES:=0,043+0,129;
           'FOR' K:=1 'STEP' 1 'UNTIL' DIKTE 'DO'
      'BEGIN'J:=2000*TETA[K];  TX[K]:=DX/LABDATET[J];
             HEATRES:=HEATRES+TX[K]
      'END';
           GRAD:=T/HEATRES;
           'FOR' K:=1 'STEP' 1 'UNTIL' DIKTE 'DO'
           TX[K]:=GRAD*TX[K];
           TX[0]:=0,129*GRAD; TOPP:=TIN-TX[0];
           B:=20*TOPP; J:=ENTIER(B);
           C4:=CMAX[J]+(B-J)*(CMAX[J+1]-CMAX[J]);
           'IF' TIK 'THEN'
    'BEGIN'NLCR(2);'FOR' K:=0 'STEP'1'UNTIL'DIKTE'DO'VASKO(4,0,K);
           NLCR(1);'FOR' K:=0 'STEP' 1 'UNTIL' DIKTE 'DO'
           VASKO(2,2,TX[K]); WRITE(''TEMPGRAD
                                        '');
           C:=TIN; 'FOR' K:=0 'STEP' 1 'UNTIL' DIKTE 'DO' 'BEGIN'
           C:=C-TX[K]; VASKO(2,2,C)  'END';
           WRITE(''TEMP.
                        WARMTEWEERSTAND'');VASKO(1,4,HEATRES);
         C:=MCI[N]; TDAUW:=1000;
         'FOR' J:=20*TIN 'STEP' -1 'UNTIL' 0 'DO'
         'IF' CMAX[J] 'LESS' C 'THEN'
      'BEGIN' A:=CMAX[J]; B:=CMAX[J+1];
              TDAUW:=0,05-(J+(C-A)/(B-A)); 'GO TO' PROC;
      'END';
PROC:     WRITE(''     DAUWPUNT''); VASKO(2,3,TDAUW);
          WRITE(''   TOPP-TDAUW''); VASKO(2,3,TOPP-TDAUW);
    'END';
  'END' TEMPDIST;

     READ(TETA); WRITE(''
                        BEGINTOESTAND'');
     'FOR' K:=1 'STEP' 1 'UNTIL' DIKTE 'DO'  'BEGIN'
     A:=TETA[K]:=b-2-TETA[K]; VASKO(0,4,A)  'END';
     DX:=0,01; XD:=1/DX; DIKMIN:=DIKTE-1; RECDIK:=1/DIKTE;
     PIEK:=PIEK+0,995;
     C1:=b-6*XD*XD-STAP; C2:=b-2*C1; C3:=BETA*XD*STAP;
     'FOR' H:=0 'STEP' 1 'UNTIL' 300 'DO'
  'BEGIN' DC1[H]:=C1*DC11[H];DC2[H]:=C2*DC22[H];RV[H]:=C3*RVO[H]
  'END';
        TYD;
```

```
            'FOR' M:=START 'STEP' 1 'UNTIL' EINDE 'DO'
   'BEGIN'  NPAG; WRITE(''MAAND''); VASKO (2,0,M);
            N:=M-12-ENTIER(M/12.1); SPACE(10);
            WRITE(''TEMP. BINNEN   BUITEN / DAMPDRUK   PIEK
                                                    '');
            SPACE(24); VASKO(2,3,MTI[N],MTE[N]); SPACE(5);
            VASKO(4,0,MCI[N],MCIP[N]);
            CI:=C3+MCI[N];  CIP:=C3+MCIP[N]; TIN:=MTI[N];
            T:=TIN-MTE[N];  TEMPDIST('TRUE');
            B:=2000*TETA[1]; L:=ENTIER(B+0.5); C5:=RV[L];
            C5:=C5+(B-L)*(RV[L+1]-C5);
            A:=720/(STAP*DIKTE)*(CI-C4*C5);
            WRITE(''
VERWACHTE WIJZIGING GEMIDDELDE VOCHTGEHALTE (MAAND) ''); VASKO(1,4,A);
            NLCR(2); SPACE(5);
            'FOR' K:=1 'STEP' 1 'UNTIL' DIKTE 'DO' VASKO(4,0,K);
            WRITE(''  GEMID.
                          BEGIN'');
            'FOR' K:=1 'STEP' 1 'UNTIL' DIKTE 'DO' VASKO(0,4,TETA[K]);

            'FOR' D:=1 'STEP' 1 'UNTIL' 30 'DO'
      'BEGIN'TEMPDIST('FALSE');
            'FOR' HH:=1 'STEP' STAP 'UNTIL' 24.001 'DO'
        'BEGIN' A:=TETA[1]; AA:=2000*A; L:=AA;
            C5:=RV[L]; C5:=C5+(AA-L)*(RV[L+1]-C5);
            'COMMENT' LINEAIRE INTERPOLATIE VAN REL. VOCHTIGHEID;
            'IF' HH 'LESS' PIEK 'THEN' DTO:=C1P-C4*C5 'ELSE'
            DTO:=CI-C4*C5;
            'FOR' K:=1 'STEP' 1 'UNTIL' DIKMIN 'DO'
         'BEGIN' B:=TETA[K+1]; AA:=1000*(A+B); J:=AA; DC:=DC1[J];
            DC:=DC+(AA-J)*(DC1[J+1]-DC);
            DTK:=(A-B)*DC+TX[K]*DC2[J];
            TETA[K]:=A+DTO-DTK;
            A:=B; L:=2000*A; DTO:=DTK;
         'END';
            TETA[DIKTE]:=TETA[DIKTE]+DTO;
        'END' UREN;
            'COMMENT'  DE WAARDE VAN DTK GEEFT DE DOORSTROMING
            DOOR HET DENKBEELDIGE VLAK OP DE PLAATS K,
            TETA[K] IS HET VOCHTGEHALTE TUSSEN K-1 EN K;

            NLCR(1); VASKO(2,0,D); C:=0;
            'FOR' K:=1 'STEP' 1 'UNTIL' DIKTE 'DO'  'BEGIN'
            A:=TETA[K]; C:=C+A; VASKO(0,4,A)  'END';
            VASKO(2,4,C*REGDIK);
       'END' DAGEN;

            TEMPDIST('TRUE');  TYD;
     'END' MAANDEN;
  'END';
        FOUT: NPAG; 'GO TO' NOGEEN;
'END';
*****************************************************************###
```

```
                ****************************************************
==A6,U=6oo,R=15,VOCHTGEHALTE DAKCONSTRUCTIES,
*****************************************************************
2.1o,
2.1o, 3.36, 5.41, 7.2o, 9.55, 13.4, 14.3, 1o.3, 6.4o, 3.8o,
2.7o, 2.1o, 1.8o, 1.4o, 1.2o, 1.2o, 1.2o, 1.2o, 1.2o, 1.25,
1.27, 1.3o, 1.32, 1.35, 1.37, 1.4o, 1.45, 1.47, 1.5o, 1.55,
1.6o, 1.7o, 1.75, 1.85, 1.95, 2.oo, 2.1o, 2.2o, 2.35, 2.5o,
3.1o, 3.8o, 4.7o, 5.6o, 7.oo, 8.5o, 1o.5, 13.o, 16.o, 2o.o,
24.o, 3o.o, 38.o, 47.o, 6o.o, 75.o, 95.o, 125 , 16o , 2oo ,
27o , 3oo , o , o , o , o , o , o , o , o ,
'COMMENT' DTETA 23-3-69;**********************

o.oo,
o.o18,o.o55,o.1o1,o.183, o.29, o.37 , o.43, o.48, o.55, o.66,
o.74, o.85, 1.oo, 1.15, 1.25, 1.35, 1.45, 1.5o, 1.6o, 1.7o,
1.75, 1.8o, 1.9o, 2.oo, 2.1o, 2.2o, 2.3o, 2.4o, 2.5o, 2.7o,
2.85, 3.oo, 3.1o, 3.25, 3.4o, 3.5o, 3.6o, 3.8o, 3.9o, 4.oo,
4.75, 5.4o, 6.oo, 6.7o, 7.2o, 7.8o, 8.5o, 9.oo, 1o.o, 1o.5,
11.3, 12.o, 13.o, 14.o, 14.5, 14.5, 14.5, 14.3, 13.6, 12.o,
 9.5,  6.1,  o.54,o.53, o.52, o.51, o.5o, o.49, o.48, o.47,
'COMMENT ' DT 25-3-69;**************************
o.oo,o.o15,o.o45,o.o83,o.13o,o.24,o.36,o.54,o.68,o.76,o.8o,
o.825,o.85,o.87,o.885,o.9,o.91,o.925,o.93,o.94,o.945,
o.95,o.955,o.96,o.96,o.96,o.965,o.97,o.97,o.975,o.98,
o.98,o.98,o.985,o.985,o.99,o.99,o.995,o.995,1,1,
1,1,1,1,1,1,1,1,1,1,
1,1,1,1,1,1,1,1,1,1,
1,1,1,1,1,1,1,1,1,1,
'COMMENT' RV 19-6-68;
*****************
61o,
  622,  635,  647,  66o,  672,  685,  697,  71o,  722,  735,
  747,  76o,  772,  785,  797,  81o,  825,  84o,  855,  87o,
  886,  9o2,  919,  935,  951,  967,  984, 1ooo, 1o17, 1o35,
 1o52, 1o7o, 1o9o, 111o, 113o, 115o, 117o, 119o, 121o, 123o,
 131o, 14oo, 15oo, 16oo, 171o, 182o, 194o, 2o6o, 22oo, 234o,
 249o, 265o, 281o, 299o, 317o, 335o, 356o, 377o, 399o, 423o,
 45oo, 476o, 5o3o, 532o, 563o, 595o, 628o, 663o, 7ooo, 74oo;
'COMMENT' MAXIMALE VOCHTGEHALTE ALS FUNCTIE VAN DE TEMPERATUUR,CMAX;
 *****************
o.185,
o.188,o.193,o.196,o.2oo,o.2o2,o.2o5,o.2o7,o.21o,o.212,o.215,
o.217,o.22o,o.222,o.225,o.227,o.23o,o.234,o.237,o.241,o.245,
o.247,o.25o,o.252,o.255,o.257,o.26o,o.262,o.265,o.268,o.272,
o.276,o.28o,o.282,o.285,o.287,o.29o,o.292,o.295,o.297,o.3oo,
o.315,o.325,o.335,o.345,o.36 ,o.37 ,o.38 ,o.39 ,o.4o3,o.415,
o.425,o.44 ,o.45 ,o.46 ,o.47 ,o.485,o.495,o.5o5,o.52 ,o.53 ,
o.54 ,o.55 ,o.565,o.575,o.585,o.6o ,o.61 ,o.62 ,o.635,o.645;
'COMMENT' WARMTEGELEIDINGSVERMOGEN ALS FUNCTIE VAN HET
 VOCHTGEHALTE, LABDATET  7-8-68;
 ******************

1o,  1,  6,  1.o8b-7,  1,  1,
***********
o,o,o,o,o,o,o,o,o,o,o,o,
23,23,23,23,23,23,23,23,23,23,23,23,
******
1686,1686,1686,1686,1686,1686,1686,1686,1686,1686,1686,1686,
1686,1686,1686,1686,1686,1686,1686,1686,1686,1686,1686,1686,
***********
1.5,1.5,1.5,1.5,1.5,1.5,1.5,1.5,1.5,1.5,1.5,1.5,
****************************************
```

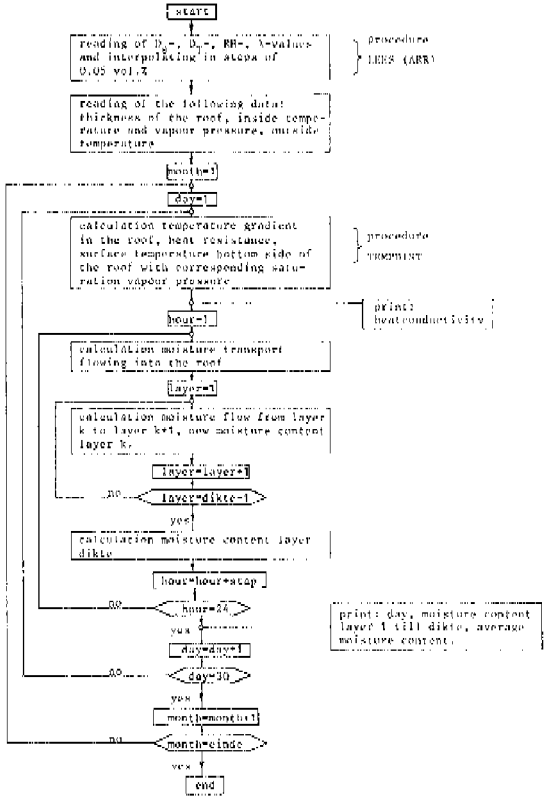

In the way discussed above the moisture transport is calculated in a roof of cellular concrete, exposed to the same summer and winter conditions for which also the experiments, discussed in Chapter 5, have been carried out. As the measurements of the diffusivities D_θ and D_T (see Sections 3.5 and 3.6) show a rather wide spread, the D_θ and D_T-curves have been adjusted within the range of uncertainty in such a way that the best agreement was found between the results calculated with these diffusivities and the experiments.

First the D_θ-curve has been adjusted on the basis of the drying curves from the roof constructions for isothermal summer conditions. Starting from this D_θ-curve next the D_T-curve was adjusted on the basis of the curves for moisture increase for winter conditions.

Both curves have been presented in Fig. 6.1 together with those derived from the measurements (Section 3.5 and 3.6) for increasing moisture content. Both the D_θ-

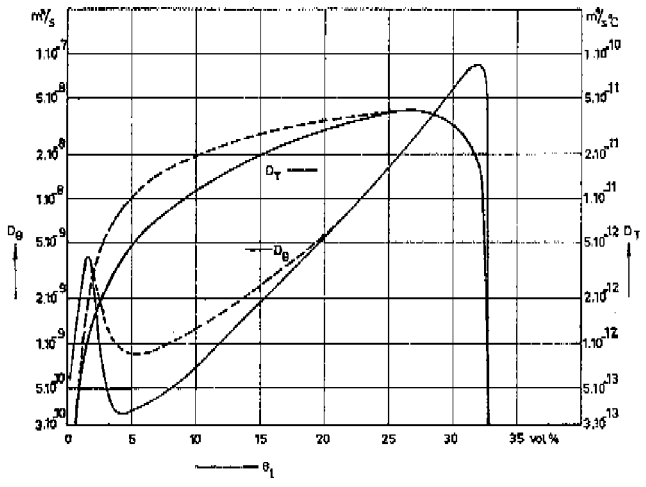

Fig. 6.1 The diffusioncoefficients D_θ and D_T as a function of the moisture content, θ_l.

——— values, applied in computer program
– – – – – values, experimentally determined

curve and the D_T-curve had to be adjusted to lower values; the values of ε remaining approximately the same. The reasons for the discrepansies between the values of D_θ found here and those found in Chapter 3 are not yet understood. One of the possible factors can be the presence of reinforcing in the roof constructions by which locally the structure of the material is changed and consequently also the moisture characteristics.

For low moisture contents ($\theta_l < 2$ à 4%) the diffusivities have been calculated from Eqs. (2.19) and (2.20), using the relation $h = h(\theta_l)$ of Fig. 3.7; this relation was also introduced in the computer program. In the present calculations the exact values of D_θ and D_T are extremely important due to their strong dependence on θ_l, especially for low moisture contents ($\theta_l < 5\%$).

The calculations of the moisture flux between layer k and layer $k+1$ of the roof were carried out with D_θ-values related to $(\theta_k+\theta_{k+1})/2$ and with D_T-values related to θ_k. This way of calculation turned out to give the most consistent results. Concerning the D_θ-values this was checked by calculating the moisture distributions for drying during summer conditions with a computer with D_θ-values related to θ_k, $(\theta_k+\theta_{k+1})/2$ and θ_{k+1} successively. Next from these moisture distributions D_θ-curves were derived in the way discussed in Section 3.6.1, and compared with the D_θ-curve originally used for the calculation. The D_T-values were related to θ_k because during winter conditions the increase of moisture content is defined mainly by the moisture

content in the surface layer. An exact D_T-value therefore is of more importance at the lower face of the roof than in the remaining part.

Information about the stability of the calculation method applied here is given by Eq. (6.9), which, with the highest possible D_θ-value ($D_\theta = 5.10^{-5}$ m^2/h at $\theta_l \approx 25\%$) and $\Delta z = 0.01$ m, yields the condition $\Delta t \leqslant 1$ h. The influence of the D_T-term has to be considered too. However, some preliminary calculations with Δt-values of 8, 4, 2, 1 and 0.5 h have proved that a really good stability is obtained for $\Delta t = 1$ h. In some cases Δt had to be decreased until 0.5 h.

About the accuracy of the calculations only little information is available. It was shown that when Δt was decreased to a certain value at which the calculation method had a good stability, a further reduction did not lead to a change in the profiles calculated. The accuracy was improved further by introducing linear interpolations at suitable places in the computer program (see for instance labels D8, E4 and F5).

It was not considered useful to compare results obtained with the computer with results calculated in an anlytical or numerical way (according to the methods given by Philip and Klute, see Section 2.1.1) because the latter calculations can be performed only for isothermal conditions and for certain simple $D_\theta(\theta_l)$-relations. A possible agreement of the results for simple $D_\theta(\theta_l)$-relations would not give information about an agreement for more complicated $D_\theta(\theta_l)$-relations, because the accuracy of the computer calculation depends also on the form of the $D_\theta(\theta_l)$-relation.

With the computer program discussed before the moisture transport in a 10 cm thick roof of cellular concrete has been calculated for exposure conditions given in Table 6.1.

Table 6.1 Exposure conditions for which the calculations were carried out

	internal		external
conditions	T_i (°C)	h_i (%)	T_e (°C)
summer conditions	23	60	23
winter conditions	23	60	0
	23	70	3

The calculations for winter conditions with internal conditions of 23°C 70% were carried out for an outside temperature of 3°C contrary to the experiments which were performed for an outside temperature of 0°C. The calculations had to be performed in this way because otherwise a surface temperature at the bottom of the roof was calculated lower than the dewpoint of the inside air, involving a too high rate of increase of moisture content. This discrepancy may have been caused by a too high outside temperature or a somewhat too low inside vapour pressure adjusted during the experiments or by a somewhat too low insulation value of the roof in the calculations. However the differences are only small and will only be found for those conditions at which nearly "surface condensation" occurs.

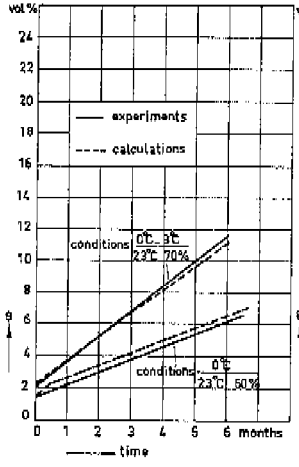

Fig. 6.2a
Increase of the average moisture content during winter conditions.

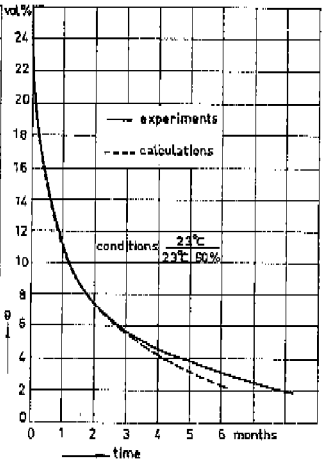

Fig. 6.2b
Decrease of the average moisture content during summer conditions.

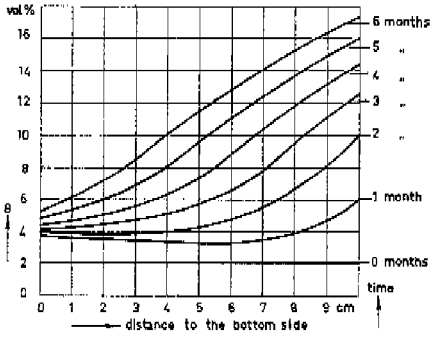

Fig. 6.3a
Calculated moisture distributions in a roof of cellular concrete exposed to the stationary winter conditions:
$T_i = 23\,°C$, $h_i = 70\%$, $T_e = 3\,°C$

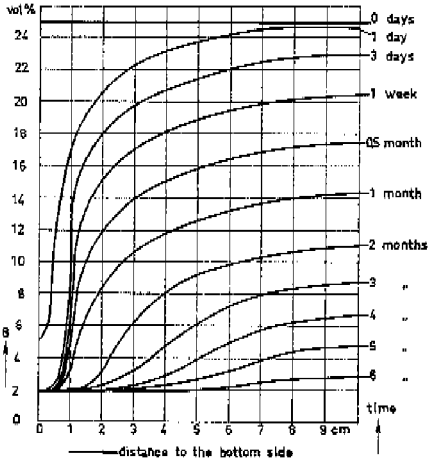

Fig. 6.3b
Calculated moisture distributions in a roof of cellular concrete exposed to the stationary summer conditions:
$T_i = 23\,°C$, $h_i = 60\%$, $T_e = 23\,°C$

The results calculated are given in Figs. 6.2 and 6.3 together with the experimental ones. Figs. 6.2a and 6.2b show the course of the average moisture content in the roof during winter and summer conditions respectively. The Figs. 6.3a and 6.3b show the corresponding calculated moisture distributions.

6.2 Comparison of experimental and calculated results

From the experiments given in Chapter 5 and the calculations described in the Sections 2.2.1, 2.2.2 and 6.1 the following results have been derived, concerning the rate of increase or decrease of the average moisture content in a roof exposed to winter and summer conditions. They are given in Table 6.2. The rate of decrease proves to be strongly dependent upon the moisture content in the roof, therefore this quantity has been given for several values of the average moisture content.

When we compare the calculated results with the results derived from experiments, according to the method of Glaser during winter conditions a too low rate of moisture increase proves to be calculated; at the conditions 23 °C 60%/0 °C this rate of moisture increase is 1,5 times too low, at the conditions 23 °C 70%/0 °C this rate of moisture increase is 2 times too low. Much greater differences exist, however, between the calculated and measured drying rates during summer conditions. Especially at high moisture contents the drying rate proves to be many times greater then is calculated according to the method of Glaser. This difference is caused in both cases by the fact that in this calculation method no attention is given to liquid flow but only to vapour transfer.

In the calculations at which the theory of Philip and De Vries is used liquid flow as well as vapour transfer have been considered. The values of the moisture increase during winter conditions, calculated by the "simple method" are in good agreement

Table 6.2 Rate of change of the average moisture content in a 10 cm thick cellular concrete roof exposed to controlled winter and summer conditions.

method by which the results have been obtained	rate of increase of the moisture content (vol.%/month) during winter conditions		rate of decrease of the moisture content (vol.%/month) during summer conditions (23°60%/23°) at an average moisture content of			
	23°60%/0°C	23°70%/0–3°C	20 vol.%	15 vol.%	10 vol.%	5 vol.%
measurements (Chapt. 5)	0.8	1.6	25	10	4	1
calculations with method of Glaser	0.5	0.8	0.6	0.6	0.6	0.6
calculations with theory of Philip & De Vries (simple procedure)	0.8	1.8	..	–	–	–
calculations with theory of Philip & De Vries (with computer)	0.8	1.5	35	9.6	3.2	1.5

with the values found from the experiments, while values concerning the drying rate during summer conditions cannot be calculated by this method. However these more complicated calculations can be performed in a satisfactory way by means of a computer. As can be seen the results calculated with a computer are in fair agreement with the experiments both for winter and summer conditions. From this we may conclude that the given computer program also may be used for the calculation of the moisture transport in cellular concrete roofs under circumstances occurring in practice.

References

1. D. A. de Vries, A. J. Peck, Austral. J. Phys. **11**, 409–423 (1958).
2. R. Casanova, Möglichkeit der Vorausbestimmung von Feuchtigkeitsverteilungen in technischen Trocknungsgütern mit Hilfe elektrischer Analogieversuche, Werkzaamheden industriële electrowarmtelaboratorium, P.L.E.M. (1965) Maastricht.
3. L. Beuken, Wärmeverluste bei periodisch betriebenen elektrischen Öfen, Diss. Bergak., Freiberg, (1936).
4. J. v. d. Kooi, K. T. Knorr, Toepassing van een elektrisch analogon met betrekking tot het vochttransport in niet geventileerde dakconstructies, rapport B II-17, Stichting Bouwresearch (1966).
5. E. Schmidt, Forsch. Ing. Wes. **13**, (1942) 177.
6. J. Crank and R. Nicholson, Proc. Cambr. Phil. Soc. **43**, (1947) 50.
7. G. Liebmann, Brit. J. Appl. Phys. **13**, (1962), 572.
8. R. J. Hanks, S. A. Bowers, Soil, Sc. Soc. Proc. **26**, (1962) 530.

Chapter 7

CALCULATION OF THE MOISTURE TRANSPORT IN ROOF CONSTRUCTIONS FOR CIRCUMSTANCES OCCURRING IN PRACTICE

7.1 Measurements of the in- and outdoor climates

To calculate the moisture transport in roof constructions under circumstances occurring in practice, we need data concerning the temperature and the vapour pressure of the in- and outdoor climate. Therefore, first measurements will be discussed to obtain these data.

The moisture content of the air inside a dwelling or building is governed by the following factors. First the moisture content of the inside air changes with the moisture content of the outside air, be it with some delay. This results in a low moisture content of the inside air during the winter season, because in this time the temperature, and consequently also the moisture content of the outside air, is low. For the same reason during summer the moisture content of the inside air is much higher.

In addition in a dwelling moisture is produced by the occupants themselves (by breathing, perspiring), by bathing and by housekeeping activities (cooking, washing, etc.). Also in some cases moisture is introduced by means of humidifying apparatus or moisture can penetrate via a dampy cellar or by way of leaky walls.

The discharge of moisture mainly occurs by ventilation with outside air, while also the moisture content is decreased by condensation on cold glass panes. Because during summer the ventilation rate is higher than during winter, the difference in moisture content between in- and outside air is in summer smaller than in winter.

Concerning the outdoor climate for the Netherlands extensive climatical data are available from the Royal Netherlands Meteorological Institute [1]. For De Bilt, the seat of the Institute, the average monthly temperatures and relative humidities are given in Table 7.1. Concerning the indoor climate however only few data are availabe. Measurements have been performed in Canada [2] and Germany [3], while also some measurements have been carried out in the Netherlands [4], [5]. To supplement these data own measurements were performed, the first results of which have been given in [6].

From these measurements it may be derived that the highest moisture content occurs in bath rooms and kitchens. The monthly average temperatures, T_i, and relative humidities, h_i, for heated kitchens have been given in table 7.1. The experimental results, however, appear to show a rather wide spread. In winter this spread is smaller than in summer. Though insufficient data are available to obtain exact information about the course of the variation, it follows from the measurements that roughly speaking the relative humidity of the inside air does not differ more than 10% (abso-

Table 7.1 Average monthly temperatures (T), relative humidities (h) and vapour pressures (p_v) for the outside climate and heated kitchens.

	outdoor climate ("normal")			indoor climate: measured values			indoor climate: increased values ("modified")		indoor climate: "peak"-values	
month	T_e (°C)	h_e (%)	p_{ve} (N/m²)	T_i (°C)	h_i (%)	p_{vi} (N/m²)	T_i (°C)	h_{im} (%)	T_i (°C)	h_{ip} (%)
January	2.3	88	633	19	41	902	19	51	19	96
February	2.5	84	613	19	41	902	19	51	19	96
March	4.9	78	679	20	42	983	20	52	20	95
April	7.8	73	774	21	44	1096	21	54	21	94
May	12.4	70	1008	23	48	1349	23	58	23	94
June	14.8	70	1176	23	51	1433	23	61	23	97
July	16.6	73	1380	23	53	1489	23	63	23	98
August	16.0	76	1383	23	52	1461	23	62	23	98
September	13.6	80	1248	23	49	1377	23	59	23	94
October	9.6	85	1020	22	44	1166	22	54	22	92
November	5.0	87	757	20	42	983	20	52	20	95
December	2.9	89	667	20	42	983	20	52	20	95

lutely) from the average value. As highest value for the relative humidity therefore a value is supposed 10% higher than the average value. The calculation of the moisture transport for circumstances occurring in practice have been based on these increased values, indicated in Table 7.1 as "modified".

It can also be derived from the measurements that during periods of high vapour production (for instance in kitchens and bath rooms) the inside vapour pressure rises sharply. During these periods the dewpoint of the air may rise above the surface temperature of the roof on the bottom side, leading to condensation. During the rest of the day this condensed water partly evaporates again. The course of the vapour pressure depends on several factors, such as the rate of moisture production, the rate of ventilation, the size of the room. As a first approximation the inside vapour pressure is increased by an amount of 1000 N/m^2 above the "modified" value during two hours a day. The corresponding climatic conditions have been presented in Table 7.1, as "peak"-values.

7.2 Calculation of the moisture transport in roof constructions by means of a digital computer

In the way discussed in Section 6.1 the moisture transport is computed for several types of cellular concrete roofs and for several climatic conditions occurring in practice. The results of these calculations have been presented in [7]; some illustrative cases will be discussed here.

The calculations have been carried out for the time of 1 year, starting 1st Oktober. In this way first the moisture transport during a winter period has been calculated,

followed by the moisture transport during the summer period. When the moisture content at the end of the summer period differed considerably from the initial situation, the calculations have been carried out for yet another year.

The results for a 15 cm thick roof of cellular concrete, exposed to inside conditions as given in Table 7.1 under "modified", have been presented in the Figs. 7.1 and 7.2 for initial moisture contents of 2 vol.% and 20 vol.% respectively. A high moisture content of 20 vol.% can occur, if the roof is wetted by rain during the construction period, before the roofing was placed.

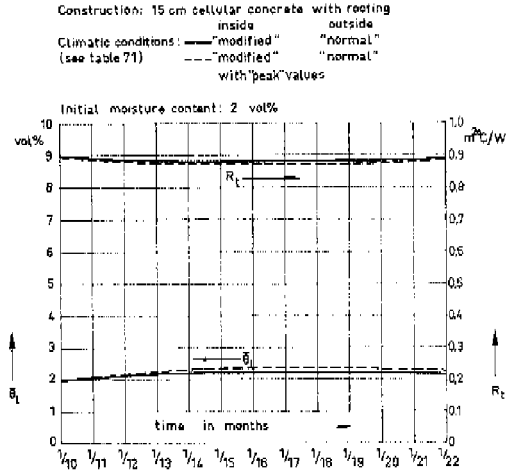

Fig. 7.1a Average moisture content, $\bar{\theta}_l$ and insulation value R_t (inclusive heat transfer resistances at both faces) as a function of time.

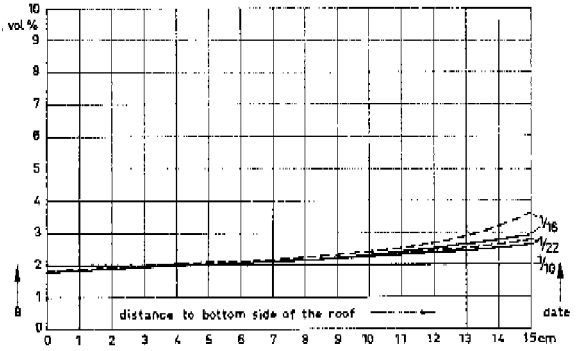

Fig. 7.1b Moisture distributions for several dates.

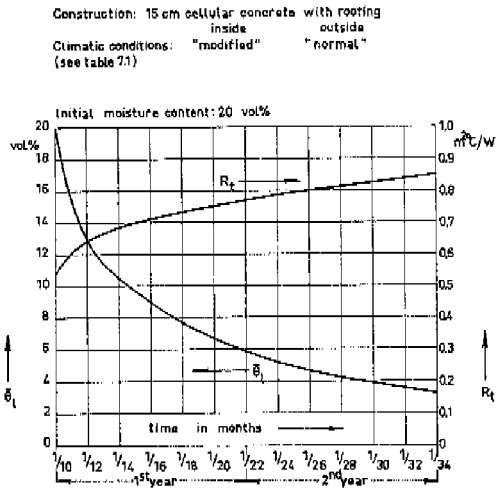

Fig. 7.2a Average moisture content, $\bar{\theta}_l$ and insulation value, R_l (inclusive heat transfer resistances at both faces) as a function of time.

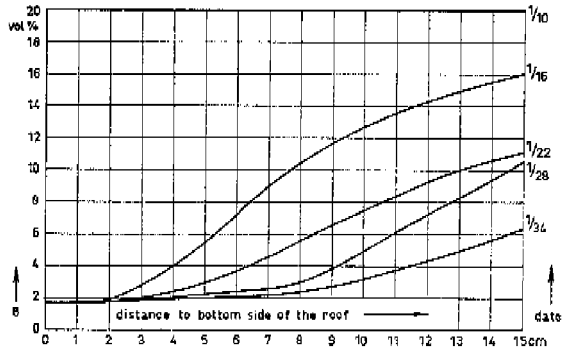

Fig. 7.2b Moisture distributions for several dates.

It can be seen that the moisture content in the roof with an initial moisture content of 2 vol.% hardly changes during the seasons. During winter as well as during summer an average moisture content has been calculated of 2.2 vol.%, with a maximum moisture content (just beneath the roofing) of 3 vol.% at the end of the winter period.

Starting from a moisture content of 20 vol.% the average moisture content decreases until about 10 vol.% during the first winter and unto 6 vol.% during the following summer, with a maximum local moisture content of 11 vol.%. During the

second year the average moisture content decreases unto 3 vol.%, with a maximum local moisture content of 6 vol.%.

For these conditions also the influence of a temporarily increased inside vapour pressure has been investigated, as may occur in bath rooms and kitchens during periods of high moisture production. The calculations have been performed for vapour pressures increased during 2 hours a day during which the conditions indicated in Table 7.1 with "peak" values hold.

For an initial moisture content of 2 vol.%, the results have been presented in Fig. 7.1, together with results for "modified" inside conditions. The influence of the temporarily increased inside vapour pressure appears to be small in this case. The

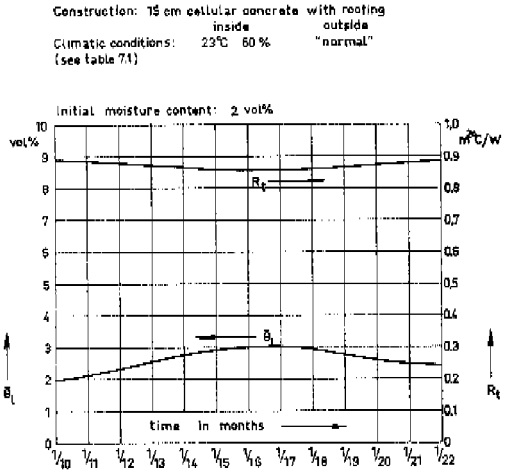

Fig. 7.3a Average moisture content, $\bar{\theta}_l$ and insulation value, R_t (inclusive heat transfer resistances at both faces) as a function of time.

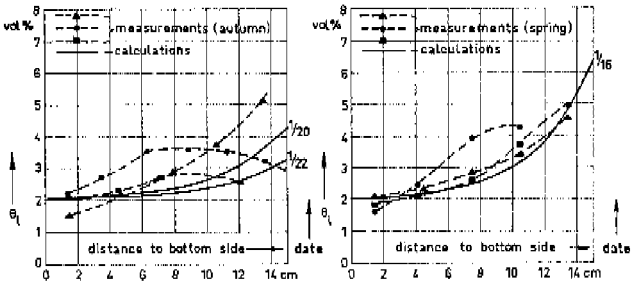

Fig. 7.3b Moisture distribution before winterperiod Moisture distribution after winterperiod

average moisture content increases unto 2.4 vol.% instead of 2.2 vol.% during winter and summer, and the maximum local moisture content at the end of the winterperiod rises to 3.5 vol.% instead of 3.0 vol.%.

Calculations have been carried out also for constant indoor conditions. The results have been presented in Fig. 7.3 for inside conditions of 23 °C, 60% and an initial moisture content of 2 vol.%. The average moisture content increases unto 3 vol.% during the winter (maximum local moisture content 6 vol.%) and decreases unto 2.5 vol.% during summer (maximum local moisture content 3 vol.%).

These theoretical values can be compared with the results of measurements, carried out in practice by Künzel [8], [9]. In one out of 35 cases investigated by him

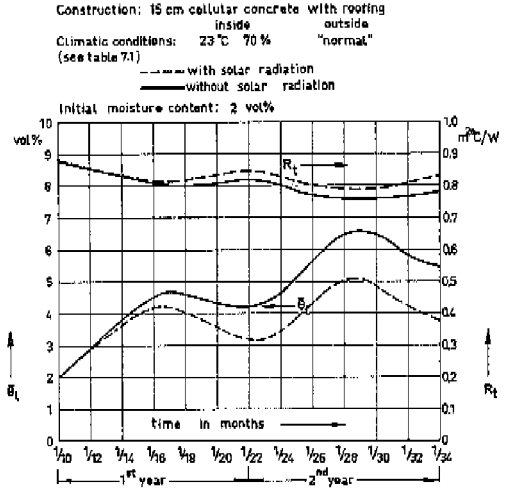

Fig. 7.4a Average moisture content, $\bar{\theta}_l$ and insulation value, R_t (inclusive heat transfer resistances at both faces) as a function of time.

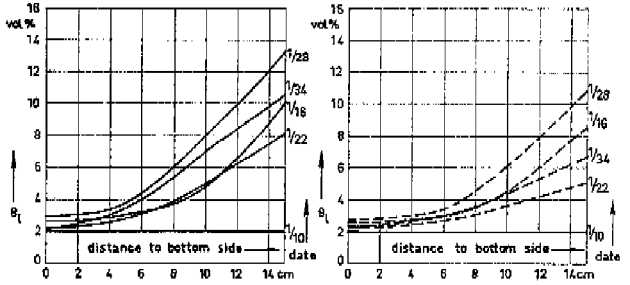

Fig. 7.4b
Moisture distributions without solar radiation Moisture distributions with solar radiation

the type of construction and the climatic conditions are nearly identical with those of our calculations. In the case considered the roof was placed above a laundry, constantly controlled at a climatic condition of 22 °C, 60%. The moisture content in the roof was measured in autumn and in spring at 3 different places. In autumn an average moisture content was found of 2.6 vol.% and in spring of 3.1 vol.%. The measured moisture distributions are presented in Fig. 7.3b together with the calculated ones. The results show a fairly good agreement.

For indoor conditions of 23 °C, 70% the results are presented in Fig. 7.4 by drawn lines. During the first winter period a rise of the average moisture content unto 4.6 vol.% is calculated (maximum local moisture content 10 vol.%) and a decrease during the summer period unto 4.2 vol.% (maximum local moisture content 8 vol.%). During the second year the average moisture content increases unto 6.5 vol.% (maximum local moisture content 13 vol.%) in the winter period and decreases unto 5.5 vol.% (maximum local moisture content 10 vol.%) during the summer period. The heat insulation value, initially 0.89 m^2 °C/W decreases in the first winter unto 0.80 m^2 °C/W and during the second winter unto 0.75 m^2 °C/W.

In the foregoing calculations the influence of solar radiation was not considered. To investigate its influence calculations have also been performed making allowance for solar radiation. In these calculations the temperature gradient inside the roof was computed for each time increment on the basis of the average monthly outside temperature in combination with the diurnal variation in temperature rise of the upper face of the roof caused by solar radiation. The latter was obtained from the values of the irradiance caused by the sun as shown in [10]. For indoor conditions of 23 °C, 70% the results have been presented in Fig. 7.4 by dotted lines, together with the results obtained without taking solar radiation into account.

As might be expected the roof dries out faster during the summer season by the influence of solar radiation. This results in an average moisture content 1 vol.% lower after 1 year and 2 vol.% lower after 2 years.

7.3 Suggestions for further work

It is shown in foregoing sections that the calculated results agree fairly well with results found experimentally in the laboratory and in practice. All calculations, however, are carried out for climatic conditions above 0 °C. In severe winters during a considerable time the outside temperature is below 0 °C. It is generally known that moisture transport is influenced by frost. Therefore a better understanding of the basic physical processes related to frost would be useful, also in connection with the occurrence of frost damage in building materials. At first sight one might expect that the moisture transport below 0 °C can be described with similar equations as those used above 0 °C, be it that the diffusion coefficients D_θ and D_T have to be adapted. The release of latent heat on freezing must be incorporated in the energy equation.

Next to this it may be useful to determine the diffusion coefficients D_θ and D_T also

for other materials, for instance wood and concrete. In practice many wooden structures, such as window frames deteriorate in an early stage by wood rot. This process among other things seems to be connected with the amount of moisture present in the wood. Therefore it may be useful to calculate the moisture flow in the structures making it possible to find requirements for lowering the moisture content in the wood.

In constructions of concrete, especially in thick ones, long times after setting a considerable creep is noticed, which is believed to be caused by too high a moisture content in the concrete. At the preparation of concrete water has to be added in excess. Especially in thick constructions due to the high resistance against vapour diffusion the drying process is a very slow one. A method for calculating the drying time therefore would be desirable, just as conditions for increasing the drying rate.

Further work also could be done in developing building materials with suitable properties with relation to moisture transport. In contrast with the way followed here, in which for the material considered the diffusion coefficients were determined and the moisture transport was calculated a different approach is to develop a material with a high value for the diffusion coefficient D_θ and a low one for D_T. It follows from the foregoing discussions that in roofs composed of such materials a low moisture content may be expected, even for high inside vapour pressures. Such suitable properties may be expected for materials with many very narrow pores, so that for low moisture contents ψ_m strongly depends on θ_l. A similar result can be obtained by making a roof material with narrow pores at the bottom side and wide pores on top or composing a roof from different materials, the material with fine pores being placed at the bottom side and the material with wide pores on top. To make such a choice of composing materials possible, the pore-size distribution of the materials should be known. Therefore it can be recommended to measure ψ_m vs θ_l for the most common building materials.

References

1. C. Braak, Het Klimaat van Nederland, Servire, Den Haag, 1950.
2. A. D. Kent, G. O. Handegord, D. R. Robson, Ashrae Transactions 72 (1966), nr. 1998.
3. W. Schüle, H. Lutz, Ges. Ing., **83**, (1962) 217–252.
4. H. P. L. den Ouden, Vocht in woningen, IG-TNO, werkrapport C 165, (1964).
5. Stichting Ratiobouw, De invloed van grindbetonwanden en centrale verwarming op de luchtvochtigheid in woningen, Verzameling Bouwstudies nr. 25, Uitgave Bouwcentrum 1964.
6. J. van der Kooi, K. T. Knorr, De vochtigheid in vijf woningen en een laboratoriumgebouw, Rapport B II-21, (1967), uitgebracht aan Stichting Bouwresearch.
7. J. van der Kooi, K. T. Knorr, Het vochtgedrag in niet-geventileerde daken van cellenbeton, publikatie nr. 33, Stichting Bouwresearch, Samsom, Alphen a/d Rijn (1970).
8. H. Künzel, K. Gertis, Untersuchungen über die Feuchtigkeitsverhältnisse in Gasbeton Dächer, Berichte aus der Bauforschung, Heft 51 (1968).
9. Untersuchungen über die Feuchtigkeitsverhältnisse in Dächer aus Gasbeton, Fachverband Gasbeton Industrie E.V. (1969)
10. Studie van de warmtewinst en van de natuurlijke verlichting van gebouwen, researchrapport nr. 10, Wetenschappelijk en technisch centrum voor het bouwbedrijf (1969).

SUMMARY

In this thesis investigations are described on the moisture transport in flat roofs of cellular concrete. Since in winter the pressure inside a building is mostly higher than that outside the building, water vapour diffuses into the roof and condenses underneath the roofing. In summer the roof partly dries out again by evaporation at the lower side. The rate of moisture change has been investigated, theoretically as well as experimentally.

In Chapter 2 several theories are discussed concerning the moisture transport in porous media. The theory of Philip and De Vries is discussed in detail. According to this theory the moisture flux in certain porous media can be described by:

$$q/\varrho_l = -D_\theta \nabla\theta_l - D_T \nabla T, \tag{1}$$

where q is the mass flow density, ϱ_l the density of water, $\nabla\theta_l$ the moisture gradient and ∇T the temperature gradient; D_θ and D_T are diffusion coefficients for transport due to these gradients.

In Chapter 2 also methods are discussed to calculate the change of moisture content in roof constructions. A calculation method of Glaser, in which only moisture transport in the vapour phase is considered, is explained and applied to the example of a roof of cellular concrete. Next a method is described to calculate the moisture transport in roof constructions using the theory of Philip and De Vries. The moisture content at the lower boundary of the roof is related to the relative humidity of the adjacent air layer by means of the relation between the hygroscopic moisture content, θ_h, and the relative humidity, h. The moisture transport inside the roof is calculated from Eq. (1). With a simplified calculation procedure some data of importance for the practical applications, can be calculated, such as the initial rate of increase of moisture content in the roof during winter. A complete calculation, however, needs the use of a computer. This calculation method and results obtained by it are described in Chapter 6.

The calculations mentioned before can only be carried out if certain properties of the roof material are known, such as the diffusion coefficients D_θ and D_T and the heat conductivity, λ, as functions of θ_l, and the relation $\theta_h = \theta_h(h)$. The measurements of these properties for cellular concrete are described in Chapter 3. The diffusion coefficients turned out to be highly dependent on θ_l. Also a hysteresis occurred for $\theta_l > 0.30$, where the curves differed considerably for increasing and decreasing moisture content. In order to calculate the diffusion coefficients the matrix potential $\psi_m = \psi_m(\theta_l)$ has been determined experimentally. The pore structure of the material has been examined with an electron microscope.

Using the expressions, derived by Philip and De Vries, in Chapter 4 the D_θ- and D_T-curves are calculated, making use of the knowledge obtained about the pore structure. Both diffusion coefficients, D_θ and D_T, can be considered as to be composed of a contribution in the liquid phase and one in the vapour phase. The contribution to D_θ in the liquid phase is calculated, from the matrix potential ψ_m and the hydraulic conductivity, K. The latter is calculated with the method of Childs and Collis-George. By adapting the method for the pore structure under consideration a fairly good agreement is found between the calculated D_θ-curve and the one determined experimentally.

The contribution of transport in the vapour phase is calculated using the theory of Maxwell, Burger en Eucken for calculating the diffusion coefficient of water vapour through a porous material, on the basis of certain assumptions about the pore structure. In these calculations also the reduction of the diffusion coefficient due to Knudsen flow is taken into account. However, the diffusion coefficient determined experimentally turned out to be about 2.5 times lower than the calculated value. This discrepancy is ascribed to the presence of blocked pores.

In the calculation of the contribution of transport in the vapour phase to D_T the influence of 'combined vapour-liquid transfer' was considered. The relations derived by Philip and De Vries needed some extension for the material under consideration, because of its complicated structure. The contribution in the vapour phase was considered as a combination of parallel transport (where in part of the pores vapour transport occurs exclusively and in the remaining part of the pores liquid transport exclusively) and series transport (where in all pores liquid islands are present so that only combined vapour-liquid transport occurs).

The calculated contribution of transport in the liquid phase turned out to be considerably lower (about ten times) than the contribution of that in the vapour phase. Summation of both contributions yielded a D_T-curve, which for $\theta_l < 30\%$ agreed fairly well with the curve determined experimentally. For $\theta_l > 30\%$ the experimental results were considerably lower, which was ascribed to the influence of large air enclosures.

In Chapter 5 experiments are discussed where in climate rooms the rate of moisture change was measured on roof specimens of cellular concrete exposed to stationary simulated summer and winter conditions. The experiments for winter conditions were started with practically dry specimens, for the experiments at summer conditions the initial moisture content was about 25%. The moisture increase turned out to occur very slowly. The drying process was much faster, especially for high moisture contents in the specimens.

In Chapter 6 calculations of the moisture content by means of a computer are described for cellular concrete roofs exposed to the same winter and summer conditions, for which the experiments in Chapter 5 were carried out. The results have been compared with the experimental ones. In order to obtain a good agreement, the D_θ- and D_T-curves used in the computer program had to be adjusted to lower values

than those determined in Chapter 3. The reason of these discrepancies is not yet understood.

For the same climatic conditions also the rates of moisture change have been calculated with the method of Glaser (see Table 6.2). These values have been compared with the experimental ones. The calculated rate of moisture increase during winter conditions turned out to be 1.5 till 2 times too low; the calculated drying rate during summer conditions was up to 40 times too low, which had to be ascribed to the fact that in this method liquid transport is left out of consideration.

In Chapter 7 the moisture transport is calculated in roofs of cellular concrete exposed to climatic conditions occurring in practice, in the same way as discussed in Chapter 6. Data on the outdoor climate have been derived from measurements of the K.N.M.I. (Royal Dutch Meteorological Institute). Data of the indoor climate have been derived from own measurements carried out in several types of dwellings. For these indoor conditions, indicated as 'modified' and for indoor conditions with a temperature of 23 °C and a relative humidity of 60 or 70% the course of the moisture content throughout the year is calculated for a cellular concrete roof with a thickness of 15 cm.

For the indoor conditions 'modified' and the conditions with a relative humidity of 60% the moisture content hardly increased during winter. For indoor conditions with a relative humidity of 70% a more rapid increase of moisture content during winter was calculated, which was higher than the decrease during summer, leading to an accumulation of moisture in the roof.

With the computer program also the influence of a temporarily increased indoor vapour pressure has been investigated, as may occur in kitchens during periods of high moisture production. For this purpose the indoor vapour pressure was increased with 1000 N/m^2 above the 'modified' indoor conditions during two hours per day. The influence of the temporarily increased vapour pressure was only small for the conditions considered here.

The influence of solar radiation on moisture transport has been investigated as well. For this purpose the computer program had to be somewhat extended. Calculations have been performed for the indoor conditions 23 °C, 70%. Due to solar radiation the drying rate during summer is increased, so that the accumulation of moisture in the roof decreases and the moisture content does not rise any further after some years.

Künzel has investigated the moisture content in roofs of cellular concrete under conditions occurring in practice. One of these roofs investigated was covering a space controlled at indoor conditions of 22 °C, 60%. Therefore the moisture behaviour could be compared with the calculations carried out for a roof with indoor conditions 23 °C, 60%. The results determined experimentally and those calculated showed a fairly good agreement.

SAMENVATTING

In dit proefschrift is een onderzoek beschreven naar het vochttransport in platte daken van gasbeton. Onder invloed van de 's winters meestal hogere waterdampdruk binnenshuis dan buitenshuis diffundeert waterdamp in een dak en condenseert hierin onder de dakbedekking, die voor water en waterdamp vrijwel ondoorlatend is. Gedurende de zomer droogt het dak gedeeltelijk uit door verdamping aan de onderzijde.

Het tempo van vochttoe- en afname is, zowel theoretisch als experimenteel, nader onderzocht.

In hoofdstuk 2 zijn – in het kort – de belangrijkste theorieën behandeld betreffende het vochttransport in poreuze materialen. Op de theorie van Philip en De Vries is dieper ingegaan. Volgens deze theorie kan het vochttransport in een poreus materiaal beschreven worden met de vergelijking:

$$q/\varrho_l = -D_\theta \nabla\theta_l - D_T \nabla T, \tag{1}$$

waarin q de vochtstroomdichtheid voorstelt, ϱ_l de soortelijke massa van water, $\nabla\theta_l$ de vochtgradiënt en ∇T de temperatuurgradiënt. D_θ en D_T zijn diffusiecoëfficiënten voor vochttransport tengevolge van deze gradiënten. θ_l is de volumefractie van vloeibaar water in het materiaal.

Eveneens zijn in hoofdstuk 2 methoden besproken om het tempo van de verandering van het vochtgehalte in dakconstructies te berekenen. Bij de door Glaser ontwikkelde methode wordt alleen damptransport beschouwd dat optreedt tengevolge van het verschil, tussen de binnendampdruk en de verzadigingsdampdruk in het dak. De methode is toegelicht aan de hand van een voorbeeld.

Daarnaast is een rekenmethode aangegeven waarbij gebruik gemaakt wordt van de theorie van Philip en De Vries. Hierbij is het vochtgehalte aan de onderzijde van het dak afhankelijk gesteld van de relatieve vochtigheid van de aangrenzende luchtlaag door middel van het verband tussen het hygroscopische vochtgehalte, θ_h, en de relatieve vochtigheid, h. Het vochttransport in het overige deel van het dak is vervolgens berekend met behulp van vergelijking (1). Volgens een vereenvoudigde methode kunnen enkele voor de praktijk belangrijke gegevens, zoals de aanvankelijke snelheid van de vochttoename gedurende wintercondities, berekend worden. Een volledige berekening van het vochttransport is vrij omvangrijk en alleen mogelijk met behulp van een computer. Deze berekening is uitgevoerd in hoofdstuk 6.

Voor de uitvoering van deze berekeningen dienen materiaaleigenschappen bekend te zijn, zoals het verloop van de diffusiecoëfficiënten D_θ en D_T en het warmtegeleidingsvermogen, λ, als functie van het vochtgehalte, θ_l, alsmede het verband $\theta_h = \theta_h(h)$. De

bepaling van deze materiaaleigenschappen is beschreven in hoofdstuk 3. D_θ en D_T blijken sterk afhankelijk te zijn van θ_l. Ook blijkt hysterese op te treden, die hoofdzakelijk veroorzaakt wordt door grote luchtinsluitsels, waardoor vooral voor $\theta_l > 0{,}30$ de diffusiecoëfficiënten sterk verschillen voor toe- en afnemend vochtgehalte. Om het verloop van de diffusiecoëfficiënten te kunnen berekenen is tevens voor gasbeton de zuigspanning, ψ_m, als functie van θ_l bepaald en is de poriënstructuur onderzocht met een elektronenmicroscoop.

Uitgaande van deze gegevens is in hoofdstuk 4 met behulp van betrekkingen, afgeleid door Philip en De Vries, het verloop van D_θ en D_T berekend. De diffusiecoëfficiënten D_θ en D_T bestaan ieder uit bijdragen tengevolge van transport in de vloeistoffase en in de dampfase. De bijdrage tot D_θ van het transport in de vloeistoffase is berekend door gebruik te maken van het in hoofdstuk 3 bepaalde verband $\psi_m = \psi_m(\theta_l)$ en het verband tussen het hydraulisch geleidingsvermogen, K, en het vochtgehalte, θ_l, berekend volgens de methode van Childs en Collis-George. Door de laatstgenoemde methode aan te passen voor de hier beschouwde poriënstructuur werd een redelijke overeenkomst met de experimenten verkregen.

Bij de berekening van de bijdrage in de dampfase is gebruik gemaakt van de theorie van Maxwell, Burger en Eucken. Uitgaande van bepaalde veronderstellingen omtrent de structurele opbouw van het materiaal is met deze theorie de diffusiecoëfficiënt voor waterdamp in het beschouwde materiaal berekend.

Voorts bleek nog rekening gehouden te moeten worden met een vermindering van de diffusiecoëfficiënt tengevolge van Knudsen-effecten. De experimenteel gevonden waarde voor de diffusiecoëfficiënten bleek nog circa 2,5 maal kleiner te zijn dan de op deze wijze berekende, hetgeen aan de aanwezigheid van geblokkeerde poriën is toegeschreven.

Bij de berekening van de bijdrage tot D_T in de dampfase is tevens het „gecombineerde damp-vloeistoftransport" beschouwd zoals beschreven in de theorie van Philip en De Vries.

Deze theorie moest voor het hier beschouwde materiaal enigszins worden uitgebreid. Het vochttransport is beschouwd als opgebouwd uit parallel transport (waarbij in een deel van de poriën alleen damptransport plaatsvindt en in de overige alleen vloeistoftransport) en uit serietransport (waarbij in alle poriën „vloeistofeilandjes" voorkomen en uitsluitend gecombineerd damp-vloeistoftransport optreedt). Door een bepaalde wijze van combineren zijn berekende en experimenteel bepaalde waarden met elkaar in overeenstemming gebracht. De berekende bijdrage in de vloeistoffase bleek aanmerkelijk kleiner te zijn dan de bijdrage in de dampfase. Voor $\theta_l < 0{,}30$ bleken de berekende en experimenteel gevonden D_T-waarden redelijk overeen te stemmen. Voor $\theta_l > 0{,}30$ werden experimenteel aanzienlijk lagere waarden bepaald, hetgeen toegeschreven is aan de invloed van grote luchtinsluitsels.

In hoofdstuk 5 zijn experimenten beschreven waarbij in een meetopstelling het vochtgedrag in proefdaken van gasbeton is onderzocht, blootgesteld aan stationaire gesimuleerde winter- en zomercondities. Bij de experimenten bij wintercondities is

uitgegaan van praktisch droge proefdaken en bij de experimenten onder zomercondities van een initieel vochtgehalte van circa 25 volumeprocent ($\theta_i = 0{,}25$). Van deze proefdaken is eveneens met regelmatige tussenpozen de warmteweerstand bepaald.

Voor dezelfde winter- en zomercondities en hetzelfde daktype is in hoofdstuk 6 met behulp van een computer het vochtgedrag berekend en vergeleken met de experimenten. Bij deze berekening werd gebruik gemaakt van de in hoofdstuk 3 bepaalde materiaaleigenschappen, zoals de diffusiecoëfficiënten D_θ en D_T. Teneinde een goede overeenstemming te krijgen tussen berekende en experimenteel gevonden resultaten bleken beide diffusiecoëfficiënten bij de computerberekeningen nog nader aangepast te moeten worden. De reden van deze aanpassing is niet geheel duidelijk.

In hoofdstuk 6 (zie tabel 6.2) zijn tevens de resultaten vermeld, berekend volgens de methode van Glaser. Het tempo van vochttoename gedurende wintercondities bleek 1,5 tot 2 maal lager te zijn dan experimenteel werd bepaald; de droogsnelheid gedurende zomercondities bleek – vooral bij een hoog vochtgehalte in de proefdaken – tot 40 maal lager te zijn dan experimenteel werd bepaald. Deze afwijkingen worden veroorzaakt door het niet in rekening brengen van het vloeistoftransport bij deze methode.

Met het in hoofdstuk 6 besproken computerprogramma is in hoofdstuk 7 het vochttransport in daken van gasbeton berekend voor in de praktijk optredende klimaatcondities. De gegevens voor het buitenklimaat zijn hierbij ontleend aan gegevens van het K.N.M.I. te De Bilt. De gegevens voor het binnenklimaat zijn afgeleid uit eigen metingen, verricht in verschillende typen woningen.

Voor deze binnenconditics, aangeduid met „modified" en voor stationaire binnenconditics met een temperatuur van 23 °C en relatieve vochtigheden van 60% en 70% is het vochttransport in een 15 cm dik dak van gasbeton berekend. Bij de binnenconditics aangeduid met „modified" en de condities met een relatieve vochtigheid van 60% blijkt het vochtgehalte in het dak gedurende de winter nauwelijks toe te nemen. Bij de binnencondities met een relatieve vochtigheid van 70% is een vrij sterke vochtstijging gedurende de winter berekend, die groter is dan de droging gedurende de zomer. Hierdoor treedt een accumulatie van vocht op die na enkele jaren tot een te hoog vochtgehalte aanleiding geeft.

Met het computerprogramma is ook de invloed van tijdelijke „oppervlaktecondensatie" nagegaan, zoals kan voorkomen in keukens tijdens perioden met grote vochtproduktie. Uitgaande van de condities „modified" is gedurende 2 uur per dag de binnendampdruk met een bedrag van 1000 N/m^2 verhoogd, waardoor gedurende deze perioden het dauwpunt van de binnenlucht hoger was dan de oppervlaktetemperatuur van het plafond. De invloed van deze tijdelijke oppervlaktecondensatie bleek gering te zijn.

Daarnaast is met een kleine uitbreiding van het computerprogramma de invloed van zonbestraling op het vochtgedrag berekend voor binnencondities met een relatieve vochtigheid van 70%. Door de zonbestraling droogt het dak gedurende de zomer-

maanden sneller uit, waardoor een geringere vochtaccumulatie optreedt en mogelijk op den duur het vochtgehalte niet verder stijgt.

Künzel heeft onder praktijkomstandigheden het vochtgehalte in gasbeton-daken gemeten. Één van de onderzochte daken bevond zich boven een ruimte met een binnenklimaat van 22 °C en 60%, en is dus vergelijkbaar met het hier berekende dak met binnencondities 23 °C en 60%. De berekende en experimenteel gevonden vochtgehaltes bleken redelijk met elkaar overeen te stemmen.

LIST OF SYMBOLS AND UNITS

a	volume fraction of gas (m^3 gas/m^3 material)	1
a_ϱ	area occupied by pores of radius ϱ to $\varrho + dr$	1
a_σ	area occupied by pores of radius σ to $\sigma + dr$	1
c	mass fraction	1
$D_{\vartheta l}$	diffusivity for liquid transport due to a moisture gradient	m^2/s
$D_{\vartheta v}$	diffusivity for vapour transport due to a moisture gradient	m^2/s
D_ϑ	total diffusivity for moisture transport due to a moisture gradient	m^2/s
D_{Tl}	diffusivity for liquid transport due to a temperature gradient	$m^2/s°C$
D_{Tv}	diffusivity for vapour transport due to a temperature gradient	$m^2/s°C$
D_T	total diffusivity for moisture transport due to a temperature gradient	$m^2/s°C$
D	diffusion coefficient of water vapour in air	m^2/s
D'	thermal diffusion coefficient	$m^2/s°C$
D_i	diffusion coefficient of particles of kind i	m^2/s
DTO	change of moisture content of layer k due to moisture flux at $(k-\frac{1}{2})\Delta z$	1
DTK	change of moisture content of layer k due to moisture flux at $(k+\frac{1}{2})\Delta z$	1
g	acceleration of gravity	m/s^2
h	relative humidity	1, %
k	„Potentialleitfähigkeit" ($= D_{\vartheta l}$)	m^2/s
K	hydraulic conductivity	kgm^2/Js ($=s$)
k	number of position increment, Δz	1
$\boldsymbol{k}$	unit vector in pos. z-direction	1
k_i	factor depending on the form of particles of kind i	1
M	molar mass	kg/kmol
M	constant for adapting the theoretical D_ϑ-curve	s/m^2
m	number of time increment, Δt	1
P	total gas pressure	N/m^2
P_0	reference value of total gas pressure ($= 1$ atm. $= 1.01325 \cdot 10^5$ N/m^2)	N/m^2
P_t	moisture tension	N/m^2
p_{ve}	external vapour pressure	N/m^2

p_{vi}	internal vapour pressure	N/m^2
p_{vsr}	saturation vapour pressure corresponding with T_r	N/m^2
p_{vss}	saturation vapour pressure corresponding with T_s	N/m^2
p_v	partial pressure of water vapour	N/m^2
p_{vs}	saturation vapour pressure	N/m^2
q	mass flow density	kg/m^2s
r	radius of capillary	m
R	universal gas constant ($\approx$ 8.31 kJ/kmol K)	J/kmol K
R_e	heat transfer resistance external	$m^2°C/W$
R_i	heat transfer resistance internal	$m^2°C/W$
R_t	thermal resistance (inclusive heat transfer resistances on both sides)	$m^2°C/W$
S	volume fraction of pores	1
T	temperature	K, °C
T_0	reference temperature (= 273 K)	K
T_r	temperature just beneath the roofing	°C
T_s	temperature at the bottomside of the roof	°C
t	time	s, h
u	mass fraction of moisture content (kg liquid/kg mat.)	1
v_i	volume fraction of particles of kind i	1
Z	diffusion resistance	m/s
z	vertical coordinate	1
α	labyrinth factor	1
β	mass transfer coefficient	m^2s/kg
β_s	reduction factor of diffusivity due to Knudsen flow	1
Γ_w	moisture content (kg liquid/m^3 material)	kg/m^3
γ	temperature coefficient of surface tension	$°C^{-1}$
δ	contact angle	1
δ	vapour transmission coefficient	s
ε	temperature gradient factor ($= D_T/D_\theta$)	$°C^{-1}$
λ	thermal conductivity	W/m°C
μ	diffusion resistance factor	1
ν_l	kinematic viscosity of water	m^2/s
θ_l	volume fraction of moisture content (m^3 liquid/m^3 material)	1, %
ϱ	density	kg/m^3
ϱ	radius of capillary	m
ϱ_m	density of dry material	kg/m^3
σ	surface tension	N/m
σ	radius of capillary	m
ψ	total hydraulic potential	J/kg (= m^2/s^2)
ψ_g	gravity potential	J/kg

ψ_m	matrix potential	J/kg
ψ_p	pressure potential	J/kg

INDICES

a	air	q	quartz
i	particles of kind i	s	series transport
k	place increment number	s	sponge material
l	liquid	v	vapour
m	time increment number	ϱ	pores of radius ϱ to $\varrho+\mathrm{d}r$
p	parallel transport	σ	pores of radius σ to $\sigma+\mathrm{d}r$

ACKNOWLEDGEMENTS

The research described in this thesis was carried out at the Institute of Applied Physics TNO-TH in Delft. I am indebted to the management of the institute for providing the facilities for carrying out this study and printing the results as a thesis.

I am grateful to Mr. Knorr for carrying out part of the experiments and to Mr. Peitsman for drawing the figures in this thesis. Next to this I am grateful to Drs. Visser for his help in composing the computer programme and to Mr. Spit for his microscopical work.

The work presented here was commissioned by the Foundation Building Research and was partially supported by this body, by the Organization for Industrial Research TNO and by the Institute of Applied Physics TNO-TH of the Central Organization for Applied Scientific Research in the Netherlands TNO.

CURRICULUM VITAE

Op aanbeveling van de Senaat volgt hier een korte levensbeschrijving van de schrijver van dit proefschrift.

Hij werd geboren te Geldrop op 8 juli 1934. Na de lagere school bezocht hij het Lorentz-Lyceum waar hij het eindexamen HBS-b aflegde in 1951. Aansluitend begon hij zijn natuurkundestudie aan de Technische Hogeschool te Delft. Hij verrichtte zijn kandidaatswerk onder leiding van Prof. dr. ir. F. A. Heijn op de afdeling der Elektrotechniek en zijn afstudeerwerk onder leiding van Prof. dr. M. J. Druyvesteyn bij de Technisch Physische Dienst TNO-TH.

Het ingenieursexamen werd afgelegd in 1959. Vervolgens vervulde hij zijn militaire dienstplicht bij de Koninklijke Landmacht en trad in 1961 in dienst bij de Technisch Physische Dienst TNO-TH, afdeling Warmte. Sindsdien is hij bij deze Dienst werkzaam.

STELLINGEN

I

De opvatting van Eichler dat een „koudebrug" gevormd door een betonvloer die door de gevel uitkraagt met een looprand niet verbeterd kan worden door het aan de buitenlucht grenzende gedeelte te bekleden met warmteisolerend materiaal, is onjuist.

F. Eichler, Bauphysikalische Entwurfslehre, deel II (1968) p. 407.

II

Een dak behoort zodanig te worden geconstrueerd dat eventueel tijdens de bouw binnengedrongen vocht of door lekkage van de dakbedekking binnengedrongen regenwater binnen redelijke tijd kan ontwijken. Het aanbrengen van dampremmende lagen aan de onderzijde van niet-geventileerde daken, zoals in de Duitse literatuur wordt aanbevolen, is daarom onjuist en leidt in de praktijk tot schadegevallen.

W. Caemmerer, Berichte aus der Bauforschung, Heft 51 (1968).
Wärmedämmungs- und Dampfsperrschichten bei Dächern und Wänden, Zentralblatt für Industriebau 2 (1965) p. 60–71.

III

Berekeningen van de te verwachten hoeveelheid condensatie volgens de methode van Glaser geven voor constructies opgebouwd uit materialen met een capillaire structuur veelal verkeerde uitkomsten. Bij dergelijke constructies wordt het vochtgedrag behalve door transport in de dampfase ook bepaald door capillair vloeistoftransport en door het hygroscopisch vochtgehalte in de desbetreffende materialen.

Dit proefschrift.

IV

Bij experimenten ter bepaling van het verloop van de diffusiecoëfficiënt D_θ als functie van het vochtgehalte θ_l voor gasbeton hebben Krischer en Mahler door een onvolledige interpretatie van hun meetresultaten het secundaire minimum in de $D_\theta(\theta_l)$-kromme bij $\theta_l \simeq 0{,}50$ niet gevonden.

Dit proefschrift.

V

De bepaling van de poriënverdeling met een vloeistofverdringingsmethode geeft bij materialen met een gecompliceerde structuur onvoldoende informatie over de structuuropbouw om de transporteigenschappen van deze materialen voor vocht te kunnen berekenen. Bij dergelijke materialen is een aanvullend microscopisch onderzoek noodzakelijk.

VI

In de woningbouw verdienen hellende pannendaken de voorkeur boven platte daken.

VII

Parken in dichtbebouwde stadswijken dienen vrije ontplooiingsmogelijkheden voor kinderen te bieden en niet onderhevig te zijn aan allerlei verbodsbepalingen. Aparte parkgedeelten voor honden zouden daarbij zijn aan te bevelen.

VIII

Bij de berekening van de temperatuur van door zon beschenen buitenwanden en daken werden door Croiset en Berthier te lage waarden voor de warmteoverdrachtscoëffiënt aangehouden.

M. Croiset, J. Berthier; Températures maximales atteintes au soleil par des parois de construction. Cahiers du Centre Scientifiques et Techniques du Bâtiment no. 58 (1962).

IX

In de bouwpraktijk worden veelal vochtklachten die veroorzaakt worden door lekkage of door de aanwezigheid van bouwvocht, ten onrechte toegeschreven aan condensatie.

X

In de norm DIN 4701 „Regeln für die Berechnung des Wärmebedarfs von Gebäuden" wordt de grotere warmteafgifte van het menselijk lichaam in de nabijheid van een koude buitenwand geacht te worden gecompenseerd door een verminderde warmteafgifte aan de lucht als gevolg van het instellen van een hogere luchttemperatuur.

Dit uitgangspunt wordt eveneens aangehouden door Kast en door Kollmar. Op deze wijze wordt echter geen behaaglijk binnenklimaat verkregen, omdat een te sterke asymmetrische warmteafgifte een gevoel van onbehagen veroorzaakt.

W. Kast; Ges. Ing. **91** (1970) 252–257.
A. Kollmar; Ges. Ing. **91** (1970) 33–41.

XI

Het luistergenot van grammofoonplaten met buitenlandse tekst waarvan het niveau uitgaat boven rijmelarij, wordt aanzienlijk verhoogd wanneer op de hoes de volledige tekst is vermeld.

J. van der Kooi
18 mei 1971